THERMODYNAMICS AND KINETICS ENHANCEMENT OF $LiNH_2$-MgH_2 SYSTEMS USING ALKALI METAL HYDRIDE DOPANTS FOR HYDROGEN STORAGE

by

TOLULOPE OLUMIDE DUROJAIYE

A DISSERTATION

Submitted in partial fulfillment of the requirements

for the degree of Doctor of Philosophy in

the Applied Chemistry Graduate

Program of Delaware State University

DOVER, DELAWARE

May 2013

DEDICATION

I dedicate my dissertation work to Almighty God and my deceased dad Isaac Durojaiye. To my mom, Florence Durojaiye for her prayers. To my lovely wife and son; Susan and Moyo for their unwavering support, patience and understanding. To my siblings, Olaolu, Titi, Seun, Seye and their families. You all are special.

I also dedicate this dissertation to my many friends and church family who have supported me throughout the process. The Sabitu, Orefuwa and Ojo family, you all are awesome. To my friends and the Chemistry Department of Delaware State University, who gave me all the support and love I needed throughout my stay at the University and in the course of this dissertation.

ACKNOWLEDGEMENT

I give all glory to God, the author, the beginning and the end of this dissertation for seeing me through.

I would like to express the deepest appreciation to my supervisor Dr. Andrew Goudy who has the attitude and substance of a genius for his all round support. Without is guidance and persistent help this dissertation would not have been possible.

I would like to thank my committee members Dr. Andrew Goudy, Dr. Bizuneh Workie, Dr. Cherese Winstead, Dr. Raymond Edziah and Dr. Tabbetha Dobbins. Thank you all for your time and willingness to be part of my committee.

Many thanks to special friends and colleagues like Dr. Hongwei Yang, Dr. Tope Sabitu, Dr. Samuel Orefuwa, Dr. Adeola Ibikunle, Esosa Iriowen and Jalaal Hayes for their support and input. You all are special.

Thanks to families like The Durojaiye, Orekoya, Kukoyi and Shuaib for their words of encouragement and prayers.

Special thanks to mother of the Chemistry Department Mrs. Leida Sanchez for your support throughout my research and during my stay at the University. You are a true mother.

ABSTRACT

The $LiNH_2/MgH_2$ systems, either in ratio 1:1 or 2:1, are promising hydrogen storage materials due to their high hydrogen storage capacities, potential reversibility and moderate operating conditions. The effects of some selected non-transition metal hydride additives (KH, RbH and CsH) were investigated on these systems. KH showed to be more effective for lowering the desorption temperature and increasing the desorption rates of the 2:1 mixtures than the 1:1 mixtures. The desorption rates of the 2:1 mixture was enhanced by ~25 times when doped with KH. The KH has no effect on the desorption rates of the 1:1 mixtures. The effects of the various selected non-transition metal hydrides on the 2:1 mixtures were also investigated and compared. All the additives proved to be effective for lowering the desorption temperature, reducing the enthalpy and increasing the desorption rates of the 2:1 mixture; hence they are referred to as "catalytic additives". Using constant pressure thermodynamics driving forces of N = 10 and at 210^{o} C, the kinetics results showed that the RbH-doped mixture released hydrogen over twice as fast as the K doped mixture, thrice as fast as the Cs doped mixture and approximately 60 times faster than the un-catalyzed sample. This is a remarkable improvement on the desorption kinetics of the $2LiNH_2/MgH_2$ system. Modeling studies using the shrinking core model and a method developed by Hancock and Sharp both indicated that the reaction rates for both the doped and un-doped mixtures of the $2LiNH_2/MgH_2$ are controlled by diffusion in the two-phase plateau region.

TABLE OF CONTENTS

LIST OF TABLES

LIST OF FIGURES

CHAPTER ONE

1.0 INTRODUCTION

At the present time the world is faced with the problems of rapidly dwindling sources of conventional energy such as fossil fuels (especially petroleum and natural gas). Burning of these fossil fuels results in several problems such as acid rains, climate change, global warming and pollution that degrades our environment and have negative effect on the quality of life. These have brought increased consciousness of the need for efficient, clean and renewable energy sources. Hydrogen is the most often discussed energy carrier because when burned in air, it produces a clean form of energy. Hydrogen's interest as energy of the future is in being a clean energy carrier source, lightest fuel, most abundant element in the universe, richest in energy per unit mass, easy storage and creation of new economy [1, 2].

Hydrogen gas can be used for various applications such as generating electricity, cooking, automobiles fuel, power industries, flying jet planes and other domestic energy requirements. It is presently being used in experimental cars, and as fuel in space programs. In the 1960s NASA's space capsule used hydrogen fuel cells to power aerospace transports to build the international space station, provide electricity and portable water for space dwellers [1].

Hydrogen is the simplest and lightest element in the universe. It has only one proton and electron and it is only available in compounds such as water and hydrocarbons. It has three times higher energy efficiency compared to petroleum [3]. The interest in hydrogen as an energy alternative has grown more in the 1990s after its initiation in the 1960s [4,5]. Hydrogen's large scale production efforts have been faced with diverse problems which inhibit the hydrogen economy implementation. Effective hydrogen storage is a major problem inhibiting the hydrogen economy. Due to low energy density and safety, cryogenic and high pressure storage is not the most suitable way for practical vehicular storage [6, 7]. Due to the reasons mentioned enormous efforts have been made to look for solid materials which can hold hydrogen reversibly according to the U.S. Department of Energy (US DOE) stated standards which include good storage capacity, low desorption temperature, low cost and low toxicity [8].

Some materials such as metal hydrides [9, 10], carbon materials [11, 12], and activated charcoal [13, 14] have been examined to fulfill the requirements above but none of them showed satisfactory performance for commercial vehicular hydrogen storage application. Lately, investigations of complex hydrides have offered a possibility to design a potential hydrogen storage system due to their light weight and number of hydrogen atoms per metal atom [1].

1.1 U.S. DOE TECHNICAL TARGETS FOR ON-BOARD HYDROGEN STORAGE SYSTEM

The goal of the U.S. Department of Energy Hydrogen Program is for hydrogen fuel to produce ten percent of our energy consumption by year 2030. In order to achieve the

widespread commercialization of hydrogen in the transportation industry the performance of hydrogen fueled vehicles must be compatible or superior to conventional gasoline powered vehicles [2]. As required by the US DOE the desired hydrogen storage technology should allow a driving range of more than 300 miles (500 km) without making significant changes to the vehicle and being available at similar cost. As a result of significant progress made on the development of hydrogen fueled vehicles and real-world driving and testing experience, valuable information has been substantially gathered. Also, information on design limitations of fuel cell vehicles, vehicle performance and customer requirements and expectations are now available. These new developments have led to the revision of the 2015 technical targets for on-board hydrogen storage system [2].

The new gravimetric hydrogen density and volumetric hydrogen density are now 5.5 wt. % and 40 g H_2 L^{-1} respectively (down from 9 wt. % and 81 g H_2 L^{-1}). New system fill time for 5-kg fill is 3.3 min (up from 2.5 min). The new storage system cost is yet to be determined as at the time of writing (old system cost was \$67/kg H_2 or \$2/kWh). The operational cycle life is unchanged - 1500 cycles. The hydrogen desorption temperature must be between 60 ^{o}C and 120 ^{o}C. Toxicity, safety, permeation and leakage should also be kept at levels that meet the federal applicable standards [15].

1.2 HYDROGEN ENERGY BENEFITS

Readily available

Hydrogen is the most abundant element found in the universe. It can be made from a wide variety of feed stocks including water, biomass, coal, natural gas, even in conjunction with wind, solar, and nuclear energy [16, 17].

Environmentally friendly

When hydrogen is burned, it leaves almost no harmful byproducts. Its byproduct is drinkable water. Hydrogen benefits the environment because it replaces older, dirtier fuels, thus reducing greenhouse gas emissions and improving air quality. Hydrogen's non-toxic nature makes it a rare fuel source among others. Nuclear energy, coal, and gasoline are all either toxic or found in hazardous environments. This makes hydrogen ideal for use in a number of ways other fuel sources can't compete against [16, 17].

Powerful and Fuel efficient

Hydrogen energy is powerful enough to propel spaceships and it is safer than using any other similar product to accomplish such an energy-intensive duty. Hydrogen has the highest energy content per unit weight of any known fuel and burns more efficiently than gasoline. This clearly means that a car loaded with hydrogen fuel will go much farther than the one using the same amount of traditional source of energy [16].

Renewable

Unlike non-renewable sources of energy which can't be produced again and again as they are limited and rapidly depleting; hydrogen is a renewable carrier of energy that can be produced on demand from replenishable resources [16].

Economic growth

Hydrogen can contribute to economic growth through job development, investment opportunities, and the creation of a sustainable, secure energy supply [17].

Energy security

Hydrogen benefits energy security through energy diversification. It could reduce our dependence on foreign oil since hydrogen can be derived from domestic sources, such as natural gas and coal, as well as renewable resources. Hydrogen used to provide transportation fuel and off-grid power makes us less vulnerable to oil price shocks from an increasingly volatile oil market [17, 18].

1.3 HYDROGEN ENERGY CHALLENGES

System Cost

On-board hydrogen storage systems cost is too high, particularly in comparison with conventional storage systems for fossil fuels such as gasoline. Low-cost media, materials of construction and balance-of-plant components are needed, as well as low-cost, high-volume manufacturing methods [19].

System Weight and Volume

The weight and volume of hydrogen storage systems are presently too high, resulting in inadequate vehicle range compared to conventional petroleum fueled vehicles. Materials and components are needed for all compact, lightweight hydrogen storage systems that allow driving ranges similar to those available today for light-duty vehicle platforms. Reducing weight and volume of thermal management components is required [19].

Charging/Discharging Rates

Hydrogen refueling times are generally too long for material based systems. There is a need to develop hydrogen storage systems with refueling times of about three minutes for a 5-kg hydrogen charge, over the lifetime of the system. Thermal management that enables quicker refueling is a critical issue that must be addressed [19].

Efficiency

Energy efficiency is a challenge for all hydrogen storage approaches. The energy required in transferring hydrogen into and out of the storage media or material is an issue for all material options. Life-cycle energy efficiency may be a challenge for chemical hydrogen storage technologies in which the spent media and by-products are typically regenerated off-board the vehicle. Thermal management for charging and releasing hydrogen from the storage system needs to be optimized to increase overall efficiency for all approaches [19].

Balance of Plant (BOP) Components

Light-weight, cost-effective balance-of-plant components are needed for all approaches of hydrogen storage, especially those requiring high-pressure or extensive thermal management. These include tubing, fittings, check valves, regulators, filters, relief and shut-off valves, heat exchangers, and sensors. System design and optimal packaging of components to meet overall volumetric targets are also required [19].

Durability/Operability

Hydrogen storage system's durability is currently inadequate. Storage media, materials of construction and balance-of-plant components are needed that allow hydrogen storage systems with a lifetime of at least 1500 cycles and with tolerance to hydrogen fuel contaminants [19].

Codes & Standards

Applicable codes and standards for hydrogen storage systems and interface technologies, which will facilitate implementation/commercialization and assure safety and public acceptance, have not been established. Standardized hardware and operating procedures, and applicable codes and standards, are required [19].

Materials of Construction

High pressure containment for compressed gas and other high-pressure approaches limits the choice of construction materials and fabrication techniques, within weight, volume, performance and cost constraints. For all approaches of hydrogen storage, vehicle

containment that is resistant to hydrogen permeation and corrosion is required. Materials to meet performance and cost requirements for hydrogen delivery and off-board storage are also needed [19].

1.4 HYDROGEN STORAGE TECHNOLOGIES

Hydrogen storage has been the leading technical barrier to hydrogen's future in the transportation sector. Current limitations in the hydrogen production and fuel cell technologies are likely to be solved through progressive or evolutionary improvements. Meeting the storage challenge will require revolutionary improvements and breakthroughs. Hydrogen can be stored in the form of gas, cryogenic liquid or adsorbed gas in solid materials [20].

Compressed gas

Compressed hydrogen is generally stored in cylindrical tanks at pressures of around 200-700 bars [21]. This in turn requires the use of specially constructed pressure vessels, which are energy consuming and expensive for large-scale applications [22]. Low pressure storage, either in tanks or underground, can be used for very large volumes. It is the cheapest method, however storage density is low. Higher storage pressures increase the storage density, but also the costs of the system and most especially the safety requirements [21].

Liquid Hydrogen

Another method of storing hydrogen is physical storage of cryogenic liquid hydrogen (cooled to -253 ^{o}C) in insulated tanks [23]. The liquefaction process itself is energy intensive, but liquid hydrogen has a very high hydrogen density, over three times that of gasoline. Highly insulated tanks are needed to minimize evaporation and these can add to the bulkiness and heaviness of on-board liquid storage system [21].

Chemical storage

Hydrogen can also be stored within the structure of advanced materials or on the surface of certain materials, as well as in the form of chemical precursors that undergo a chemical reaction to release hydrogen [23]. Metal hydrides are metal alloys that can store hydrogen within their chemical structure. Hydrogen is bonded to the surface of small particles of the material and is only released on application of heat. Hydrogen can also be stored within carbon materials and in the form of liquid hydrides [21].

1.5 METAL HYDRIDES

Metal hydrides contain typically heavy elements (transition metals) [24]. Hydrogen reacts with several transition metals and their alloys at high temperatures to form hydrides. The electropositive elements such as Sc, Y, lanthanides, actinides and members of the Ti and V groups are the most reactive. The binary hydrides of transition metals are metallic in character and are known as metallic hydrides [25]. The storage of hydrogen in molecular

and/or atomic form can be achieved, depending on the binding energy between metal adsorbents and hydrogen. Heat is either absorbed (endothermic) or released (exothermic) during metal-hydrogen interaction. This makes metal hydrides prime candidates for heat storage systems [26]. A typical metal-hydrogen reaction is stated as:

$$M + \frac{x}{2} H_2 \longrightarrow MH_x \qquad (1)$$

Several of these compounds, (MH_x), display large deviations from ideal stoichiometry (n = 1, 2, 3) and can exist as multiphase systems. The lattice structure is that of a typical metal with hydrogen atoms in the interstitial sites. They are called interstitial hydrides for that reason (Fig 1).

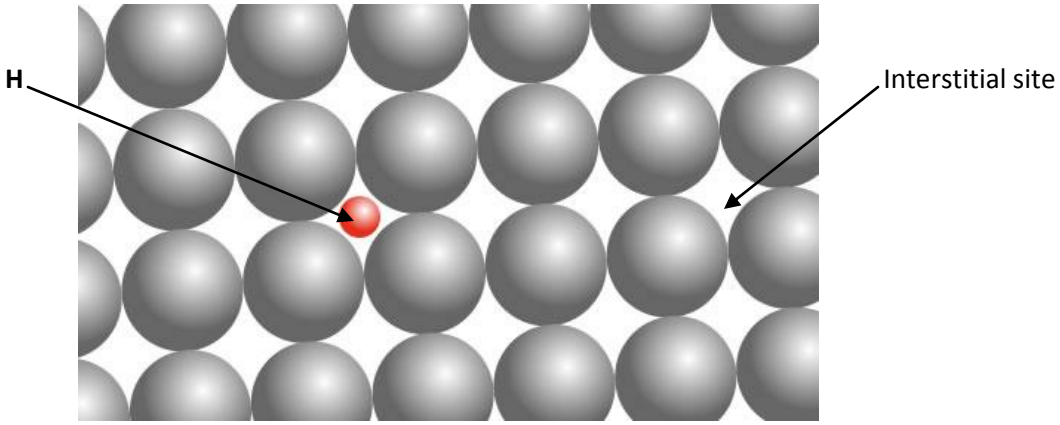

Figure 1.0 Metal lattice with interstitials

This type of structure is limited to the compositions MH, MH_2, and MH_3, with the hydrogen atoms fitting into tetrahedral or octahedral holes in the metal lattice or a combination of the two [25]. Metal hydrides of intermetallic compounds, in the simplest case the ternary system AB_xH_n are particularly interesting because the variation of the

elements allows the properties of these hydrides to be tailored. Element A is usually a rare earth or alkaline earth metal and tends to form a stable hydride while element B is often a transition metal that forms only unstable hydrides. Some well defined ratios of B:A, where x = 0.5, 1, 2, 5, have been found to form hydrides with a hydrogen to metal ratios [25].

A major challenge is to find metal hydrides with sufficiently large hydrogen mass density. This is restricted by the minimum distance between two hydrogen atoms, which is typically ~2Å [24]. Conventional high capacity metal hydrides require high temperatures (~300° C-350 °C) to liberate hydrogen, but sufficient heat is not generally available in fuel cell transportation applications. Currently existing low temperature hydrides, however, suffer from low gravimetric energy densities and require too much space on board or add significant weight to the vehicle [27]. MgH_2 is one of the most studied metal hydride.

1.6 LIGHT WEIGHT COMPLEX HYDRIDES

Enormous efforts have been made to find solid storage materials which can reversibly store hydrogen at moderate temperatures. A suitable solid material for hydrogen storage should have low desorption temperature (60-120 ^{o}C), cheap to produce and have low toxicity. Due to their light weight and number of atoms per metal atom, complex hydrides offered a chance to design a potential hydrogen storage system. A complex hydride is a group of materials which are a combination of hydrogen and group 1, 2, 3 light metals

e.g. Li, Na, B and Al [25 and 28]. Some complex hydrides include alanates [29-37], borohydrides [38-42], amides and imides [43-49], amino borane [50-53], alane [54 and 55] etc.

Several works have been carried out to optimize the hydrogen storage properties of many of the light weight complex hydrides using additives. Alanates are attractive to study because of their easy accessibility. The most popular of the group is $NaAlH_4$ and it is commercially available. $TiCl_3$ was reported to have a good catalytic effect on $NaAlH_4$ [56]. Remarkable improvements have been reported in the kinetics of La_2O_3 doped $NaAlH_4$ compared to the un-doped $NaAlH_4$ [57].

Borohydrides are promising hydrogen storage materials because of their high gravimetric and volumetric hydrogen capacity. High hydrogen desorption temperature and poor reversibility due to formation of stable intermediate or loss of diborane has limited their usage [58-60]. Significant improvement was reported in desorption kinetics of $LiBH_4$ when mixed with MgH_2 and doped with NbF_5 [61]. Improved desorption rates of $Mg(BH_4)_2/Ca(BH_4)_2$ mixtures over individual borohydrides have been reported by Ibikunle *et al* [62]. $Ca(BH_4)_2$ reversibility by doping with $TiCl_3$ has been reported but NbF_5 was reported as the best performing catalyst for the rehydrogenation [63, 64].

Practical use of amides and imides has been limited by their poor absorption kinetics despite their high hydrogen capacity and moderate operating temperatures. Mechanical ball-milling using catalyst doping has been identified as a way to overcome their kinetic barriers. Several works have been reported on many systems in this group such as $LiNH_2$,

Li_2NH, $Mg(NH_2)_2$, $Ca(NH_2)_2$, Li-Mg-N-H, Li-Ca-N-H and Li-Al-N-H [1]. Some of these works are discussed extensively in the subsequent section.

Amino boranes are basically compounds of borane groups having ammonia addition [65]. They are considered as promising candidate for chemical hydrogen storage applications due to their low molecular weight and high hydrogen content of 19.6 wt. %. It was reported that mechanical milling with metal catalysts enhanced hydrogen release in solid state ammonia borane. Also the onset temperature of hydrogen release was reportedly reduced by the addition of nanophase boron nitride [66, 67].

Poor reversibility and slow desorption kinetics are reasons limiting the practical use of alane as an effective hydrogen storage material. It was reported that doping AlH_3 with a small amount of LiH, NaH and KH resulted in speeding up hydrogen desorption rates at low temperatures [68].

1.7 $LiNH_2/MgH_2$ SYSTEMS FOR HYDROGEN STORAGE

Among several systems investigated so far, the Li-Mg-N-H system has shown promising characteristics for onboard vehicular application. It shows significant decrease in enthalpy of reaction and favors reversible hydrogen storage near ambient conditions [1]. Different studies have been carried out on various Mg:Li ratios in the literatures. Luo and Sickafoose reported Mg:Li = 1:2 [69, 70], Xiong reported 3:6 ratios ($3Mg(NH_2)_2+6LiH\leftrightarrow 3Li_2Mg(NH)_2+6H_2$) [71, 72], Luo and Ichikawa reported ratios 3:8 ($3Mg(NH_2)_2+8LiH\leftrightarrow 4Li_2NH+Mg_3N_2+8H_2$) [69 , 73] and Orimo *et al* reported 1:4 ratios

($3Mg(NH_2)_2+12LiH \rightarrow 4Li_3N+Mg_3N_2+12H_2$ [44, 74]. It was found in the above reactions that the reversible capacity increases when decreasing the Mg content. However, studies showed that most of the combined ratios exhibits high desorption temperatures to achieve full hydrogen desorption (up to 500 ^oC). This is due to stability of the transitory imide phases. The ratio 1:2 combination is the most promising material/combination because of its high capacity (~5.6 wt %) and relatively low operating temperature around 200 ^oC [1].

1.7.1 $LiNH_2+MgH_2$ SYSTEM (1:1)

Hydrides of period 2 and 3 elements are promising for hydrogen storage but their high heats of reaction are too high to be utilized for fuel cell vehicles. Alapati *et al* [75] estimated that for dehydrogenation temperatures to fall between 50 and 150 ^oC, it is necessary that ΔH lies between 30 and 60 kJ/mol H_2. Reactions with ΔH values higher than 60 kJ/mol H_2 will not have appreciable hydrogen pressures until the temperature is too high, which is unacceptable. If the ΔH is significantly lower than 30 kJ/mol H_2, the material will show very poor reversibility. Using DFT calculations a number of reactions that have promising properties in terms of both reaction enthalpies and hydrogen storage capacities were identified. The reaction below is predicted to have a hydrogen storage capacity of 8.2 % and ΔH value of 31.9 kJ/mol.

$$LiNH_2+MgH_2 \rightarrow LiMgN+2H_2 \qquad (2)$$

Due to the promising predictions made by Alapati *et al* using DFT calculations, studies have been carried out on Eq. 2 above. Lu *et al* [76] reported that the above reaction releases ~8.1wt % of hydrogen between 160 and 220^oC which is close to the reported

theoretical value of 8.19 wt %. Rehydrogenation of the binary nitride LiMgN was also achieved by doping with 4 wt % of $TiCl_3$ with 2000 psi of hydrogen pressures applied at 160 ^oC. TGA results showed that a total of 8.0 wt % can be stored in the Ti doped LiMgN. Using information obtained from XRD and FTIR techniques, the hydrogenation reaction of LiMgN was proposed as follows:

$$LiMgN+2H_2 \rightarrow 1/2Mg(NH_2)_2+1/2MgH_2+LiH \quad (3)$$

The need to determine isothermal plateau pressures and analyze desorbed gases of the $LiNH_2/MgH_2$ system (ratio 1:1) led to new discoveries by Osborn *et al* [77]. PCI isotherms showed that less than 3.4 wt. % H_2 is released at a plateau pressure near 20 atm at 210 ^oC. Further XRD results obtained showed the absence of LiMgN but the presence of $Li_2Mg_2(NH)_3$ and some starting materials. Analysis of the desorbed gas also shows large quantities of ammonia are released from the system. The overall dehydriding reaction at 210^oC is proposed to be;

$$LiNH_2+MgH_2 \rightarrow 1/3Li_2Mg_2(NH)_3+H_2+1/3MgH_2+1/3LiH \quad (4)$$

Formation of $Li_2Mg_2(NH)_3$ rather than LiMgN was reportedly due to its fast kinetics or more favorable thermodynamic driving force than LiMgN.

Liu *et al* [78] reported their findings after ball milling the system for 36 hrs using planetary ball milling machine and subsequent heating up to 390 ^oC. A total of 6.1 wt. % of hydrogen was released from the mixtures. XRD and FTIR examinations revealed the exchange of the NH_2 group between $LiNH_2$ and MgH_2 first to produce $Mg(NH_2)_2$ and

LiH during ball milling. The products consist of Mg_3N_2, $Li_2MgN_2H_2$ and LiH after heating to 390 ^oC. Poor reversibility was also reported in the system.

Since studies by several research groups on ball-milled $LiNH_2$-MgH_2 (1:1) mixture resulted in different dehydrogenation processes, Liang *et al* [79] were motivated towards understanding the underlying mechanisms of the chemical reaction between $LiNH_2$ and MgH_2 (1:1). By using FTIR and XRD they found that the reaction pathway for dehydrogenation/hydrogenation of $LiNH_2/MgH_2$ (1:1) system is strongly dependent on the duration of the milling due to the presence of two competing reactions in different stages. They reported the initial conversion of the binary mixture $LiNH_2/MgH_2$ to the ternary mixture $0.5Mg(NH_2)_2/LiH/0.5MgH_2$ system in the initial ball-milling stage. During extended ball-milling, newly formed $Mg(NH_2)_2$ reacted readily with MgH_2 to yield MgNH with evolution of hydrogen. However, at high temperatures (~250 ^oC) $Mg(NH_2)_2$ showed preference in reacting with LiH rather than MgH_2.

Anton *et al* [80] investigated the effect of two metal oxide additives (Fe_2O_3 and V_2O_5) on the sorption kinetics of (1:1) $LiNH_2/MgH_2$ mixture. It was found that the addition of both metal oxides significantly reduced the amount of ammonia emission during the initial decomposition. However, the V_2O_5 modified mixture showed faster sorption kinetics than the Fe_2O_3 modified mixtures after four isothermal sorption cycles.

Price *et al* [81] also investigated the effects of some metal halide modifiers ($TiCl_3$, VCl_3, $ScCl_3$ and $NiCl_2$) on the sorption properties of the 1:1 molar ratio of $LiNH_2/MgH_2$. The investigations showed that the modified mixtures contained $LiNH_2$, MgH_2 and LiCl. The

metal halide modifiers also reduced the hydrogen desorption temperatures in the order $TiCl_3 > ScCl_3 > VCl_3 > NiCl_2$. Little improvement was reported in the isothermal sorption kinetics of the modified mixtures over the unmodified mixtures after the first dehydrogenation cycles but drastic improvement was observed in the rehydrogenation cycles.

1.7.2 $2LiNH_2+MgH_2$ SYSTEM (2:1)

Following the reports of Chen *et al* [82, 83, 84] on the discovery of lithium nitride/imide system with a high hydrogen storage capacity of 11.5 wt. % and the system's operating conditions which are not satisfactory for automobile application; there has been motivation for extensive studies on the amide/imide family for hydrogen storage possibilities.

Luo reported the preparation of a new type of hydrogen storage system by partial substitution of Li by Mg in lithium amide ($2LiNH_2/MgH_2$). The new storage material can reversibly store hydrogen at 32 bars and 200 ^oC [69].

When $LiNH_2$ and MgH_2 are ball-milled together in ratio 2:1, the dehydrogenation product is a ternary imide $Li_2Mg(NH)_2$. The dehydrided product can be formed using two methods. The first method involves subjecting a mechanically milled mixture of $2LiNH_2/MgH_2$ to dehydrogenation and evacuation at 300 ^oC [85]. The reaction is shown below;

$$2LiNH_2+MgH_2 \rightarrow 3Li_2Mg(NH)_2+6H_2 \qquad (5)$$

Luo *et al* [70] suggested the second method which involves the formation of mixed imide phase. It is a two step process. In this method, $LiNH_2$ and MgH_2 undergo initial conversion to $Mg(NH_2)_2$ and LiH when heated for 2 hrs at 200 ^oC under 100 bar of hydrogen, these products are reversibly decomposed to form $Li_2Mg(NH)_2$ with evolution of hydrogen. The reaction is shown below;

$$2LiNH_2+MgH_2 \rightarrow Mg(NH_2)_2 +2LiH \leftrightarrow Li_2Mg(NH)_2+H_2 \qquad (6)$$

Luo and Ronnebro [86] studied the desorption isotherm of ($2LiNH_2+MgH_2$) at 200, 220 and 240 ^oC. A Van't Hoff plot generated from this data was used to determine the enthalpy of desorption for this material. The desorption enthalpy was calculated to be 39 kJ/mol-H_2. They also reported that the mixture of ($2LiNH_2+MgH_2$) converts to $Mg(NH_2)_2$ +2LiH after a desorption/re-absorption cycle.

In an attempt to analyze the origin of the kinetic barrier in reaction (7), Xiong *et al* [72] reported that the PCT curve recorded at 220 ^oC contains a distinct plateau region and a sloping region.

$$Mg(NH_2)_2 +2LiH \leftrightarrow Li_2Mg(NH)_2+H_2 \qquad (7)$$

About 2/3 of hydrogen desorption was reported to occur at the distinct plateau region at a pressure of 46 bar while the sloping region accounts for the remaining 1/3 hydrogen desorption. They suggested that the strong affinity of $H^{\delta+}$ (from $Mg(NH_2)_2$) and $H^{\delta-}$ (from LiH) may lead to induction of formation of an intermediate phase between $Mg(NH_2)_2$ and LiH. The reaction scheme below was proposed;

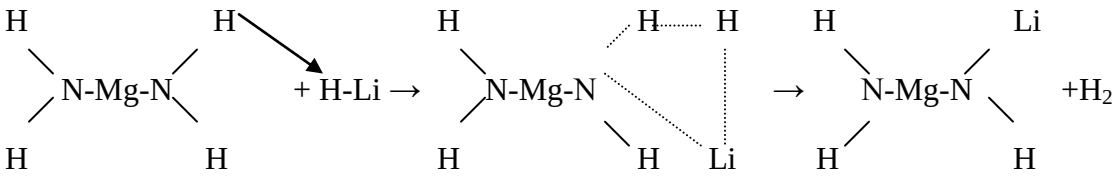

Scheme 1. Reaction mechanism

They suggested the structure NH_2-Mg-NHLi may not be stable. Based on their proposal they suggested that the way to decrease the activation energy can be achieved either by enhancing the attraction of $H^{\delta+}$-$H^{\delta-}$ or by weakening of Li-H and N-H bonds. These can be achieved by a choice catalyst (chemical) with those specific functions of enhancing attraction or weakening of bonds. In addition, they suggested that in order to increase the reaction rates, better contact between amide and hydride is probably crucial.

Chen *et al* [87] reported that a mechanically milled $LiNH_2/MgH_2$ mixture can reversibly store about 4.3 wt. % of hydrogen at 200 ^oC and 90 % of it can be desorbed within one hour. They also observed that the hydrogen storage capacity and dehydriding rate of the material is significantly decreased when the operating temperature was lowered. They suggested that more work is needed in compositional adjustment to enhance the hydrogen storage capacity. Also, exploration of suitable catalysts to kinetically enhance the reversible dehydrogenation/rehydrogenation reactions was also suggested.

In the quest to explore compositional adjustment, Xiong *et al* [88] prepared and investigated three Li-Mg-N-H samples with $LiH/Mg(NH_2)_2$ ratio 1:1, 2:1 and 3:1. They

observed that the reduction of LiH content induced ammonia release. However, higher content of LiH led to increased desorption temperature.

Cheng *et al* [89] carried out the isothermal and non-isothermal kinetic measurements on the chemical reaction between $Mg(NH_2)_2$ and LiH. They also studied thermal decomposition of $Mg(NH_2)_2$. The differences in Arrhenius parameters obtained for both chemical processes revealed that the thermal decomposition of $Mg(NH_2)_2$ is unlikely to be an elementary process in the chemical reaction of $Mg(NH_2)_2$-2LiH. From the observed linear relationship between time and the extent of the reaction of $Mg(NH_2)_2$-2LiH, it showed that the interface reaction in the earlier state of the reaction may be responsible for the kinetic barrier. As the reaction progressed, there was increase in the resistance of mass transport through the product layer and this became the rate-determining step. They also reported that the particle size and the degree of mixing of reacting species will affect the overall kinetics.

Luo *et al* [90] investigated the effect of water-saturated air on the starting mixture of fully dehydrided and fully rehydrided ($2LiNH_2$+MgH_2) material. They reported that the materials showed no degradation of its hydrogen storage properties after exposure to water saturated air at 25 ^oC. A decrease of the times for reaching the same H_2 wt. % after exposure to the water-saturated air for both absorption and desorption was also reported. An accelerating effect is also present for immediately preceding runs and subsequent ones.

In order to optimize the hydrogen storage properties of $Mg(NH_2)_2$-2LiH system, Sudik *et al* [91] investigated the effect of product seeding on the kinetic improvement of the system. The result of 5, 10 and 15 wt. % seeding showed that all are effective for reducing the peak hydrogen desorption temperature relative to the neat material (220 ^oC). An optimal effect was reported with the incorporation of 10 wt. % excess product seed, this corresponds to a 40 ^oC reduction in the peak hydrogen desorption temperature. A reported 11.8 kJ/mol decrease in activation energy was also observed. This corroborates the kinetic enhancement. Analysis of the effluent gas composition showed significant decrease in ammonia release. They also reported a 25 % decrease in kinetic performance after 13 charge/discharge cycles for the seeded sample. They suggested the 25 % decrease is likely due to deterioration of seed quality. Isothermal desorption kinetics at 180 ^oC and 220 ^oC was reported to show a dramatic improvement in kinetic response for the seeded composition.

Ammonia formation is a parallel, competing process with hydrogen release during the desorption process of the Li-Mg-N-H. With the aid of a Draeger Tube Luo *et al* [92] determined the ammonia concentration in the desorbed hydrogen. They reported that ammonia concentration increases with the desorption temperature, from 180 ppm at 180 ^oC to 720 ppm at 240 ^oC.

In order to clarify the effects of the LiH ratio on the properties of the system, Aoki *et al* [93] investigated the dehydriding and rehydriding properties of $3Mg(NH_2)_2$+nLiH (n = 6, 8 and 12) using p-c isotherm and XRD measurements. They found out that the amount of hydrogen desorbed on a unit mass basis decreased with increased n. The features of the p-

c isotherm were reported to be similar to each other. $Li_2Mg(NH)_2$ was observed in XRD profiles of all the mixtures after the p-c isotherm measurements. They suggested that the dehydriding reactions of the mixture of $3Mg(NH_2)_2$+nLiH (*n* = 6, 8 and 12) under hydrogen pressure is not dominantly affected by the value of *n*. They also reported that the amounts of ammonia desorbed from the mixtures detected by mass spectroscopy decreased with increased *n*.

Janot *et al* [94] investigated the hydrogen storage performances of the Li-Mg-N-H system either from (1:2) $Mg(NH_2)_2$-LiH or (1:2) MgH_2-$LiNH_2$ mixtures. They reported ammonia release for (1:2) MgH_2-$LiNH_2$ mixtures if the first heating is conducted under a dynamic vacuum. They suggested that this could lead to fast degradation of the material. They reported that the desorption kinetics of the ball-milled (1:2) $Mg(NH_2)_2$-LiH mixture are fast: a total of 5.0 wt.% is reportedly desorbed in 25 minutes at 220 ^oC. They also suggested that the formation of two pressure plateaus reveals the existence of an intermediary phase between $Li_2Mg(NH)_2$ and the rehydrided material, which is the (1:2) $Mg(NH_2)_2$-LiH mixture.

Rijssenbeek *et al* [95] used a combination of synchrotron X-ray diffraction and neutron diffraction to determine the hydrogen storage reactions of mixtures of lithium amide and magnesium hydride. The dehydrogenation product of the material was reported to be α-$Li_2Mg(NH)_2$. Two structural phase transitions were reportedly observed as the imide was heated further to over 500 ^oC at 12 ^oC/min. The first transition was reported to start at 350 ^oC, when the orthorhombic α-phase was gradually replaced by a primitive cubic phase (β-$Li_2Mg(NH)_2$). A second transition started at about 500 ^oC, at which point the primitive

cubic phase quickly became face-centered cubic (γ- $Li_2Mg(NH)_2$). However, when cooled the γ- $Li_2Mg(NH)_2$ was converted back to β- $Li_2Mg(NH)_2$. The regeneration of the α- $Li_2Mg(NH)_2$ could only be achieved by cycling under hydrogen pressure. Similar reactions were reportedly observed when the starting mixture was $Mg(NH_2)_2$-2LiH.

Liu *et al* [96] reported that the equilibrium concentrations of ammonia in the volatile products of the reaction between $Mg(NH_2)_2$ and 2LiH are strongly dependent on the reaction temperature. The equilibrium concentrations of ammonia calculated at 90 and 25 ^oC are ca. 30 and 17 ppm respectively.

Markmaitree *et al* [97] compared the dehydrogenation kinetics of ($2LiNH_2$+MgH_2) and ($LiNH_2$+LiH) systems and their vulnerabilities to the ammonia emission problems. They also investigated the two systems to understand their different degrees of mechanical activation. Their results showed that the dehydrogenation of ($2LiNH_2$+MgH_2) mixture had lower onset temperature and higher hydrogen pressure than ($LiNH_2$+LiH). Their report showed that the rate of the ($2LiNH_2$+MgH_2) mixture to generate hydrogen at 210 ^oC was higher than that of the ($LiNH_2$+LiH) mixture. The reaction rate between MgH_2 and NH_3 was reported to be lower than that between LiH and NH_3. This creates ammonia emission problem for the ($2LiNH_2$+MgH_2) mixture. High-energy ball milling was reported to increase the reaction rates and alleviates the ammonia emission problem. Based on the XRD and FTIR results and the desorbed gas analysis a reaction pathway was proposed for reaction (8) below:

$$2LiNH_2+MgH_2 \rightarrow Li_2Mg(NH)_2+H_2 \qquad (8)$$

Firstly, the $2LiNH_2$ decomposes as shown below;

$$2LiNH_2 \rightarrow Li_2NH + NH_3 \quad (9)$$

The NH_3 formed then reacts with MgH_2 in (8)

$$NH_3 + 1/2MgH_2 \rightarrow 1/2Mg(NH_2)_2 + H_2 \quad (10)$$

The $1/2Mg(NH_2)_2$ decomposes

$$1/2Mg(NH_2)_2 \rightarrow 1/2MgNH + 1/2NH_3 \quad (11)$$

The $1/2NH_3$ formed from (11) reacts again with un-reacted MgH_2 according to reaction (10). The $Mg(NH_2)_2$ formed decomposes again according to reaction (11) to form MgNH and NH_3. This reaction cycle continues according to reactions (10) and (11) until all MgH_2 has reacted with NH_3. The products from this reaction cycle are H_2 and MgNH. The MgNH formed reacts with the Li_2NH from reaction (9) in the reaction below;

$$MgNH + Li_2NH \rightarrow Li_2Mg(NH)_2 \quad (12)$$

Since the FTIR spectra do not show the $Mg(NH_2)_2$ phase at any stage of the reaction, they suggested that reaction (10) must have proceeded relatively slowly in comparison with reaction (11) so that $Mg(NH_2)_2$ is not accumulated to a level detectable by FTIR.

Shahi *et al* [98] investigated the ball milling (5-45 hrs) followed by dehydrogenation kinetics of the $LiNH_2$-MgH_2 mixture. Their findings revealed the formation of $Mg(NH_2)_2$ for mixtures ball milled for more than 15 hours. There was also appreciable increase in the desorption kinetics as milling duration increased from 5 to 45 hours. The enhancement was attributed to the formation of $Mg(NH_2)_2$ during this process.

Size-dependent kinetic enhancement in hydrogen absorption and desorption of the Li-Mg-N-H system was investigated by Liu *et al* [99]. Their XRD and IR results showed

that a polymorphic transformation was induced from the orthorhombic α-$Li_2Mg(NH)_2$ phase to the cubic β- $Li_2Mg(NH)_2$ phase during 36 h ball milling. They found that the particle size of the sample was reduced from >800 nm to 100-200 nm after 36 h ball-milling as observed with scanning electron microscopy. The onset of hydrogen desorption for the ball-milled sample was dramatically lowered to 80 ^oC and the dehydrogenation kinetics was reported to be significantly improved after hydrogenation at a much lower temperature. Diffusion of small ions in the sample is reported to be the rate controlling step of the hydrogen desorption reaction.

Hu and Fichtner [100] investigated the formation and stability of ternary imides in the Li-Mg-N-H hydrogen storage system. By varying the molar ratio of $Mg(NH_2)_2$ to LiH in the proximity of 1:2 (1:1.5, 1:1.8, 1:2.0, 1:2.2, 1:2.5 and 1:2.7), they reported that a maximal amount of hydrogen and low level of ammonia generation were observed for the mixture with molar ratio 1:2. They also confirmed that $Li_2Mg(NH)_2$ is a thermodynamically favored dehydrogenation product in the hydrogen storage system.

Markmaitree and Shaw [101] reported the phase pure synthesis of $Li_2Mg(NH)_2$ by dehydriding treatment of ball-milled $2LiNH_2+MgH_2$ mixture. They reported that the isothermal hydriding process of $Li_2Mg(NH)_2$ is very sluggish and holding at 200 ^oC for 10 hrs only resulted in 3.75 wt. % hydrogen uptake. They reported that detailed kinetic analysis revealed that the rate-limiting step for the hydriding process of $Li_2Mg(NH)_2$ is diffusion. In order to enhance the hydriding kinetics of $Li_2Mg(NH)_2$, they suggested nano-engineering to minimize the diffusion distance and high-energy ball milling to introduce

lattice defects and thus increase the diffusion co-efficient. They also suggested doping to increase the lattice distortion and thus the diffusion rate.

Catalytic enhancement of the $2LiNH_2+MgH_2$ system has been widely studied in order to improve the hydrogen storage properties of the system. Cheng *et al* [102] reported the effect of various carbon additives on a rehydrogenated sample of Li-Mg-N-H. The carbon additives studied included as-prepared single-walled carbon nanotubes (A-SWNTs), purified single-walled carbon nanotubes (P-SWNTs), purified multi-walled carbon nanotubes (P-MWNTs), graphite (G-carbon) and activated carbon (A-carbon). Their report showed that an optimum hydrogen storage capacity was achieved in the 2.15:1 $LiNH_2/MgH_2$ mixture. They also reported that the addition of a small amount (5 wt. %) of SWNTs improved the dehydriding kinetics of $Mg(NH_2)_2$/LiH materials. The dehydriding kinetics was reported to be 3 times faster for the SWNTs containing samples when compared with the un-catalyzed sample at 200 ^oC.

In order to alter the thermodynamics and kinetics of the $Mg(NH_2)_2$ +2LiH system, Liu *et al* [103] altered the chemical composition of the Li-Mg-N-H system by partially substituting NaH for LiH or substituting $NaNH_2$ for $Mg(NH_2)_2$. They reported that the desorption peaks of the samples containing Na compounds occurred at a temperature ~14 ^oC lower than that of the un-catalyzed Li-Mg-N-H sample. The activation energies of the substituted samples were reduced by approximately 8 and 13 kJ/mol when compared to that of the un-catalyzed sample. Lohstroh and Fichtner [104] reported that the addition of 2 mol % $TiCl_3$ to the $2LiNH_2$-MgH_2 system shifted the endothermic hydrogen release to lower temperatures but it does not have a catalytic effect on the reversible reaction.

Barison *et al* [105] tested the effectiveness of the presence of additives (Nb_2O_5, $TiCl_3$ and graphite) and of a prolonged milling time in improving the kinetics of the hydrogen absorption/desorption processes. Their results showed that a milling time of 24 hrs or longer using high energy mill gave a better kinetics than the milled for lesser times sample. The kinetics improvement was suggested to be due to reduced average crystallite size, which led to an increased surface to bulk ratio which enhanced the solid-solid reactivity and shortened the hydrogen diffusion paths.

Motivated by the mechanistic understanding of the essential amide/imide Ma *et al* [106] experimentally examined the catalytically reversible dehydrogenation of the $Mg(NH_2)_2$ +2LiH system using Ru/C catalyst (a metal catalyst). Compared to the neat sample, they reported that the Ru/C doped samples exhibited enhancement of the dehydrogenation /rehydrogenation kinetics particularly at lowered temperatures. They reported that the catalytic enhancement was achieved without penalty of the capacity of the material. It was reported that the isothermal dehydrogenation behaviors suggested that the enhanced dehydrogenation kinetics may result from the Ru-catalyzed interface reaction between amide and imide solid phases.

Ma *et al* [107] investigated the effect of Li_3N additive with respect to reversible dehydrogenation performance of the Li-Mg-N-H system. Their results showed that varying Li_3N additions (5, 10, 20 and 30 mol %) proved effective for improving the hydrogen desorption capacity. Optimum results were achieved with 10 mol % Li_3N with a capacity increase from 3.9 wt. % to approximately 4.7 wt. % hydrogen at 200 ^oC. The enhanced capacity was reported to be stable over 10 dehydrogenation/rehydrogenation

cycles. The Li_3N additive was reportedly transformed into $LiNH_2$ and LiH phases which remained in the dehydrogenation/rehydrogenation cycle. Using combined structure/property investigations they suggested that the in situ-formed $LiNH_2$ should be responsible for the capacity enhancement. It was presumed that the incorporated $LiNH_2$ acted as stable nucleation sites for promoting the growth of intermediate $LiNH_2$. They also reported that the concurrent incorporation of LiH is effective in reducing ammonia release.

In order to catalytically improve the hydrogen storage properties of Li-Mg-N-H system, Wang *et al* [108] investigated the effect of potassium (a non-transition metal dopant) on the hydrogen storage properties of $Mg(NH_2)_2$ /2LiH. Their results showed that complete hydrogen desorption can be achieved at circa 107 ^oC which is much lower when compared with the un-catalyzed sample (i.e > 180 ^oC). They reported that potassium diffused into the imide and /or amide phases and combined with nitrogen thereby weakening the amide N-H bonds and imide Li-N bonds which considerably enhanced the dehydrogenation. They suggested any potential catalyst has to be dissolved in the reaction region in order to be approachable by the reacting species. Their temperature programmed desorption (TPD) results showed that the desorption peak of the potassium modified sample shifted downwards by 50 ^oC. Also the release of ammonia was reported to be hardly detectable in the temperature range of 75-200 ^oC. The enthalpy change of hydrogen release was reported to be 42 kJ/mol H_2. They reported that similar performance can be achieved by introducing other potassium salts such as KF, KNH_2,

KOH, K_2CO_3 and K_3PO_4 to the $Mg(NH_2)_2$ +2LiH system however KH and K-N containing compounds are always the effective species.

Wang *et al* [109] investigated the nature of the Ti species in the Li-Mg-N-H system for hydrogen storage. They reported a slight improvement in the hydrogen desorption kinetics of the TiN and TiF_3 doped samples. The activation energies reported for dehydrogenation with or without TiF_3 additive are 81.45 kJ/mol and 92.2 kJ/mol respectively. The TiF_3 additive showed very little catalytic effect on Li-Mg-N-H system. The Ti in $Li_2MgN_2H_2$ was reportedly calculated and determined as $Li_7TiMg_4(N_2H_2)_4$ by a first principles approach.

Shahi *et al* [110] studied the effect of vanadium and vanadium based (V, V_2O_5 and VCl_3) catalysts on the dehydrogenation characteristics of $Mg(NH_2)_2$ /2LiH. Their results showed that all the additives are capable of lowering the initial decomposition temperature, however the VCl_3 proved the most effective by lowering the initial decomposition from ~80 ^oC to ~60 ^oC. The addition of 2 mol % of VCl_3 to the mixture also increased desorption kinetics by ~38 %. They also reported that the absorption kinetics of the un-catalyzed material also increased with the addition of 2 mol % vanadium based additives at 10 MPa of H_2 pressure and 220 ^oC. The hydrogen uptake capacity of the un-catalyzed material, V, VCl_3 and V_2O_5 doped samples were found to be ~2.8, ~3.8, ~4.2, and ~3.25 wt. % within 10 hrs respectively. The optimal desorption conditions for the VCl_3 doped sample were reported as 5.2 wt. % at 220 ^oC within 150 min. Good reversibility at 180 ^oC with a hydrogen storage capacity of ~4.9 wt. % after 10 cycles was reported also for the VCl_3 doped mixture.

Ball-milling is a good way to achieve smaller/finer particles and uniform mixing of reactants. Aggregations of fine particles are reportedly common during dehydriding and rehydriding of mixtures. Aggregation leads to reduction of surface area as well as the extension of the mass transport path followed by a reduction in hydrogen sorption performance. In an attempt to maintain the physical state of reactants in the cycling of the Li-Mg-N-H system, Wang *et al* [111] investigated the effects of triphenyl phosphate (TPP) on the hydrogen storage performance of the $Mg(NH_2)_2$-2LiH system. The TPD report showed that for the un-catalyzed $Mg(NH_2)_2$ -2LiH sample, the peak desorption temperature was increased by ~20 ^oC after one cycle while the TPP doped sample experienced a reduction of ~10 ^oC lower than that of the un-catalyzed sample in the first desorption. A further 4 ^oC downward shift was also reported after 4 cycles. They reported that TPP reacted with LiH and $Mg(NH_2)_2$ exothermically to form more stable compound(s) during ball-milling. The compound(s) formed do not change during hydrogen absorption/desorption by the Li-Mg-N-H system. TPP was reported to effectively prevent the aggregation of ternary imide $Li_2MgN_2H_2$ in the dehydrogenation and the crystallization of $Mg(NH_2)_2$ in hydrogenation; this favors cyclic durability. They reported that the addition of TPP significantly affected both the thermodynamics and kinetics. It was reported that the persistence of amorphous $Mg(NH_2)_2$ in cycling by doping with TPP was the reason for the thermodynamic changes compared to the un-catalyzed sample while the reduction of the crystallite size of the reactants by ~7 nm was responsible for the faster kinetics at lower temperatures.

Nayebossadri [112] studied the effects of elemental Si and Al on the dehydrogenation kinetics of Li-Mg-N-H. He reported that the addition of elemental Si had no appreciable effect on the hydrogen desorption profile of the sample. The addition of Al was reported to shift desorption temperature peak to a higher temperature by ~100 ^{o}C. He reported that examination of the phases after dehydrogenation showed that elemental Si was not incorporated into the dehydrogenated phases but remained intact. The dehydrogenated phases contained a cubic $Li_2MgN_2H_2$. No ammonia was reported in the evolved gas analyses.

In an effort to lower the operating temperatures and enhance the dehydrogenation /hydrogenation rate of the $Mg(NH_2)_2$ -2LiH system by catalyst addition, Liang *et al* investigated the effect of NaOH additive on the enhancement of dehydrogenation/hydrogenation kinetics. They reported that the onset temperatures for hydrogen desorption were lowered by ~30 ^{o}C when compared to the un-catalyzed sample while a 36 ^{o}C reduction was observed for the peak hydrogen desorption temperature. Ammonia generation was reportedly reduced and was almost undetectable for the sample with 0.5 mol NaOH. It was also reported that hydrogen desorption was dramatically sped up with the addition of NaOH. The $Mg(NH_2)_2$-2LiH-0.5 NaOH sample released ~48 % of hydrogen capacity within 750 min while < 15 % of hydrogen capacity was released by the un-catalyzed sample in the same period of time. They reported that approximately 65 % of the hydrogen storage capacity could be recharged into the dehydrogenated NaOH doped sample within 300 min at 100 ^{o}C while only 31 % of hydrogen capacity could be recharged into the un-catalyzed sample. A reversible 2.5 wt. % could be achieved at 150

^{o}C and 105 atm. This is lower than the un-catalyzed sample with 4.9 wt. % reversibility [113].

Luo *et al* [114] reported a comparative study for hydrogen storage characteristics of un-doped and KH-doped $2LiNH_2+MgH_2$. Their results showed that the solid state conversion ($2LiNH_2+MgH_2 \rightarrow Mg(NH_2)_2+2LiH$) is an exothermic process and this explained why the rehydrogenation of the spent material ($Li_2MgN_2H_2$) terminates at ($Mg(NH_2)_2+2LiH$) without forming ($2LiNH_2+MgH_2$) during subsequent absorption cycles. They reported the effectiveness of the KH catalysis which dramatically improved the hydrogen absorption rate. Absorption was almost completed for the KH-doped samples within about 0.1 hr at 200 ^{o}C, while the un-doped sample was only 70 % completed after 0.5 h. The absorption rate was reported to be dramatically improved at 115 atm and 180 ^{o}C. A "self heating" effect was also reported to benefit the absorption rate.

Durojaiye and Goudy [115] studied the kinetics of the lithium amide/magnesium hydride system at constant pressure thermodynamic driving forces using N-value of 10 and at 210 ^{o}C. The N-value is the ratio of the mid-plateau pressure, P_m to the opposing pressure P_{opp}. Their result showed that the KH is more effective on $2LiNH_2$-MgH_2 system than the $LiNH_2$-MgH_2 system. The desorption temperature was significantly lowered for the 2:1 mixture compared to the 1:1 mixture when doped with KH. The desorption rates of KH-doped $2LiNH_2+MgH_2$ mixture was reported to be ~25 times faster than the un-doped $2LiNH_2+MgH_2$ mixture.

Using density functional theory Velikokhatnyi and Kumta [116] determined the theoretical enthalpy: $Mg(NH_2)_2 + 2LiH \leftrightarrow Li_2Mg(NH)_2 + H_2$. The theoretical value obtained is 53.4 kJ/mol H_2. However, they reported the experimental value to be 44.1 kJ/mol, which is ~20 % different from the theoretical value. They suggested the observed variation might lie in the inherent difficulty to treat the random distribution of Li and Mg atoms with fractional occupation numbers using the Vienna Ab initio Simulation Package (VASP).

In this study we investigate and compare the effects of KH, RbH and CsH on the $LiNH_2/MgH_2$ systems. The capability of magnesium amides to form a wide range of mixed amido complexes with alkali metal ions $M_2[Mg(NH_2)_4]^{2-}$ (M= K, Rb and Cs) is one of the reason for considering KH, RbH and CsH additives for this study [120, 121 and 122].

1.8 GOALS OF THE RESEARCH

The goals for this research are highlighted below:

- To perform comparative thermodynamics, dehydriding kinetics and modeling studies on KH doped and un-doped ($2LiNH_2/MgH_2$) and ($LiNH_2/MgH_2$) systems. Kinetics will be compared using constant pressure thermodynamic driving forces.

- To investigate the effect of RbH on the thermodynamics and dehydriding kinetics of ($2LiNH_2/MgH_2$) system. The KH doped and un-doped samples will also be compared.

- To perform comparative thermodynamics, dehydriding kinetics and modeling studies on KH, RbH, CsH doped and un-doped ($2LiNH_2/MgH_2$). Kinetics will be compared using constant pressure thermodynamic driving forces.

CHAPTER TWO

2.0 EXPERIMENTAL SECTION

2.1 SAMPLE PREPARATIONS

All materials used for this research were obtained from the Sigma Aldrich Corporation. The $LiNH_2$ was 95 % pure and the MgH_2 was of hydrogen storage grade, 98 % pure. The rubidium metal was 99.6 % pure and the cesium metal was 99.95 % pure. RbH and CsH were self-produced from their metals in the laboratory. KH was 30 wt. % dispersed in mineral oil (mineral oil was removed by washing severally with n-Heptane before use). KBr was FTIR grade and 99 % pure. All sample handling, weighing and loading were performed in a Vacuum Atmospheres argon-filled glove box that was capable of achieving less than 1 ppm oxygen and moisture. The glove box was vacuum-cleaned several times using purified argon gas to remove air and moisture that can contaminate the reagents and samples.

2.2 SYNTHESIS OF RbH and CsH CATALYSTS

RbH and CsH catalysts were synthesized by modifying the reactive ball milling method described by Elansari *et al* [117]. Approximately 4-5 g of the alkali metal was added into a 45 ml vial followed by 10 Tungsten Carbide (WC) balls ~10 mm in diameter each in a purified argon filled glove box. The vial was covered with a special lid that allowed the vial to be pressurized and depressurized. Vacuum was pulled on the vial to remove the

argon and hydrogen pressure of about 90 psi was introduced into the vial. The vial was placed in a planetary mill (Fritsch pulverisette 7). A rotation rate of 100 rpm was kept for 15 min. The rotation rate was progressively increased by 25 rpm; the 15 min milling time was kept constant until 250 rpm is reached. This was repeated thrice starting from 100 rpm. At 250 rpm a 12 hr milling period was observed which included 36 cycles of 20 min milling and 10 min pause times. It should be noted that before the start of each milling cycle the vial was re-pressurized at 90 psi. The lid of the vial was changed when 175 rpm was reached because of the spread of alkaline metal onto the inside of the lid which might prevent effective pressurization of the vial. After 12 hrs milling was completed the vial was re-pressurized and placed in an oven at 120 ^{o}C for 1 hr. A white powdered was formed at the end of the incubation when observed in the argon filled glove box. Results of the XRD are discussed in the result section in chapter four.

2.3 BALL MILLING OF SAMPLES

In this study the un-doped and doped samples were mixtures of $LiNH_2$ and MgH_2 in a molar ratio 2:1.1. An excess of 10 % MgH_2 was added to prevent the escape of NH_3 from the system during synthesis. For the doped sample, 3.3 mol % of the additives KH, RbH and CsH were added and prepared separately. The weighing balance was zeroed before each measurement and a weight correction was done for the weighing paper. The samples were handled in an argon filled Vacuum Atmosphere Company glove box, NEXUS DRI-TRAIN model equipped with a trace oxygen analyzer. Prior to use, the stainless steel sample holder and the balls were washed and oven dried for thirty minutes. They were

later removed and cooled to room temperature in open air. They were then transferred to the ante chamber of the glove box. The ante chamber was vacuum cleaned about six times to remove air and moisture trapped in it during the transfer of the milling vials and balls into it. The ante chamber was opened from the inside of the glove box and the sample holder was placed inside the glove box. A 5g mixture of the sample was placed in a clean stainless steel sample vial containing stainless steel balls in an argon filled glove box. The sealed stainless steel sample vial was taken out of the glove box and clamped in the jaws of the 8000M Mixer/Mill. The crank was tightened firmly and the small locking tab on the treaded rod was also tightened to prevent the jaws from loosening while milling is in progress. The machine was turned on and 2 hrs of milling was programmed for all the samples. The sample holder was returned to the glove box via the cleaning process described earlier when milling was completed and the mixed samples were transferred into clean transparent glass sample bottles for further analysis.

Figure 2.1 The Vacuum Atmosphere Glove Box

Figure 2.2 The 8000M and 8000D Mixer/Mills

2.4 X-RAY DIFFRACTION (XRD) MEASUREMENT

X-ray diffraction measurements of both the starting materials and the products formed were carried out using a PANalytical X'pert Pro X-ray Diffractometer Model PW3040 Pro. The instrument was equipped with an accelerator detector that allowed for rapid analyses. A dry x-ray analysis sample holder was cleaned and placed in the side chamber of the glove box. The chamber was cleaned several times as described earlier to remove air and moisture before transferring the sample holder into the glove box. Each sample was transferred into the sample holder, leveled with a razor to ensure an even surface and covered with a transparent polyimide film (Kapton) for protection from air and moisture outside of the glove box during analyses. Kapton has very high transmittance to X-rays

such that no adjustment is required. The lid was then fastened to hold the thin film tightly onto the x-ray sample holder. The prepared sample for x-ray analysis was removed from the glove box and transferred to the PANalytical X'pert Pro X-ray Diffractometer.

Figure 2.3 PANalytical X-ray Diffractometer

The instrument's light was turned on and the sample holder was mounted on the stage. It was ensured that the doors of the instrument were tightly shut. The x-ray diffraction analysis program was started on the desktop by clicking X'pert data collector. This connects the instrument to the computer. The analysis took approximately 20 minutes and a diffraction pattern was produced. The operation conditions for the XRD data collection were Cu K-Alpha radiation, 40kV, 20 mA and 0.02 ^{o}/step. The diffraction pattern was recorded in the 2θ range and scan range was between 5 and 120 degrees. The analysis

was performed by using the X'pert data viewer software on the desktop to confirm the formation of a new phase.

2.5 THERMAL GRAVIMETRIC AND DIFFERENTIAL THERMAL MEASUREMENTS.

A combination of Thermal Gravimetric and Differential Thermal Analysis using the Perkin Elmer Simultaneous TGA / DSC model Pyris Diamond High Temperature 115 housed in Argon filled glove box was carried out on the samples. The TGA measures the weight lost by the sample.

Figure 2.4 The Lab System-Diamond TG/DTA (TGA)

The TGA machine was turned on and allowed to stand for some minutes until option "linkwait" was displayed on the instrument's LCD monitor. The TGA was operated by a

Pyris program. The Pyris program was started on the computer and the sample and program information were inputted. Located on the left side of the instrument is the open/close button. The open button was used to open the sample stage. Two identical ceramic pans reference (left) and sample (right), were located on the two beams covered by the stage. The weights of the two ceramic pans were zeroed. This was repeated several times to ensure equilibration of the weight of the ceramic pans. The sample ceramic pan was removed with forceps and loaded with approximately 5-10 mg of the sample to be analyzed before carefully placing it on the beam. The stage was closed and the weight of the sample was measured by clicking on the displayed weight icon on the monitor. This was repeated several times to ensure equilibration. The program was started by clicking the start button on the program. The heating rate for the samples was 4 ^{o}C per minute starting from 30 to 350 ^{o}C. Different heating rates were also conducted in order to calculate the activation energies by the Kissinger method.

2.6 TEMPERATURE PROGRAMMED DESORPTION (TPD) AND PRESSURE COMPOSITION ISOTHERM MEASUREMENTS.

The ball milled mixture was subsequently subjected to a dehydriding treatment followed by series of hydriding and dehydriding isotherm measurements at various temperatures using a commercial Sieverts'-type pressure-composition isotherm (PCI) unit (Advanced Materials Corporation, PA) . The unit was fully automated and controlled by a Lab View-based software program. The TPD and PCI analyses were done on freshly milled samples. Prior to analysis, the sample chamber was cleaned and transferred to the glove

box approximately 0.5 g of sample was loaded into the sample holder. The chamber was attached to the instrument via a quick connect fitting. Labview software was used to control the system as well as to collect and analyze the data. The TPD analyses were done in the 30-250 ^{o} /300 ^{o}C range at a heating rate of 4 ^{o}C/min. The PCI absorption and desorption measurements were carried out at temperatures ranging from 190-230 ^{o}C. Data obtained were used to calculate the enthalpy of each system from van't Hoff plot. No activation procedure was carried out prior to sample measurements.

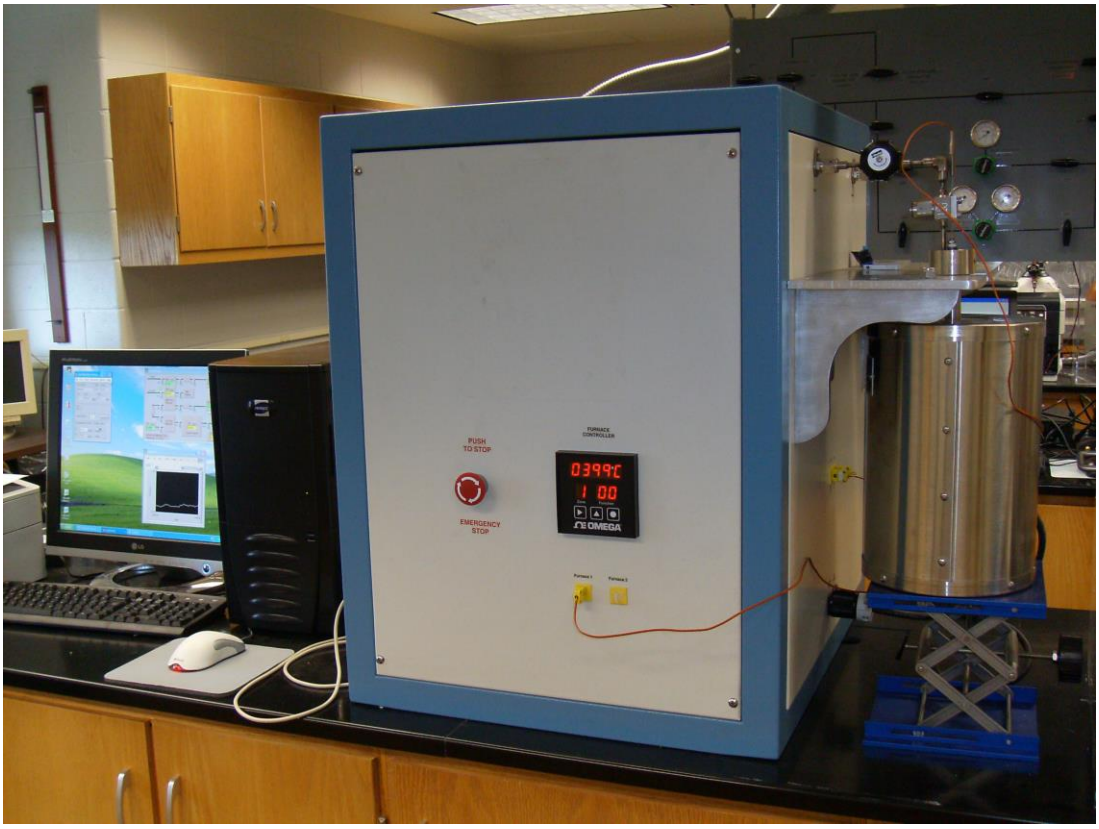

Figure 2.5 Pressure Composition Isotherm Automated Hydriding Apparatus

2.7 RESIDUAL GAS MEASUREMENT

Stanford Research Systems Residual Gas Analyzer (SRS RGA) model RGA Pro-2500 fitted with a quadrupole mass filter, faraday cup detector and a thoria-iridium filament was used to quickly identify the gas species present in the desorbed gases and monitor the level of NH_3 and H_2 in the desorbed gases of heated samples. The RGA was pre calibrated before use. The RGA was coupled to the Advanced Materials Corporation PCI unit. The sample holder was filled with about 0.5 g of the sample to be analyzed in argon-filled glove box. The sample holder was plugged with glass wool and covered. The sample was placed in its compartment and removed from the glove box. The sample holder compartment was clamped on to the PCI unit and connected to the RGA via a 1/8" sampling line. With the sample holder valve closed, a leak test was carried out and the sample and system was purged. The air pressure which controlled valve opening was set at 40 psi. The RGA was turned on. The roughing pump was turned on followed by the RGA switch. The turbo pump was turned on and monitored until the pressure in the chamber/frequency was around 10^{-4} mbar/1500 Hz. The RGA must not be operated if the pressure in the chamber is greater than 10^{-4} Torr. The manifold was cleared of residual gases before use. This was done by closing valve 1. Valve 2 and 3 were opened until the desired pressure in the manifold had been reached. Note: Valve 3 will not open unless valve 2 has already been opened for 5 seconds. The manifold clearing must always be done prior to use or after the user has finished investigating the current gas sample. The RGA software was started by double clicking on the RGA 3.0 icon on the desktop. The RGA head was connected by clicking on the tool bar's RS232 set up button. A dialogue box showing "buffer is full" was displayed and OK was clicked. The RGA list was

upgraded on a new dialogue box displayed and the port (COM1) to which the RGA head is connected was selected on the connector column and the connect button clicked. The connection is made when “connected” is displayed in the status column and the tool bar’s GO button turns green. The connector list was closed when the connection was completed. The filament was turned on by clicking on the tool bar’s filament button. A green status LED on the back panel of the ECU box indicates the emission status of the filament at all times and it provides the fastest way to verify if the filament is emitting electrons. On the tool bar the mode was clicked and the pressure versus time (P v T) mode was selected. The background measurement was done at room temperature by opening the by-pass valve followed by valve 1 then valve 2 because the measurement will be done at low pressure and the desorbed will be allowed to flow directly to the RGA. The toolbar’s GO button was clicked and after a small delay, the P v T scan data starts to be displayed on the screen. The graph was rescaled by selecting Auto scale from the graph menu. From the background set up on the software “background –scan data” was selected before sample measurements. A sample measurement was carried out the same way as the background measurement with the temperature ramped to about 400 ^{o}C. After a few seconds, the display of the selected species appeared on the screen with different pressure readings as the temperature rose.

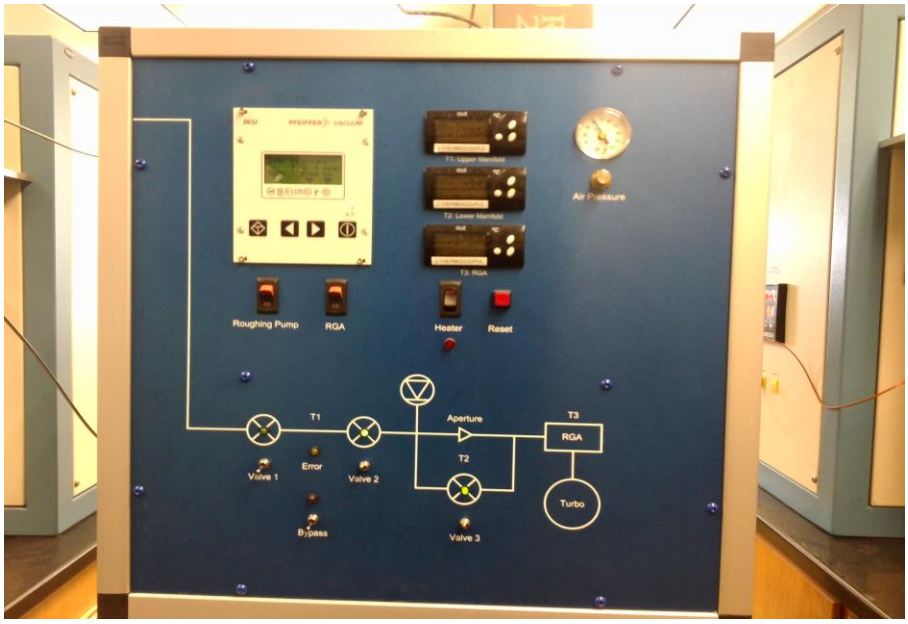

Figure 2.6 The Residual Gas Analyzer coupled to the Advanced Materials PCI unit

2.8 FOURIER TRANSFORM INFRARED (FTIR) MEASUREMENT

The N-H vibrations of the samples were determined by an IR Prestige-21 Fourier Transform Infrared Spectrophotometer model 8400S from the Shimadzu Corporation. A fraction of the sample was mixed with KBr (ratio 1:10), the mixture was ground into fine powder using an agate mortar and pestle in an argon filled glove box. The ground mixture was transferred to a pellet press holder and pressed at 13 ksi for ~ 1-2 min to form a pellet of ~12 mm in diameter and 0.5 mm in thickness. There was brief exposure of sample pellets to air during hydraulic pressing and transfer to sample compartment of the spectrometer.

Figure 2.7 IR Prestige-21 Fourier Transform Infrared Spectrophotometer.

The FTIR spectrophotometer was powered on and the IR solution icon on the monitor was double clicked to open the template. The instrument was initialized via the IR solution software. Sample information and other data such as measurement mode, number of scans and range were inputted. The background was measured first by clicking on the BKG (background) icon on the screen of the computer. The prepared pellet was carefully placed in the sample compartment and the sample measurement taken with the compartment closed. After 16 scans were accumulated, a final infra red spectrum was produced. The sample measurements were taken under room conditions. Background measurement of air was obtained prior to each measurement. The background measurement was automatically subtracted from the sample measurement by the spectrometer.

2.9 KINETICS MEASUREMENT

Kinetics measurements were carried out using a Sieverts type apparatus. The experiments were carried out using a method that allowed samples to be compared at the same constant pressure driving force. The Sieverts type apparatus was made of stainless steel and equipped with both inlet and outlet ports for adding and venting hydrogen. Installed pressure regulators control the hydrogen pressure applied to the sample and allow hydrogen to flow in and out of the sample into a remote reservoir. With the back pressure regulator, constant pressure is maintained in the sample chamber during desorption analyses. Daqview software was used in data collection. A leak test was conducted before each experimental procedure to ensure that all the valves were tightly connected and by so doing prevent pressure leakage. After passing the leak test, desorption kinetics for each sample was conducted.

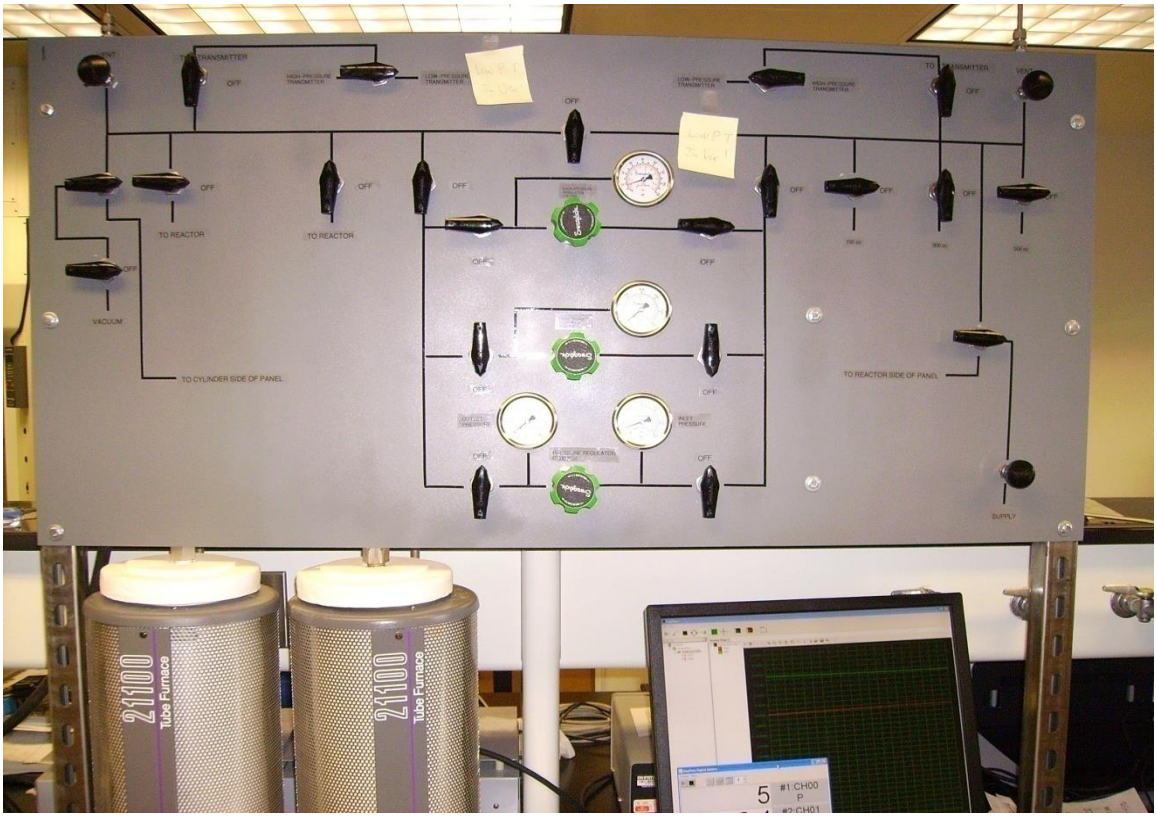

Figure 2.8 Sieverts Apparatus

Approximately 2 g of each sample mixture was measured and placed inside the sample holder in the glove box to prevent sample contamination by moisture. The sample holder was removed from the glove box, placed inside a tube furnace 21100 controlled by Barnstead thermolyne model F21135 and connected to the kinetics apparatus via a quick connect fitting. Desorption kinetics measurements for doped and un-doped mixtures of $LiNH_2/MgH_2$ were done at 210 ^oC. Once the sample holder was attached to the apparatus, the reservoirs were vented and vacuumed for few minutes. The reservoir valves were then closed so that the pressure inside them would remain in vacuum. The middle valve was closed and a pressure slightly higher than the mid-plateau pressure P_m was set in the

sample chamber. An opposing pressure P_{op}, determined from each sample's PCI plateau was set in the remaining system. The ratio of both pressure values (P_m/P_{op}) is defined as the N-value and it is kept constant for all samples measured. The vacuumed reservoir valves were then opened and the Daqview software was used for data collection. A low pressure transducer was used to collect data for opposing pressures lower than or equal to 100 psi while a high pressure transducer was used to collect data for opposing pressures higher than 100. The sample holder valve was opened after one minute of starting the experiment and the program was triggered to collect data every 30 seconds. Further data analyses were done using Microsoft excel.

CHAPTER THREE

3.0 DESORPTION KINETICS OF LITHIUM AMIDE/MAGNESIUM HYDRIDE SYSTEMS AT CONSTANT PRESSURE THERMODYNAMIC DRIVING FORCES.

3.1 XRD MEASUREMENTS

The ($2LiNH_2/MgH_2$) system reacts with hydrogen according to the following reaction;

$2LiNH_2+MgH_2 \rightarrow Li_2Mg(NH)_2+H_2$ (Dehydriding) (13)

$Li_2Mg(NH)_2+H_2 \leftrightarrow Mg(NH_2)_2 +2LiH$ (Rehydriding) (14)

XRD analyses were done in order to confirm that this system could absorb and release hydrogen in a reversible manner. Fig. 3.1 contains the XRD patterns of the fresh as-milled, dehydrided, and rehydrided samples of potassium hydride doped ($2LiNH_2/MgH_2$) containing the molar ratios: ($1.9LiNH_2+1.1MgH_2+0.1KH$). In this sample, 5 mol % of the $LiNH_2$ has been replaced by KH dopant. The KH dopant comprises 3.3 mol % of the entire mixture. The XRD pattern of the as milled sample shows that most peaks can be assigned to $LiNH_2$, MgH_2 and KH. Peaks corresponding to $Mg(NH_2)_2$ and LiH were not identified in the sample even after ball milling of mixtures for 2 hr. This shows that ball milling for 2 hr does not induce any reaction or major phase transformation after milling ($2LiNH_2 + 1.1MgH_2$). The XRD pattern of ($2LiNH_2/1.1MgH_2$) without the KH dopant is essentially the same as that of ($1.9LiNH_2 + 1.1MgH_2 + 0.1KH$) with the exception of the KH peak occurring at (~27 ^{o}). After placing the as-milled sample under vacuum for 15 hrs at 210 ^{o}C the ($1.9LiNH_2 + 1.1MgH_2 + 0.1KH$) system resulted in the pattern

displayed in Fig. 3.1 (c). It can be seen that the diffraction pattern for the dehydrided sample is composed mostly of peaks belonging to $MgLi_2(NH)_2$. The peak at (~27 ^{o}) is due to KH. Fig. 3.1 (d) contains the pattern for the rehydrided sample. Most of the peaks are due to $Mg(NH_2)_2$ and LiH. The peak at (~27 ^{o}) which is due to KH can still be seen clearly after the rehydrogenation. Reactions in the ($LiNH_2$ + MgH_2) system can be described by the following equations:

$$LiNH_2 + MgH_2 \rightarrow LiH + 1/2Mg(NH_2)_2 + 1/2MgH_2 \quad (15)$$

$$LiH + 1/2Mg(NH_2)_2 + 1/2MgH_2 \leftrightarrow 1/2Li_2Mg(NH)_2 + 1/2MgH_2 + H_2 \text{ (Dehydrogenation)} \quad (16)$$

$$1/2Li_2Mg(NH)_2 + 1/2MgH_2 + H_2 \leftrightarrow LiMgN + H_2 \text{ (Further dehydrogenation)} \quad (17)$$

Fig. 3.2 contains the XRD patterns of the mixture ($0.934LiNH_2 + 1.1MgH_2 + 0.066KH$). This system, like the previous one, contains 3.3 mol % KH. The XRD pattern of the as milled sample (Fig. 3.2 (b)) shows that most of the peaks are due to $LiNH_2$ and MgH_2. Only few peaks are due to LiH which is one of the expected products of ball milling. The peak due to KH cannot be clearly differentiated due to an overlap with MgH_2 peak at ~27 ^{o}. In the dehydrided sample (Fig. 3.2 (c)) there are several peaks due to LiMgN, however peaks due to $Mg(NH_2)_2$ and LiH are observed at ~33 ^{o} and ~44 ^{o} respectively. In the rehydrided sample (Fig. 3.2 (d)) most peaks are due to $Li_2Mg(NH)_2$ and MgH_2. These XRDs indicate that the phase transformations are incomplete even after dehydriding for ~15 hrs or rehydriding at pressures up to 200 atm at various temperatures.

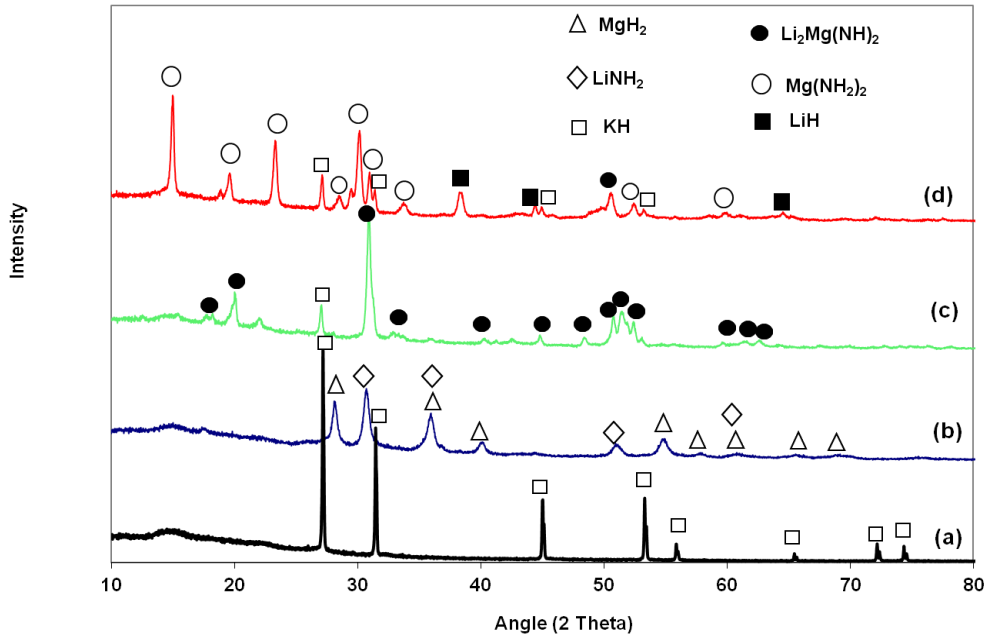

Fig. 3.1 XRD patterns for the (a) KH (b) as milled, (c) dehydrogenated, and (d) rehydrogenated samples of composition ($1.9LiNH_2 + 1.1MgH_2 + 0.1KH$) at 210 ^oC.

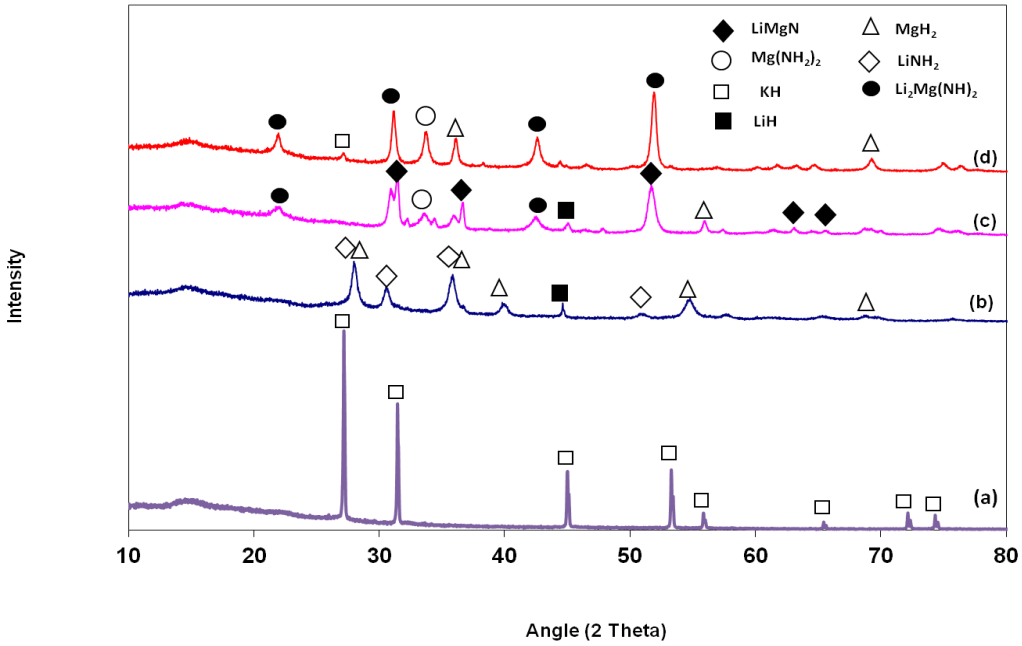

Fig. 3.2 XRD patterns for the (a) KH (b) as milled, (c) dehydrogenated, and (d) rehydrogenated samples of composition ($0.934LiNH_2 + 1.1MgH_2 + 0.066KH$) at 220 ^oC.

3.2 TPD MEASUREMENTS

Temperature Programmed Desorption (TPD) measurements were done to determine the temperatures at which the sample mixtures released hydrogen. Fig. 3.3 represents the TPD analyses of the doped and un-doped samples of ($LiNH_2$/ MgH_2) mixtures. Each sample mixture was heated to approximately 350 ^oC at a rate of 4 ^oC/min. It can be seen that the doped samples have lower desorption temperatures than their un-doped samples. The mixture (1.9$LiNH_2$ +1.1 MgH_2 + 0.1KH) has the lowest onset desorption temperature (75.3 ^oC) with its corresponding un-doped sample having the highest onset desorption temperature (109 ^oC). These values are summarized in Table 3.1. These results confirm that KH is a more effective dopant for reducing the desorption temperature of the (2$LiNH_2$/1.1MgH_2) mixture. All the samples showed hydrogen desorption slightly greater than 5 wt. %.

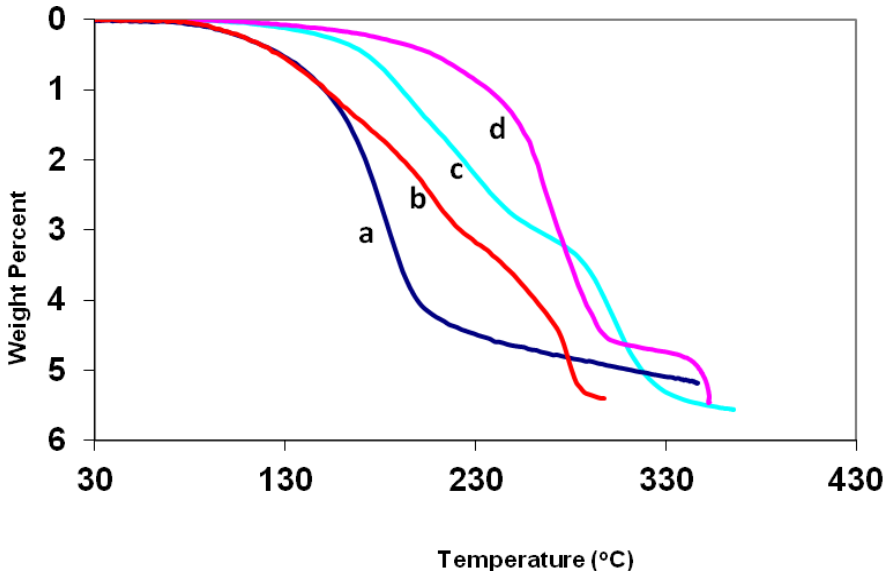

Fig. 3.3 TPD curves for (a) 1.9$LiNH_2$ + 1.1MgH_2 + 0.1KH, (b) 0.934$LiNH_2$ + 1.1MgH_2 + 0.066KH, (c) $LiNH_2$ + 1.1MgH_2, and (d) 2$LiNH_2$ + 1.1MgH_2 samples.

3.3 KINETICS MEASUREMENTS

In addition to having low desorption temperatures, it is also important that samples have fast reaction rates. Desorption kinetics measurements were done as described in [123] on each sample at 210 ^{o}C. In addition to this, all measurements were performed at constant pressure driving forces. This was accomplished by adjusting the hydrogen pressure in the reactor to a value just slightly higher than that of the mid-plateau pressure (P_m), to assure that only the hydrogen rich phase was initially present, and sealing off the reactor. The plateau pressures of the various samples at 210 ^{o}C are summarized in Table 3.1. The pressure in the remaining system (P_{opp}) was then adjusted to a value such that the ratio of the mid-plateau pressure to the applied pressure was a small whole number. This was accomplished by using the same ratio of the equilibrium plateau pressure (P_m) to applied hydrogen pressure (P_{opp}). This ratio is defined as the N-value, is equal to the ratio (P_m/P_{opp}). The N-value was set at 10 in all the experiments that were carried out. In these experiments, hydrogen was allowed to flow out of the sample, through a regulator and into a low pressure reservoir. As the sample released hydrogen, the regulator prevented any pressure change in the sample reactor by allowing the necessary amount of the hydrogen to flow out of the reactor and into the pressure reservoir.

Fig. 3.4 contains plots of the pressures in the sample reactor and in the remote pressure reservoir at N = 10. The plots show that the opposing pressure, P_{opp} remains nearly constant as hydrogen is desorbed by the sample. Thus the driving force remains constant. The pressure in the remote pressure reservoir increases over time as hydrogen flows from the sample reactor into the reservoir. The rate of pressure increase in this reservoir is a direct measure of the reaction kinetics.

It can be seen from Fig. 3.5 that the doped ($1.9LiNH_2 + 1.1MgH_2 + 0.1KH$) sample has the fastest desorption reaction kinetics while its un-doped ($2LiNH_2 + 1.1MgH_2$) sample has the slowest desorption reaction kinetics. The un-doped sample ($2LiNH_2 + 1.1MgH_2$) takes nearly 4000 min under these reaction conditions before it gets to completion whereas the doped sample is virtually complete in 400 min.

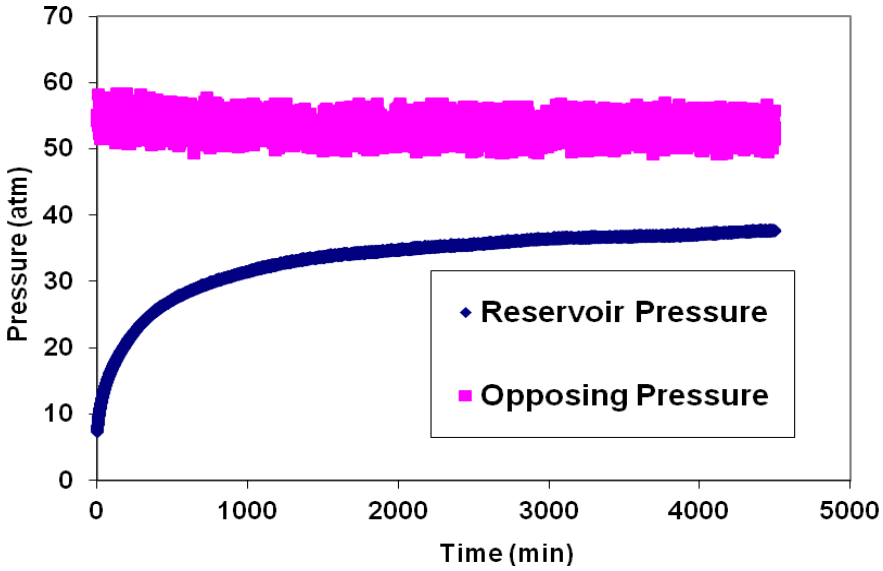

Fig. 3.4 Pressure transducer readout for kinetics on the ($2LiNH_2 + 1.1MgH_2$) sample at N=10 and 210 ^{o}C.

It is interesting to note that the times required for these reactions to reach 90 % completion (T_{90}) are significantly less than this: 1600 and 62 min, respectively. The KH seems to have no effect on desorption kinetics of ($0.934LiNH_2 + 1.1MgH_2 + 0.066KH$) when compared with its un-doped sample, ($LiNH_2 + 1.1MgH_2$). The doped and un-doped samples both take approximately the same time for hydrogen desorption. The times

required for all of these reactions to reach 90 % completion (T_{90}) are summarized in Table 3.1.

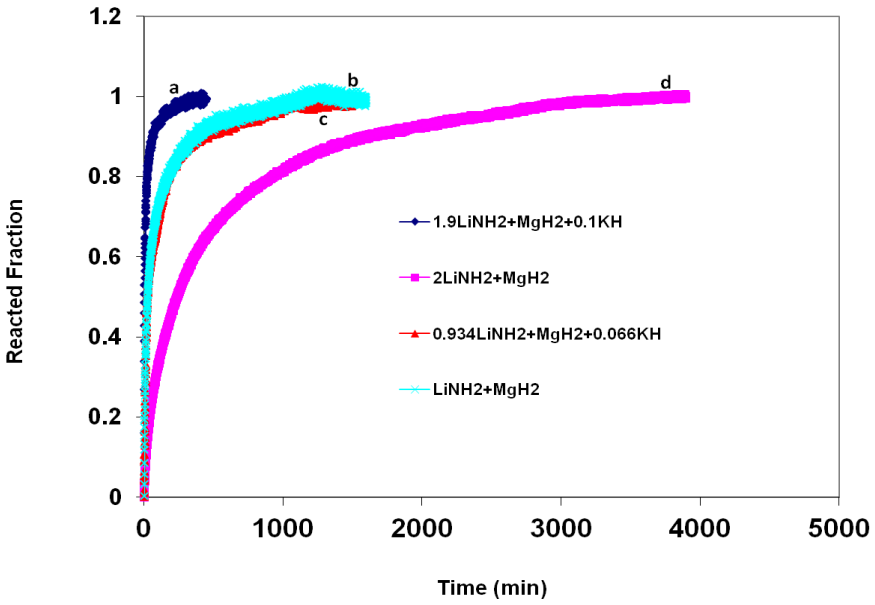

Fig. 3.5 Desorption kinetics curves at 210 ^{o}C in which the N-value was set at 10 for (a) $1.9LiNH_2 + 1.1MgH_2 + 0.1KH$, (b) $LiNH_2 + 1.1MgH_2$, (c) $0.934LiNH_2 + 1.1MgH_2 + 0.066KH$ and (d) $2LiNH_2 + 1.1MgH_2$.

3.4 KINETIC MODELING STUDIES

The classical equation for nucleation and growth processes can be written as:

$$F = 1-\exp(-Bt^m) \text{ or } -\ln \ln (1-F) = \ln B + m \ln t \quad (18)$$

where F is the reacted fraction, B is a constant which depends in part on the nucleation frequency and linear rate of grain growth, and m is a constant that can vary according to the geometry of the system. A method for comparing the kinetics of isothermal solid-state reactions based on the classical equation for analysis of nucleation-and-growth has been developed by Hancock and Sharp [118]. In that method, plots of -ln ln(1 - F) vs. ln t can

be used to distinguish reaction mechanisms. The slope (m) can be used to indicate the rate controlling process. According to the analysis, 'm' values in the 0.54-0.62 range indicate diffusion controlled reactions. Values in the 1.00-1.11 range indicated phase boundary controlled reactions. This type of analysis was applied to the systems used in the current study. Fig. 3.6 contains plots of –ln ln(1 - F) vs. ln t for the doped and un-doped systems studied.

In each case the reacted fraction values in the 0.15-0.50 range were used to determine whether the reaction rate is diffusion or phase boundary controlled. The values of 'm' obtained for each system are tabulated in Table 3.1. It can be seen that the values for all the systems except ($0.934LiNH_2 + 1.1MgH_2 + 0.066KH$) correspond most closely to those expected for diffusion-controlled reactions. This reaction had an 'm' value of 1.00 which corresponds to a phase-boundary-controlled reaction. There are actually four types of diffusion controlled reactions mentioned by Hancock and Sharp [118] but it is difficult to distinguish among them based solely on this analysis.

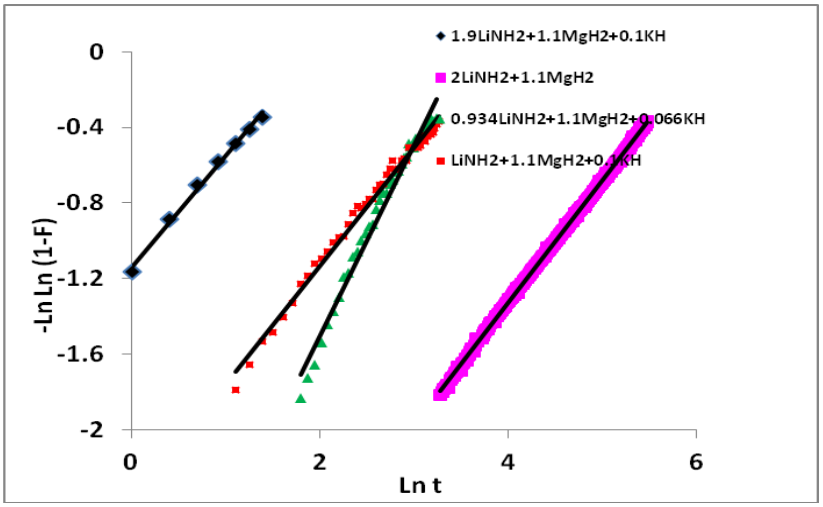

Fig. 3.6 Kinetics modeling results based on the method of Hancock and Sharp.

3.5 DIFFERENTIAL THERMAL ANALYSIS CURVES AND KISSINGER PLOTS

To further understand the effects of KH on the dehydrogenation of the $LiNH_2/MgH_2$ mixtures, the activation energies for dehydrogenation from the samples were investigated using the Kissinger method [119];

$$\ln\left(\frac{\beta}{T_{\max}^2}\right) = -\frac{E_a}{R}\left(\frac{1}{T_{\max}}\right) + F_{KAS(\alpha)} \qquad (19)$$

where T_{max} is the temperature at the maximum reaction rate, β, the heating rate, E_a, the activation energy, α, the fraction of transformation, $F_{KAS}(\alpha)$ a function of the fraction of transformation, and R is the gas constant. In this method, Differential Thermal Analysis (DTA) curves for all the ball milled samples were carried out at different heating rates between 4 and 20 ^oC per minute.

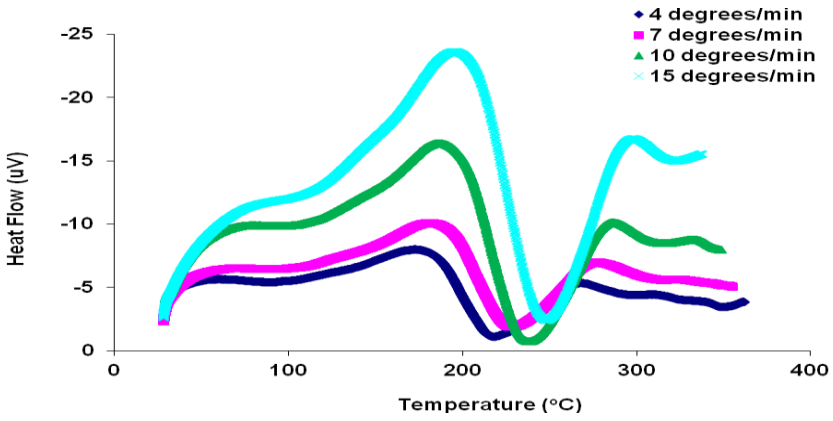

Fig. 3.7 DTA curves for $0.934LiNH_2 + 1.1MgH_2 + 0.066KH$ at heating rates of 4, 7, 10 and 15 ^oC/min.

Fig. 3.7 shows the DTA curves for one of the samples ($0.934LiNH_2 + 1.1MgH_2 + 0.066KH$). These are typical of the types of curves seen for the other mixtures studied.

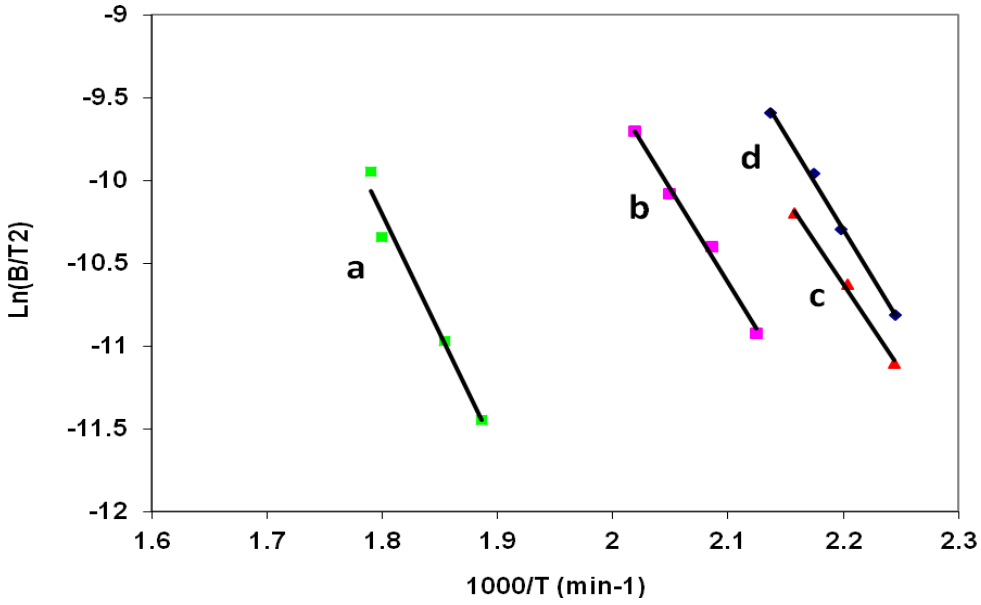

Fig. 3.8 Kissinger plots for (a) $2LiNH_2 + 1.1MgH_2$, (b) $LiNH_2 + 1.1MgH_2$, (c) $1.9LiNH_2 + 1.1MgH_2 + 0.1KH$ and (d) $0.934LiNH_2 + 1.1MgH_2 + 0.066KH$.

Using the DTA curves, the Kissinger plots shown in Fig. 3.8 were made in order to determine the activation energy for each of the samples. In each case plots of $Ln(\beta/T^2)$ versus 1/T were constructed and the slopes were used to determine the activation energy (E_a). The activation energies are summarized in Table 3.1 along with the other kinetic data. Results show that the samples with high activation energies generally react slower than those with low activation energies and samples with low activation energies also have low desorption temperatures.

Table 3.1. Summary of desorption parameters for thermodynamic and kinetics results

Sample	Onset. Des. Temp. (^oC)	E_a (kJ/mol)	M	P_m at 210 ^oC (atm)	T_{90} (min)
$0.934LiNH_2+1.1MgH_2+0.066KH$	81	99±0.1	1.00	78.8	380
$LiNH_2+1.1MgH_2$	99	94±0.1	0.62	25.6	350
$1.9LiNH_2+1.1MgH_2+0.1KH$	75.3	87±0.7	0.58	46.1	62
$2LiNH_2+1.1MgH_2$	109	119±1.7	0.64	34.2	1600

3.6 CONCLUSION

This study has shown that the potassium doped (2:1) mixture has a lower desorption temperature and a faster desorption rate than the potassium doped (1:1) mixture. The KH dopant is able to lower the hydrogen desorption temperatures of both mixtures however the extent of temperature lowering is more significant in the (2:1) doped mixture. The study has also shown KH to be a very effective catalyst in increasing the hydrogen desorption rates from the (2:1) mixture but it has almost no effect on the hydrogen desorption rates of the (1:1) mixture. The desorption rates of the (2:1) doped mixture is ~25 times faster than that of the un-doped (2:1) mixture. The reason for this effect may be due to the fact that the rate controlling step for hydrogen release from the (2:1) mixture changes upon adding the dopant, whereas the dopant has no effect on the rate-controlling step in the (1:1) mixture. It might also be due to the stoichiometric difference of the mixtures. Modeling results indicate that a diffusion process controls the reaction

rates in all the reactions except the $0.934LiNH_2+1.1MgH_2+0.066KH$ mixture. In that sample mixture it appears that a phase boundary process is rate controlling.

Results also show that the samples with high activation energies generally react slower than those with low activation energies. It is also interesting to note that, in general, the samples with low desorption temperatures also have low activation energies.

CHAPTER FOUR

4.0 RUBIDIUM HYDRIDE – AN EXCEPTIONAL DEHYDROGENATION CATALYST FOR THE LITHIUM AMIDE/MAGNESIUM HYDRIDE SYSTEM

4.1 DOPANTS ANALYSIS

XRD analysis of the synthesized dopants (RbH and CsH) and commercially obtained KH are shown in figure 4.1. The XRD of commercially obtained KH is included for comparism. The X-ray peaks are sharp, indicating a good crystalline organization of the powders. The peaks correspond to Face Centered Cubic (FCC) unit cell with the Miller indices of the same parity. The intensities and the peak positions fits well with that reported in [117] except for the RbH and this is due to the experimental conditions which involved the use of (MoKα) that provokes an intense fluorescence with rubidium. The peak positions and intensities also fit well with the ones obtained from the X'Pert High Score Plus library. The '*a*' parameters obtained for KH, RbH and CsH are 5.70 ± 0.01 Å, 6.01 ± 0.01 Å and 6.37 ± 0.02 Å respectively. The values matched those reported in [117]. Table 4.1a, 4.1b and 4.1c shows the lattice parameter calculations. Reactive ball milling under hydrogen pressure constitutes an easy and reproducible way for preparation of pure alkali metal hydrides. Moderate rotation rate employed during ball milling and the low hardness of the reactants minimizes the risk of contamination of the reactants by impurities from the shocks between balls and vial walls. It was suggested that this method can be adapted for industrial applications [117].

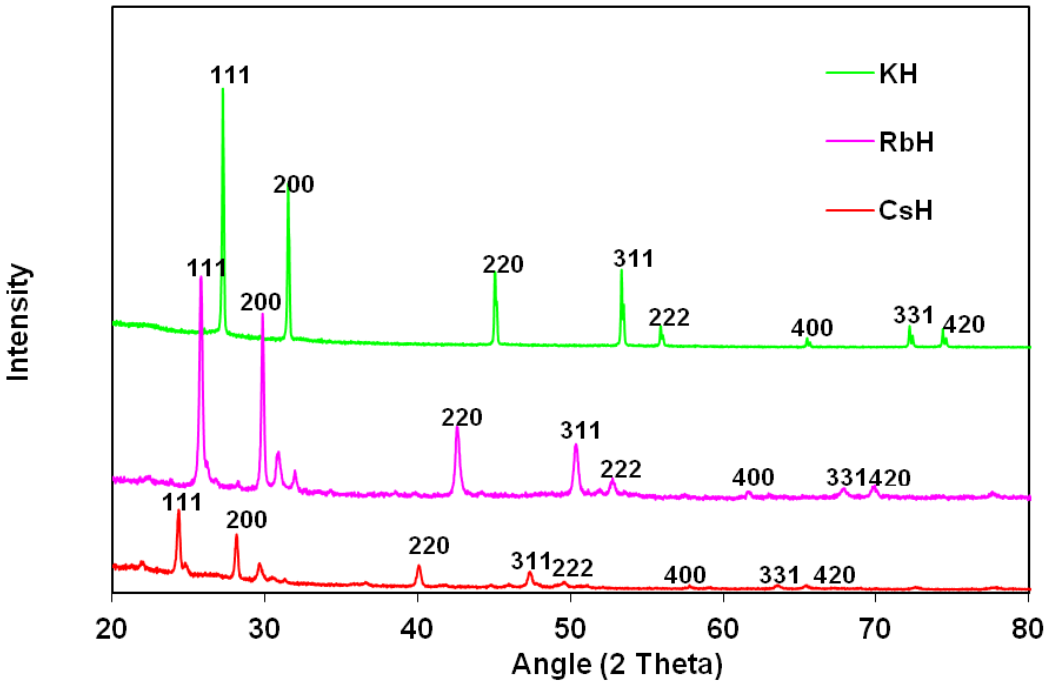

Fig. 4.1 XRD patterns for KH, RbH and CsH dopants.

KH

2θ	θ	sinθ	(sinθ)^2	Δ(sinθ)^2	Whole #		N	h,k,l	a	Std. Dev.
27.196	0.2373	0.2351	0.0553	0.055274	1.0108	3	3	111	5.6792689	
31.47	0.2746	0.2712	0.0735	0.018267	0.33405	1	4	200	5.6853641	
45.02	0.3928	0.3828	0.1465	0.073006	1.33507	4	8	220	5.6957266	
53.31	0.4652	0.4486	0.2012	0.054683	1	3	11	311	5.6995717	
55.87	0.4875	0.4684	0.2194	0.018212	0.33305	1	12	222	5.7006269	
65.46	0.5712	0.5406	0.2923	0.072845	1.33212	4	16	400	5.7035777	
72.17	0.6298	0.589	0.3469	0.054622	0.99888	3	19	331	5.7050704	
74.35	0.6488	0.6042	0.3651	0.018175	0.33236	1	20	420	5.7057257	
82.86	0.7231	0.6617	0.4378	0.072731	1.33004	4	24	422	5.70759	
89.13	0.7778	0.7017	0.4924	0.054589	0.99827	3	27	333	5.7083895	
									5.6990912	0.00974

Table 4.1a Lattice parameter calculation for KH

RbH

2θ	θ	sinθ	(sinθ)^2	Δ(sinθ)^2	Whole #		N	h,k,l	a	Std. Dev.
25.76	0.2248	0.2229	0.0497	0.04969	1.01025	3	3	111	5.990057	
29.80	0.26	0.2571	0.0661	0.01642	0.33384	1	4	200	5.996537	
42.54	0.3712	0.3627	0.1316	0.06547	1.33113	4	8	220	6.011047	
50.32	0.4391	0.4252	0.1808	0.04918	1	3	11	311	6.013673	
52.70	0.4599	0.4439	0.197	0.01626	0.33051	1	12	222	6.016376	
61.59	0.5375	0.512	0.2621	0.06511	1.32389	4	16	400	6.022782	
67.86	0.5922	0.5582	0.3116	0.04945	1.0055	3	19	331	6.019837	
69.85	0.6095	0.5725	0.3277	0.01614	0.32813	1	20	420	6.022228	
									6.011567	0.012096

Table 4.1b Lattice parameter calculation for RbH

CsH

2θ	θ	sinθ	(sinθ)^2	Δ(sinθ)^2	Whole #		N	h,k,l	a	Std. Dev.
24.301	0.2121	0.2105	0.0443	0.0443	1.01434	3	3	111	6.34379	
28.09	0.2451	0.2427	0.0589	0.0146	0.33423	1	4	200	6.352921	
40.04	0.3494	0.3423	0.1172	0.05827	1.33426	4	8	220	6.369839	
47.29	0.4127	0.4011	0.1608	0.04367	1	3	11	311	6.375079	
49.54	0.4323	0.4189	0.1755	0.01467	0.33593	1	12	222	6.374184	
57.79	0.5043	0.4832	0.2335	0.05794	1.32654	4	16	400	6.381962	
63.50	0.5541	0.5262	0.2769	0.04343	0.99449	3	19	331	6.385862	
65.38	0.5705	0.54	0.2917	0.01477	0.33813	1	20	420	6.38373	
									6.370921	0.015111

Table 4.1c Lattice parameter calculation for CsH

4.2 XRD MEASUREMENTS

The $2LiNH_2/1.1MgH_2$ system reacts with hydrogen according to the reactions described in Eq. 6. XRD measurements were done on the hydrided and dehydrided mixtures, with and without RbH dopant, to confirm that the doped $2LiNH_2/1.1MgH_2$ system could absorb and release hydrogen reversibly. Figure 4.2 (a) shows the XRD pattern for the RbH catalyst; Figure 4.2 (b) contains a pattern for the “as milled” sample; while Figures 4.21(c) and 4.2 (d) contain patterns for the hydrided and dehydrided mixtures,

respectively. A comparison of the patterns shows some significant differences in the hydrided and dehydrided samples. The pattern for the as-milled sample in Figure 4.2 (b) contains peaks for the reactants MgH_2 and $2LiNH_2$. Upon complete dehydrogenation, the pattern in Figure 4.2c contains only peaks for the expected dehydrogenated product, $Li_2Mg(NH)_2$. This product has an orthorhombic structure and it agrees very well with that reported by Hu and Fichtner [100]. No RbH peaks appear in this XRD pattern. However, upon rehydrogenation, the pattern in Figure 4.2 (d) is obtained. No peaks for the initial reactants MgH_2 and $2LiNH_2$ are seen. This XRD pattern contains peaks for ($Mg(NH_2)_2$ +LiH), as indicated in Eq. 7 along with peaks for the RbH catalyst. This confirms that the reaction in Eq. 7 occurs reversibly. Since RbH was reformed this indicates that it was not consumed during the reaction and that it is truly behaving as a catalyst. The behavior displayed in Figure 4.2 for the RbH-catalyzed $2LiNH_2/1.1MgH_2$ system has also been observed for the KH-catalyzed system by Luo *et al,* Markmaitree *et al*, and Durojaiye *et* [70, 97, and 115].

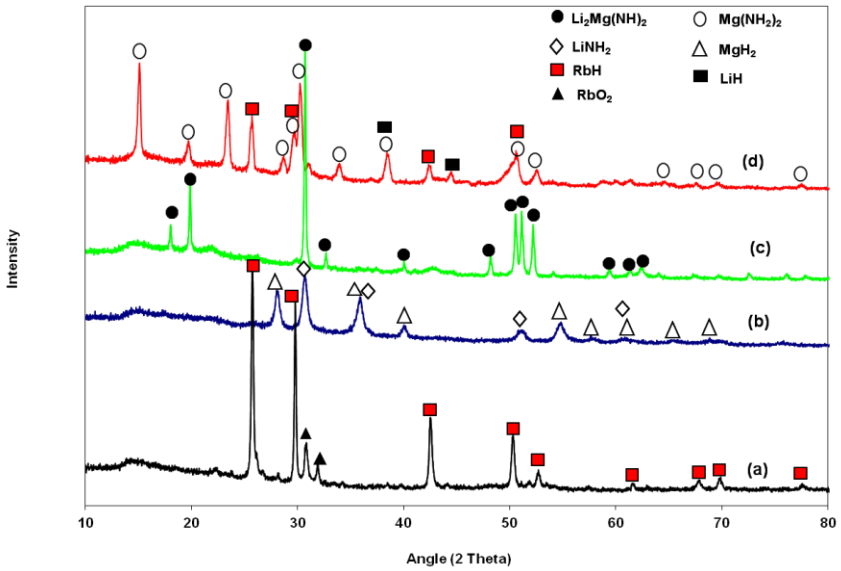

Fig. 4.2 XRD profiles for $2LiNH_2/1.1MgH_2$ mixture catalyzed by RbH (a) RbH catalyst (b) as milled (c) dehydrided and (d) rehydrided mixture

4.3 TPD MEASUREMENTS

It has already been established that KH is among the most effective catalysts for lowering the desorption temperature of the $2LiNH_2/1.1MgH_2$ system (See chapter 3 of this dissertation). Therefore temperature programmed desorption measurements were performed on this system using RbH and KH catalysts in order to compare their effectiveness. The samples were heated from 30 to 250/350 ^oC at 4 ^oC/min. The results are shown in Figure 4.3. When reporting TPD results, it is a common practice to report the onset temperatures of the dehydrogenation process, but onset temperatures can be misleading since they are the temperature at which dehydrogenation just begins to occur. This temperature is often much lower than that during which the bulk of the hydrogen is

released. Therefore a decision was made to compare desorption temperatures that correspond to the inflection point of the TPD curve.

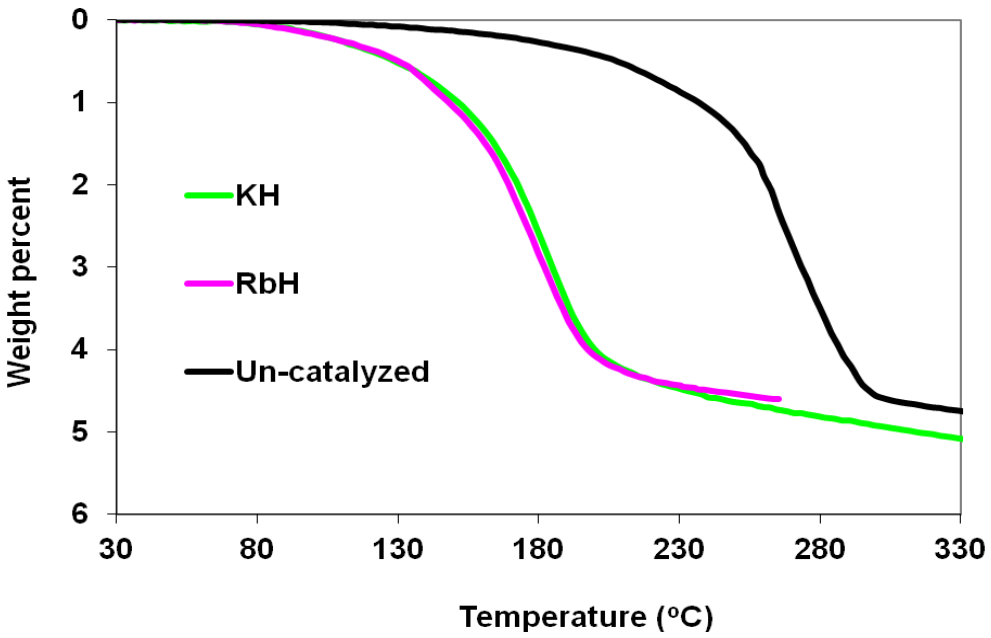

Figure 4.3 TPD Profiles for catalyzed and un-catalyzed $2LiNH_2/1.1MgH_2$ mixtures

The results in Figure 4.3 show that the desorption temperatures, T_d, are in the order: RbH ≤ KH << Un-catalyzed. The onset temperatures and desorption temperatures for these materials are reported in Table 4.2. The fact that RbH and KH-catalyzed mixtures have much lower desorption temperatures than the un-catalyzed mixture is a bit surprising. If the RbH and KH are truly behaving as catalysts, they should not have any effect on the desorption temperature of this system. Therefore it was useful to determine the thermodynamic stabilities of these mixtures.

4.4 PCI MEASUREMENTS AND van't HOFF PLOTS

Thermodynamic stabilities were determined from pressure composition temperature (PCT) isotherm measurements that were carried out on the catalyzed and un-catalyzed mixtures. Measurements were made in the 200 - 230 ^{o}C range. Figure 4.4a contains the PCT isotherms for the RbH-doped mixture and Figure 4.4b contains the PCT isotherms for the un-catalyzed mixture. PCI for KH doped mixture is shown in fig. 4.4c. The isotherms show a well-defined plateau region at each temperature. The plateau pressures for the RbH-doped mixture are higher than those for the un-catalyzed mixture under the same temperature conditions. The plateau pressures were used to construct van't Hoff plots and the slopes were used to determine the ΔH values for the desorption reactions. Van't Hoff plots for the RbH-doped, KH-doped and un-catalyzed samples are shown in Figure 4.5. The enthalpy values obtained for the different mixtures are shown in Table 4.2. The desorption enthalpy values obtained for the RbH doped mixture (42.7 kJ/mol) and the KH doped mixture (42.0 kJ/mol) are similar in magnitude. This is to be expected since the hydrogen desorption temperatures of both of these mixtures are nearly the same. These enthalpies are significantly lower than the (65 kJ/mol) found for the un-catalyzed mixture.

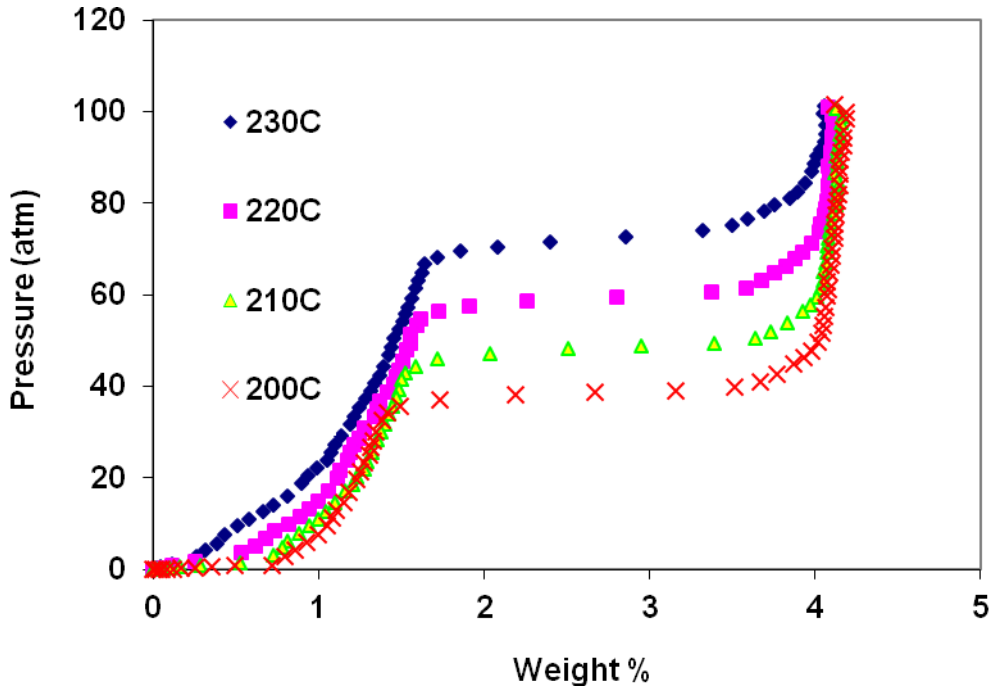

Figure 4.4a Desorption PCT isotherms for the RbH-doped $2LiNH_2/1.1MgH_2$ mixture

This is also expected since desorption of hydrogen from the un-catalyzed mixture occurs at a much higher temperature than those for the catalyzed mixtures. It should also be noted that the desorption enthalpy for the un-catalyzed mixture is in the same range as the 53.4 kJ/mol that was reported based on DFT calculations [116].

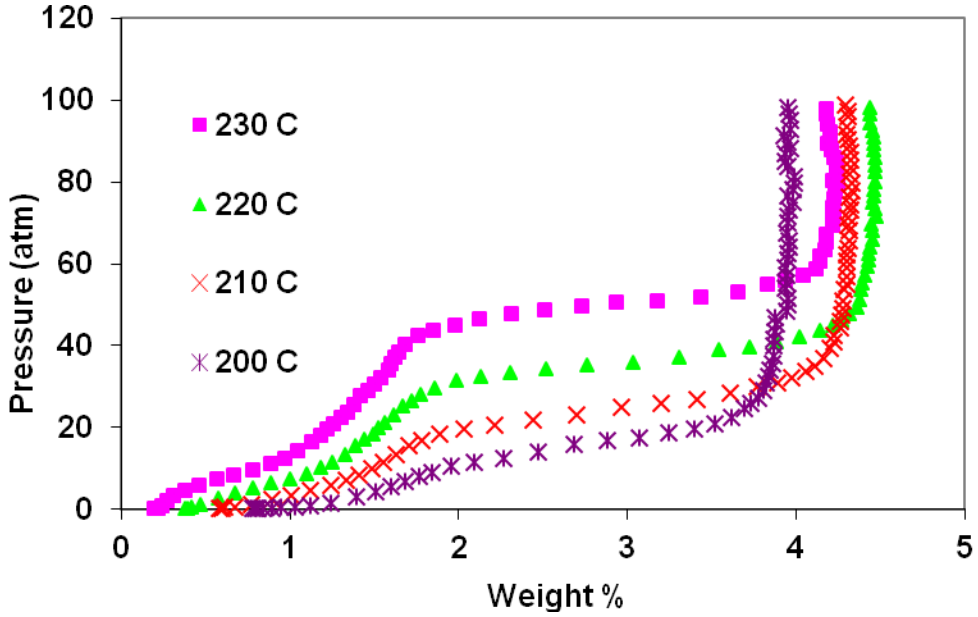

Figure 4.4b Desorption PCT isotherms for the un-catalyzed $2LiNH_2/1.1MgH_2$ mixture

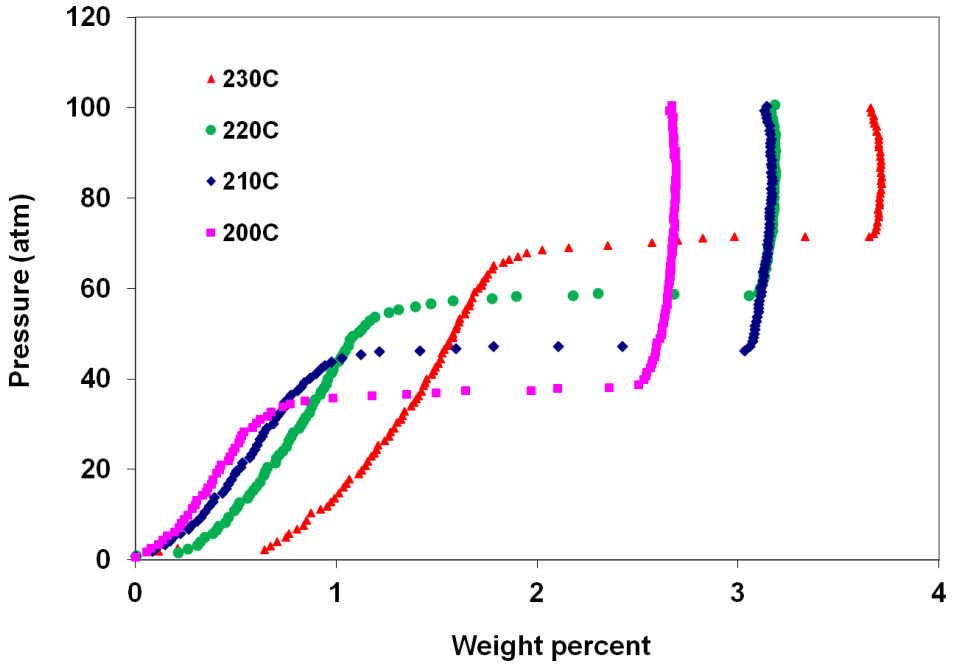

Figure 4.4c Desorption PCT isotherms for the KH-doped $2LiNH_2/1.1MgH_2$ mixture

Table 4.2 Summary of desorption parameters for thermodynamics and kinetics results

	KH	RbH	Un-catalyzed
Onset Temp. (^oC)	75	76	109
Desop. Temp., T_d, (^oC)	146	143	237
Desop. ΔH (kJ/mol)	42.0±0.12	42.7±0.03	65.8±0.04
T_{90} (min)	62	27	1600
Ea (kJ/mol)	87.0±0.7	86.8±0.1	119.0±1.7
Pm at 210 ^oC (atm)	46.1	48.3	34.2
'm' values	0.587	0.652	0.647

Some other investigators have reported desorption enthalpies in the 40-44 kJ/mol range [85, 108 and 114] but these are not consistent with our findings. Our findings can be explained based in part on the fact that Rb and K have the same Pauling electronegativity value, 0.82. Apparently both of these electropositive elements have nearly equal destabilizing effect on the N-H bond. This destabilization results in significant reductions in desorption temperature and enthalpy. Thus we see that RbH and KH are behaving as more than just catalysts. Perhaps a better term would be "catalytic additive".

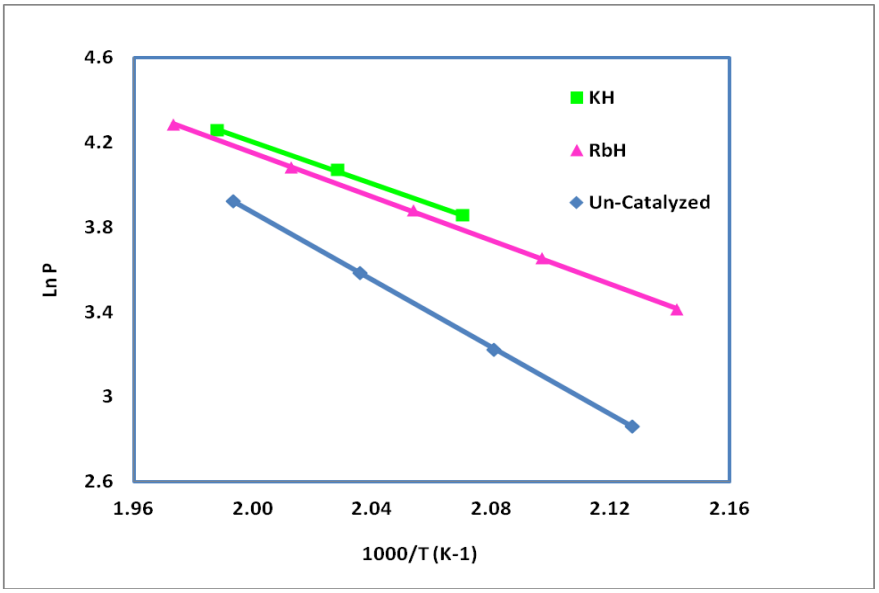

Figure 4.5 Van't Hoff plots for hydrogen desorption from the catalyzed and un-catalyzed $2LiNH_2/1.1MgH_2$ mixtures.

4.5 DTA MEASUREMENTS AND KISSINGER PLOTS

Differential Thermal Analysis curves (DTA) were carried out in order to better understand the effects of the catalytic additives on the dehydrogenation of $LiNH_2/1.1MgH_2$ mixtures. The DTAs were carried out for the catalyzed and un-catalyzed mixtures at different heating rates between 4 and 20 ^oC per minute. Figure 4.6 shows the DTA curves for the RbH doped mixture at different heating rates. The plots show that the desorption temperatures increase with increasing scan rates. These scans are typical of those that were obtained for the other mixtures. There is a relationship between the scan rate and the activation energy that is described by the Kissinger Eq. (19) in Chapter 3. Kissinger plots for various mixtures were constructed from the data obtained from the DTA curves. The slopes of these plots, shown in Figure 4.7, were used to determine the activation energies of each mixture. The activation energies for KH and RbH doped

mixtures are 87 kJ/mol and 86.8 kJ/mol respectively, which is much smaller than the activation energy (119 kJ/mol) for the un-catalyzed mixture. The similar activation energies for the two catalyzed mixtures can be correlated with the electronegativity values of Rb and K in the same way as was done for desorption temperatures. Table 4.2 shows the activation energy values of all the mixtures.

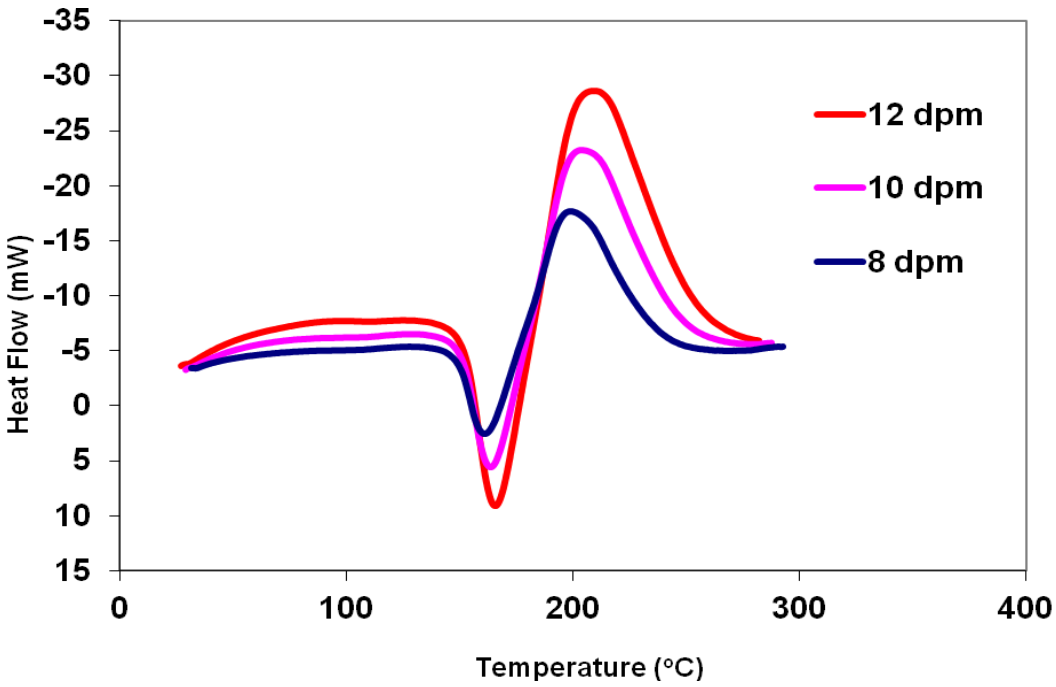

Figure 4.6 Differential thermal analysis plots for a $2LiNH_2/1.1MgH_2$ mixture catalyzed by RbH

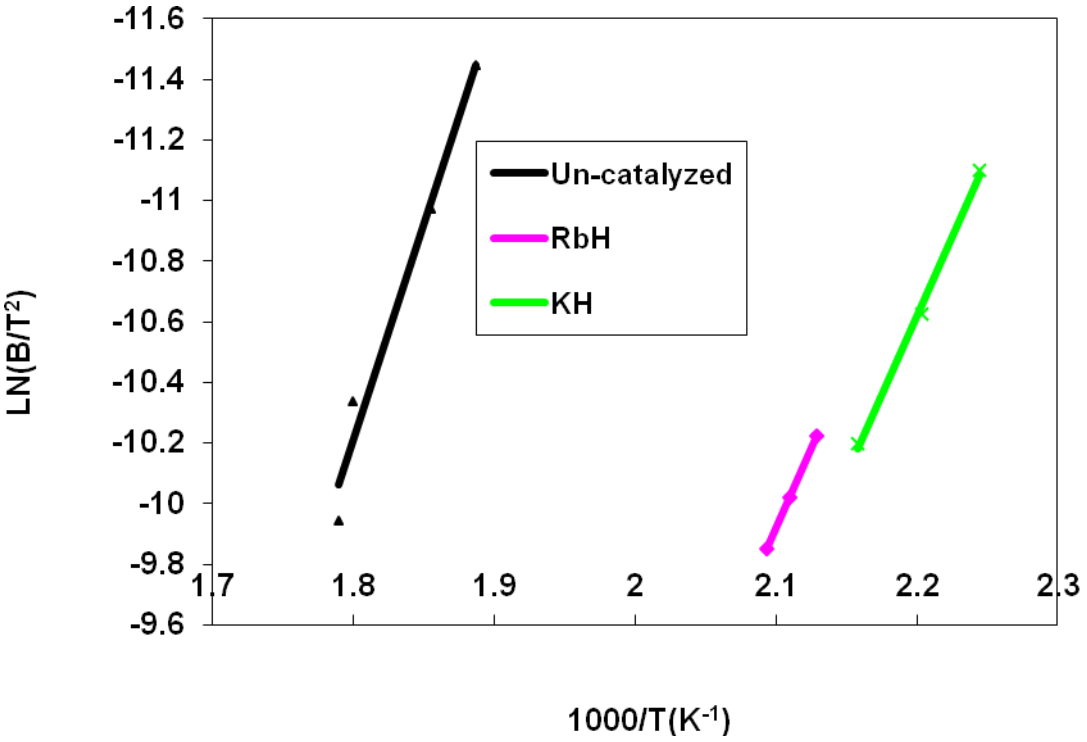

Figure 4.7 Kissinger plots for catalyzed and un-catalyzed $2LiNH_2/1.1MgH_2$ mixtures

4.6 KINETIC MEASUREMENTS

Fast reaction rate is just as important as low desorption temperatures according to the DOE requirements for hydrogen storage systems. Therefore comparisons were made of the desorption kinetics of the catalyzed and un-catalyzed systems. Kinetics measurements were carried out for each mixture in the two-phase plateau region at 210 ^{o}C using constant pressure thermodynamics forces. Constant pressure thermodynamic force is achieved by keeping the ratio of the plateau pressure to the applied pressure constant for all measurements. The ratio has been defined as the N-Value. In these experiments, an N-Value of 10 was applied to all samples. A summary of the plateau pressures at 210 ^{o}C is

shown in Table 4.2. Figure 4.8 contains the desorption kinetics plots of $2LiNH_2/1.1MgH_2$ mixtures with and without RbH and KH catalysts. It can be seen that the order of reaction kinetic rates is RbH > KH >> Un-catalyzed. The RbH doped mixture desorbs hydrogen about twice as fast as the KH doped and about 60 times as fast as the un-catalyzed mixture. The times taken by the various reactions to reach 90 % completion (T_{90}) are shown in Table 4.2.

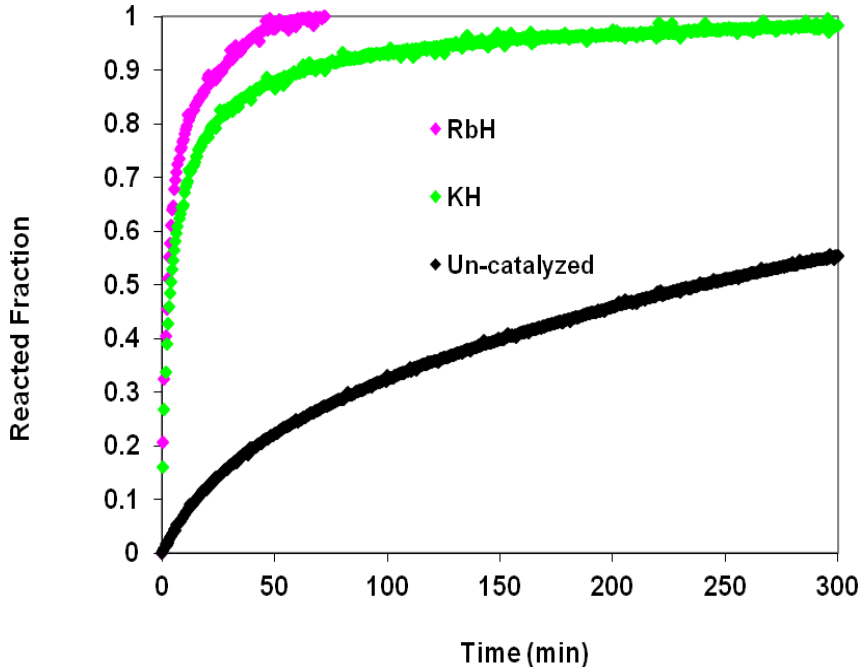

Figure 4.8 Desorption kinetics plots for catalyzed and un-catalyzed $2LiNH_2/1.1MgH_2$ mixtures at N=10 and 210 ^oC.

4.7 KINETIC MODELING STUDIES

The fact that the RbH doped mixture desorbs hydrogen twice as fast as the KH doped mixture was unexpected based on the fact that both Rb and K have the same electronegativity. Therefore kinetics modeling studies were conducted to determine if there was a plausible explanation for this. Smith and Goudy performed kinetics modeling studies on the $LaNi_{5-x}Co_x$ hydride system (x = 0, 1, 2 and 3) and used two theoretical equations based on the shrinking core model to model the system [119]. These same equations were used to model the $2LiNH_2/1.1MgH_2$ system. They are as follows:

$$\frac{t}{\tau} = 1 - \left(1 - X_B\right)^{1/3} \tag{20}$$

where $\tau = \dfrac{\rho_B R}{b k_s C_{Ag}}$

$$\frac{t}{\tau} = 1 - 3\left(1 - X_B\right)^{2/3} + 2\left(1 - X_B\right) \tag{21}$$

where $\tau = \rho_B R^2 \big/ 6 b D_e C_{Ag}$,

Where t is the time at a specific point in the reaction and X_B is the fraction of the metal reacted. R is the initial radius of the hydride particles, 'b' is a stoichiometric coefficient of the metal, C_{Ag} is the gas phase concentration of reactant, D_e is the effective diffusivity of hydrogen atoms in the hydride, ρ_B is the density of the metal hydride and k_s is a rate constant.

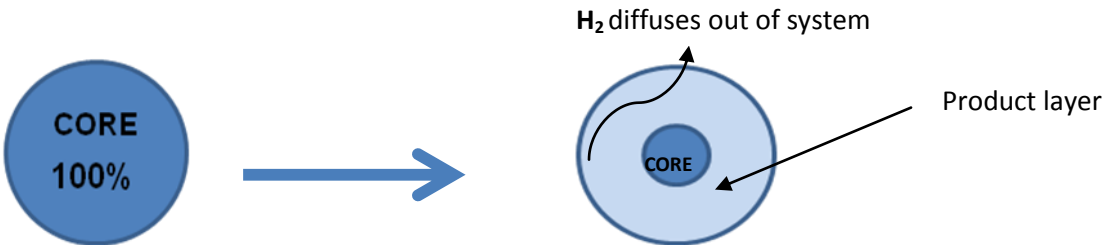

Figure 4.9. Diffusion process in shrinking core model

In the shrinking core model as the reactant core is consumed it decreases and the product layer grows bigger till all the reactant is fully consumed.

Equation (20) is based on a shrinking core model with chemical reaction at the phase boundary controlling the rate whereas Equation (21) is based on a process in which diffusion controls the reaction rate. Figures 4.10 (a – c) show kinetic modeling results for the RbH doped, KH doped and un-catalyzed mixtures respectively. Equations (20 and 21) were fitted to the kinetic data in Figure 4.8 for each of the sample mixtures to determine which kinetic model best describes the reactions in this study. In order to determine the theoretical curves, it was first necessary to determine a value for the constant, τ. This was accomplished through a series of statistical data analyses to determine a value which resulted in the smallest standard deviation between the experimental and theoretical data. Figure 4.10a, for the RbH doped mixture, shows three curves. One is an experimental curve taken from Figure 4.8; a second curve was calculated from Equation (20) and a third curve was calculated from Equation (21). As shown in Figure 4.10a, the data generated from the model with diffusion controlling the overall rate fits the experimental data better than the data generated from the model with chemical reaction controlling the overall reaction rate. This is true only during the first 70 % of the reaction. During the

last 30 % of the reaction, neither model was a good fit with the experimental data. The reason for this is that during the first 70 % of the reaction, desorption occurred along the plateau region where the pressure remained relatively constant. Therefore the N-Value was constant and thus the thermodynamic driving force was constant. When the reaction reached the left edge of the plateau region the pressure decreased sharply and the thermodynamic driving force decreased. At this point the kinetics slowed more rapidly than either model predicted. The modeling results in Figure 4.10b for the KH catalyzed mixture and in Figure 4.10c for the un-catalyzed sample showed similar results. In all cases, the data generated from the model with diffusion controlling the overall rate fit the experimental data better than the data generated from the model with chemical reaction controlling reaction rate. In all the models, diffusion controlled the rates only along the two-phase plateau region. The fact that diffusion is the rate-controlling process could be used to explain why the desorption rate in the RbH doped mixture is faster than the KH doped mixture. The atomic radius of Rb is 248 pm whereas the radius of K is only 227 pm. Since Rb is larger, it would cause a slight expansion of the lattice, thereby allowing the diffusing species to move faster through the lattice.

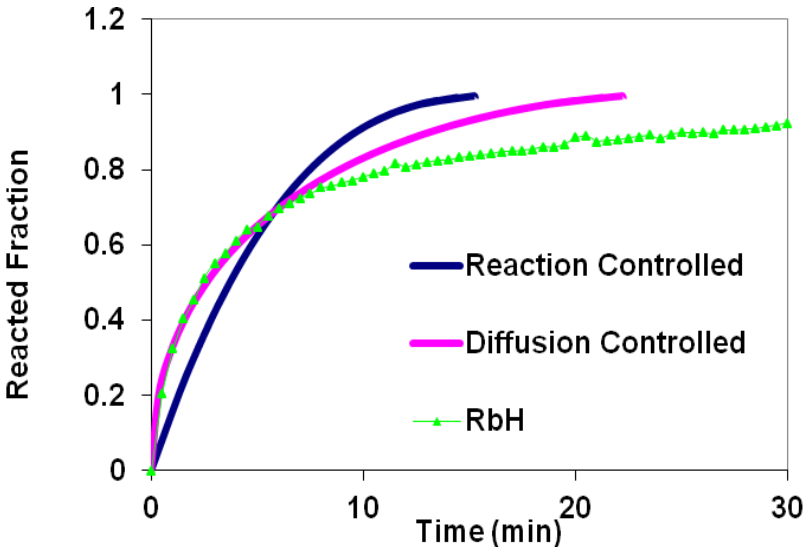

Figure 4.10a Modeling plots for the RbH doped mixture

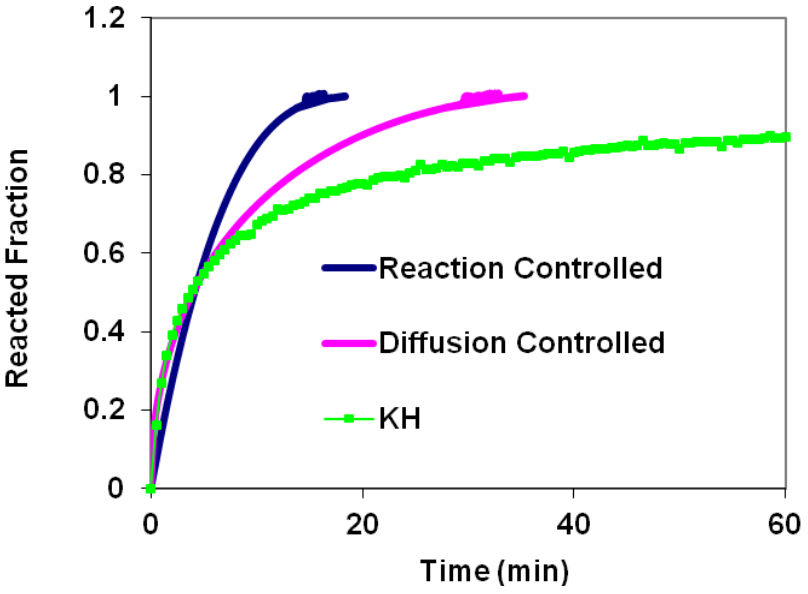

Figure 4.10b Modeling plots for the KH doped mixture

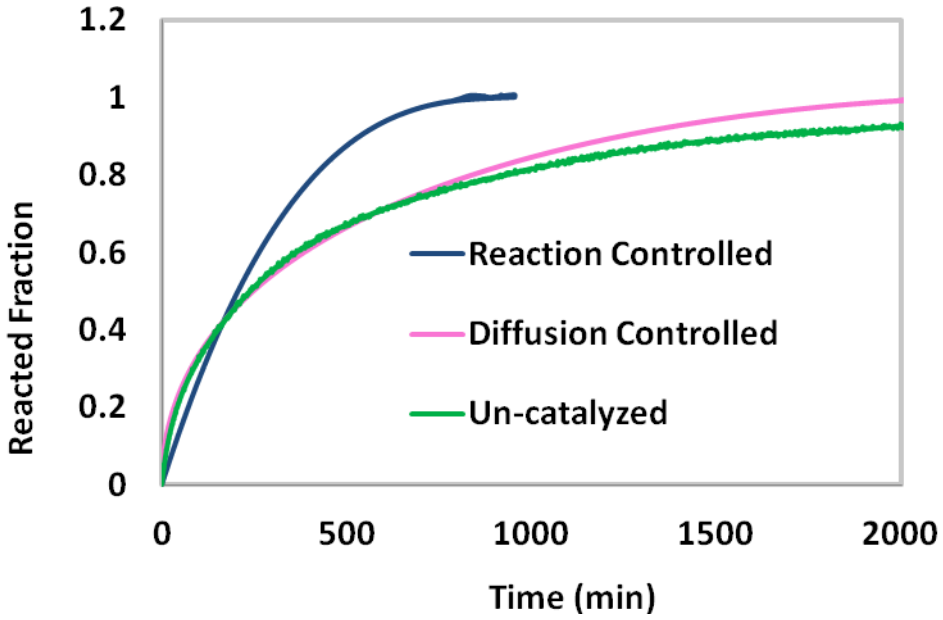

Figure 4.10c Modeling plots for the un-catalyzed mixture

In order to confirm that diffusion controls the reaction rates, a second modeling technique for comparing the kinetics of solid-state reactions was applied. This method, which is based on the classical equation for analysis of nucleation-and-growth, was developed by Hancock and Sharp [118]. This method has been discussed in detail in chapter 3.

The values of 'm' obtained from the slope of the graph in Figure 4.11 for each mixture are tabulated in Table 4.2. The data shows that the values for all the systems correspond most closely to those expected for diffusion-controlled reactions. Thus, two entirely different approaches have both indicated that diffusion is the rate-controlling process in the $2LiNH_2/1.1MgH_2$ system.

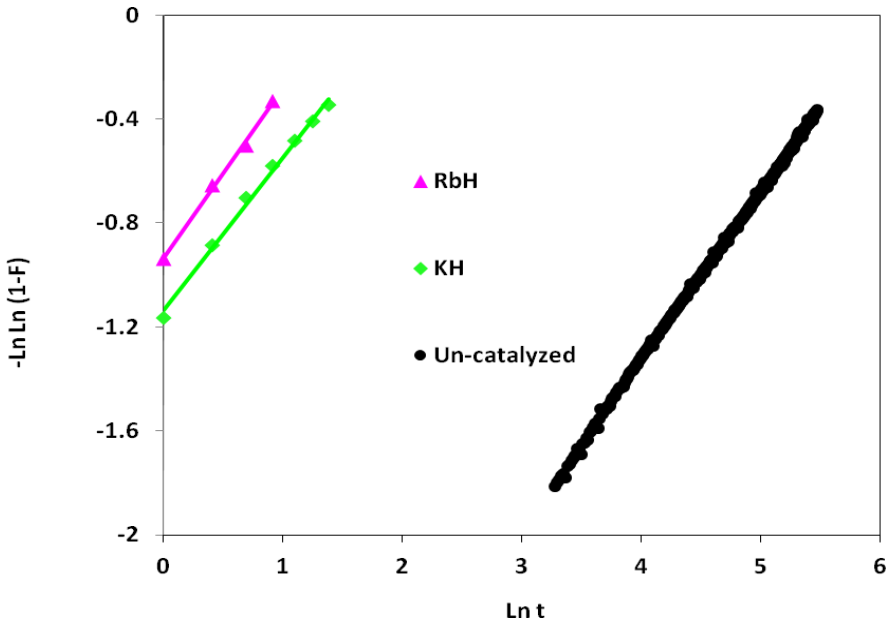

Figure 4.11 Modeling plots for catalyzed and un-catalyzed $LiNH_2/1.1MgH_2$ mixtures based on the method of Hancock and Sharp

4.8 CONCLUSION

The results of this study show that the new catalytic additive, RbH, is significantly better than KH for enhancing hydrogen desorption from the $2LiNH_2/1.1MgH_2$ system. The RbH and KH additives have nearly the same capability for lowering the hydrogen desorption temperature of the $2LiNH_2/1.1MgH_2$ mixture. This is believed to be largely due to the fact that both Rb and K have the same electronegativity and thus similar destabilizing effect on the N-H bond. The fact that the desorption enthalpy for hydrogen release from the un-catalyzed mixture was much higher than that from the catalyzed mixtures is consistent with these findings. The kinetics results show that the RbH-doped mixture releases hydrogen over twice as fast as the K doped mixture and approximately 60 times

faster than the un-catalyzed sample. The fact that the activation energy enthalpy for hydrogen release from the un-catalyzed mixture was much higher than that from the catalyzed mixtures is consistent with these findings. The modeling studies using the shrinking core model and a method developed by Hancock and Sharp both indicated that the reaction rates are controlled by diffusion in the two-phase plateau region. The faster kinetics in the RbH doped mixture is attributed to the fact that Rb has a larger radius and is thereby able to expand the lattice, thus facilitating the diffusion process.

CHAPTER FIVE

5.0 COMPARATIVE STUDIES OF SELECTED NON-TRANSITION METAL HYDRIDES OF GROUP I ON THE $2LINH_2/MgH_2$ SYSTEM

5.1 XRD MEASUREMENTS

Fig. 5.1a shows the XRD of the "As Milled" samples with and without the catalysts. It has been widely reported by Luo *et al*, Markmaitree *et al* and Durojaiye *et al* [70, 97, and 115] that the peaks occurring at 27.9, 35.7, 39.7, 54.5, 57.5 and 30.5, 35.7, 50.7, 60.3 degrees for the mixture doped with KH and the un-doped mixture are mostly due to MgH_2 and $LiNH_2$ respectively, though the peaks are wide at the base due to low crystallinity when milled. The RbH and CsH doped mixtures also follow the same pattern. The catalysts' peaks could not be identified and the peak intensities of $LiNH_2$ and MgH_2 also decreased.

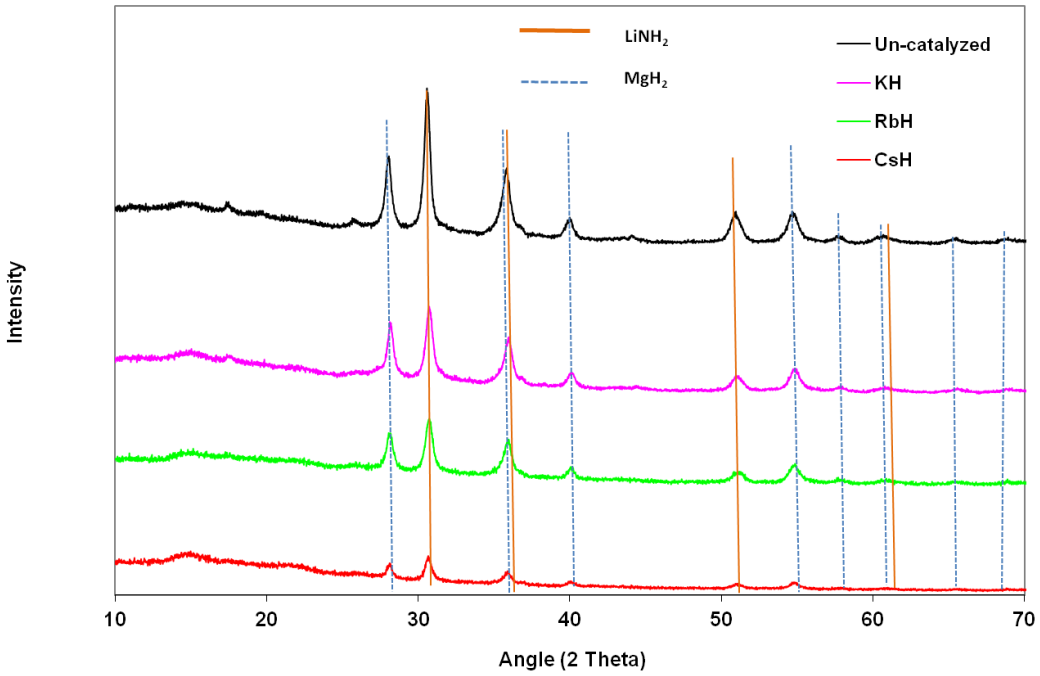

Fig. 5.1a XRD patterns for doped and un-doped as milled $2LiNH_2/1.1MgH_2$ mixtures

Fig. 5.1b shows the dehydrided XRD profile of the mixtures. The dehydrided mixtures of the KH doped and the un-catalyzed mixtures were reported by some groups Markmaitree *et al*, Wang *et al*, and Luo *et al* [97, 108 and 114]. Their reports confirmed the formation of a new ternary imide compound known as $Li_2Mg(NH)_2$ after dehydriding the $2LiNH_2+MgH_2$ mixtures. The RbH doped mixtures exhibits the same XRD pattern as the un-catalyzed and KH doped mixtures when dehydrided. The CsH doped sample showed different XRD peaks compared to the rest when dehydrided. The set of peaks at 18.3 and 20.2 degrees exhibited by other dehydrided mixtures could not be found in the dehydrided mixture of the CsH doped sample. It also possesses a strong singlet peak at

51.6 degrees. This characteristic XRD is similar to the one reported as cubic $Li_2Mg(NH)_2$ by Wang *et al* [108]. Also, a peak belonging to KH at ~27 degree can be seen in the dehydrided mixture of the KH doped mixture, this is due to the dehydrogenation temperature of ~210 ^oC employed which is lower than the decomposition temperature of the KH which is ~400 ^oC. The decomposition temperatures of RbH and CsH is ~170 ^oC for both samples. This is why the peaks of RbH and CsH are not present in the RbH and CsH doped mixtures of the dehydrogenated mixtures.

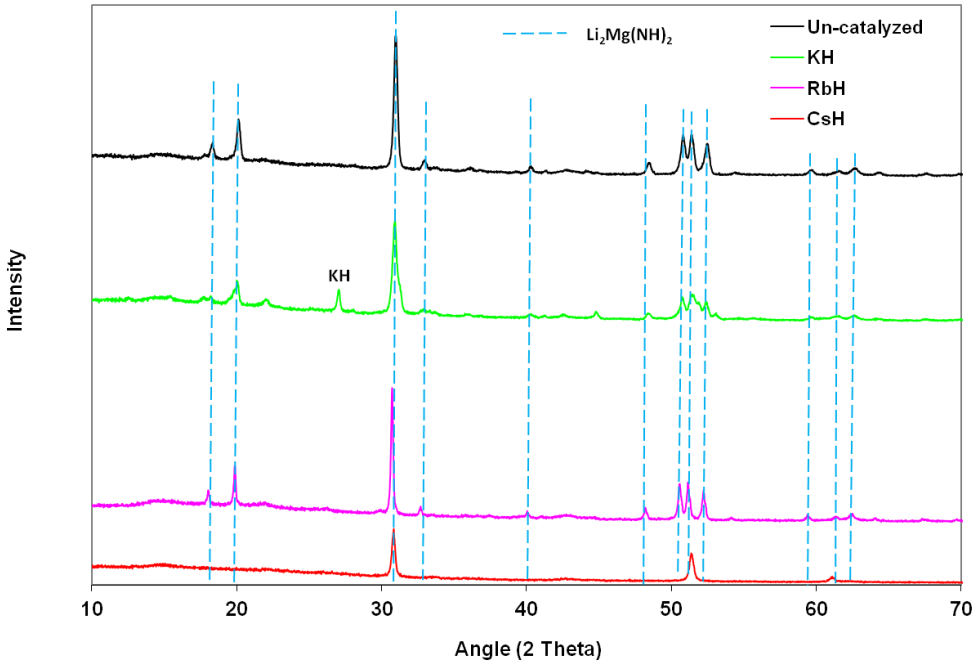

Fig. 5.1b XRD patterns for doped and un-doped dehydrided $2LiNH_2/1.1MgH_2$ mixtures

Fig. 5.1c shows the XRD profiles of the rehydrided mixtures. The simulated $Mg(NH_2)_2$ peaks are also included in the rehydrided XRD profile. It has been established that when the dehydrided mixtures are rehydrided the resultant compounds are $Mg(NH_2)_2$+2LiH

[70, 87, 114 and 115]. So, the mixtures potentially cycle between $Mg(NH_2)_2$+2LiH and $Li_2Mg(NH)_2$. The KH doped mixtures have been reported to show regeneration of peaks belonging to that of the KH catalyst at 27.2 degrees when the dehydrided mixture is rehydrided [108 and 115]. The RbH peak was also regenerated at 25.8 degrees in the RbH doped mixture. The CsH doped mixture shows slight variation in the rehydrided peaks. It is not clear whether the CsH peaks were regenerated. However it is possible that the CsH peak may have overlapped with the $Mg(NH_2)_2$ peaks at 23.5 degrees. This can be confirmed by comparing the ΔH of the various systems. An unknown peak was also observed at 26.6 degrees but this peak could not be assigned to $Mg(NH_2)_2$, LiH or CsH directly. The peak might be due to a peak shift in the synthesized CsH at 28.0 degrees. Peak shift in figure 5.1c by the doped samples are due to the increasing atomic size of the metals.

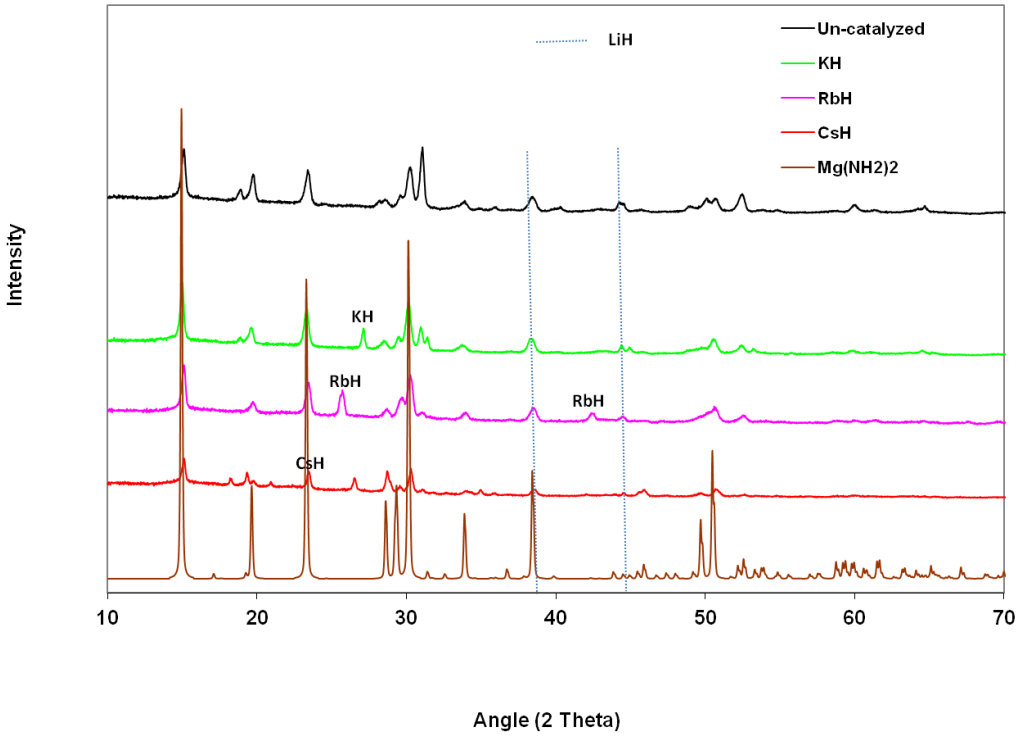

Fig. 5.1c XRD patterns for doped and un-doped as rehydrided $2LiNH_2/1.1MgH_2$ mixtures

5.2 TPD MEASUREMENTS

Fig. 5.2 shows the Temperature Programmed Desorption (TPD) curves of the various synthesized mixtures of $2LiNH_2+1.1MgH_2$ with and without the catalysts. The samples were heated from 30 ^oC to 250 ^oC/350 ^oC) at 4 ^oC/min. The mixture doped with CsH has the lowest onset temperature (63 ^oC).

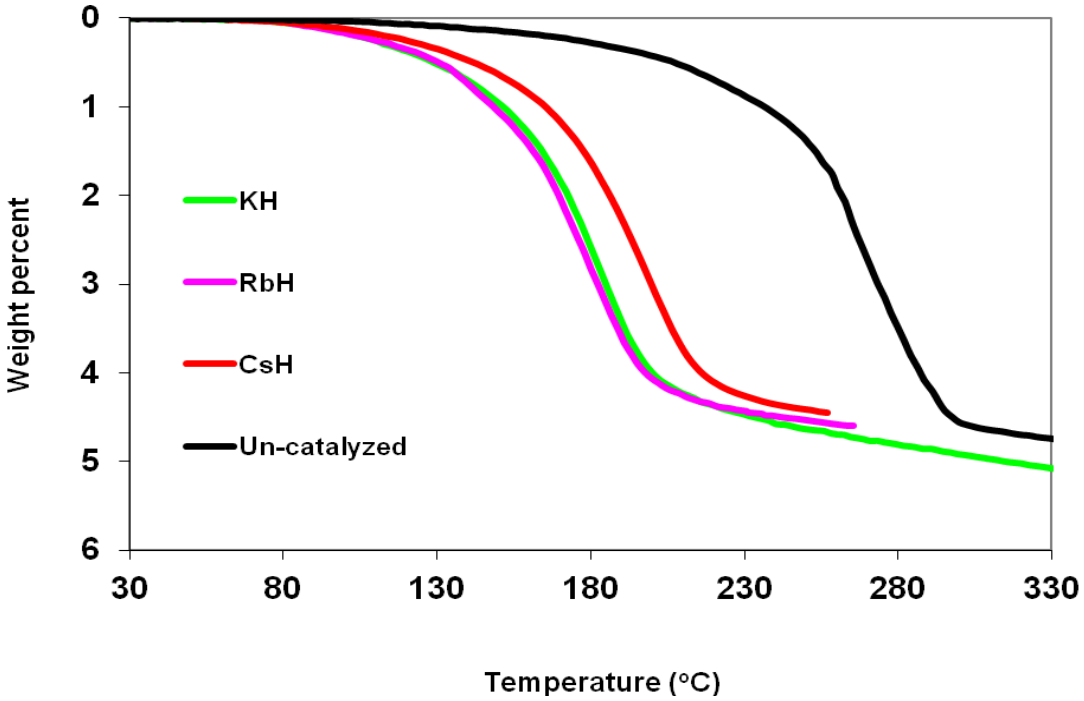

Fig. 5.2 TPD Profiles for catalyzed and un-catalyzed $2LiNH_2/1.1MgH_2$ mixtures

This might be due to the high reactivity of the Cs compared with other metals used. The relationship between the onset temperatures and the electronegativity of the corresponding metals is shown in Table 5.1. As the reactions proceed above 100 ^{o}C, the mixture doped with RbH shows the lowest desorption temperature (T_d), (143 ^{o}C). The order of desorption temperature, T_d, is RbH< KH< CsH< Un-catalyzed. The desorption temperature, T_d, corresponds to the inflection point of the TPD curve.

Rb and Cs diffused into the imide/amide phases and combined with nitrogen, and then the amide N-H and imide Li-N are weakened. This enhanced dehydrogenation. This was reported for K as well in [108].

5.3 PCI MEASUREMENTS

Desorption pressure composition isotherm measurements were carried out on the mixtures in order to determine the plateau pressures at different temperatures (200 ^{o}C-230 ^{o}C). The obtained plateau pressures were used to make van't Hoff plots and determine the ΔH values for the desorption reactions.

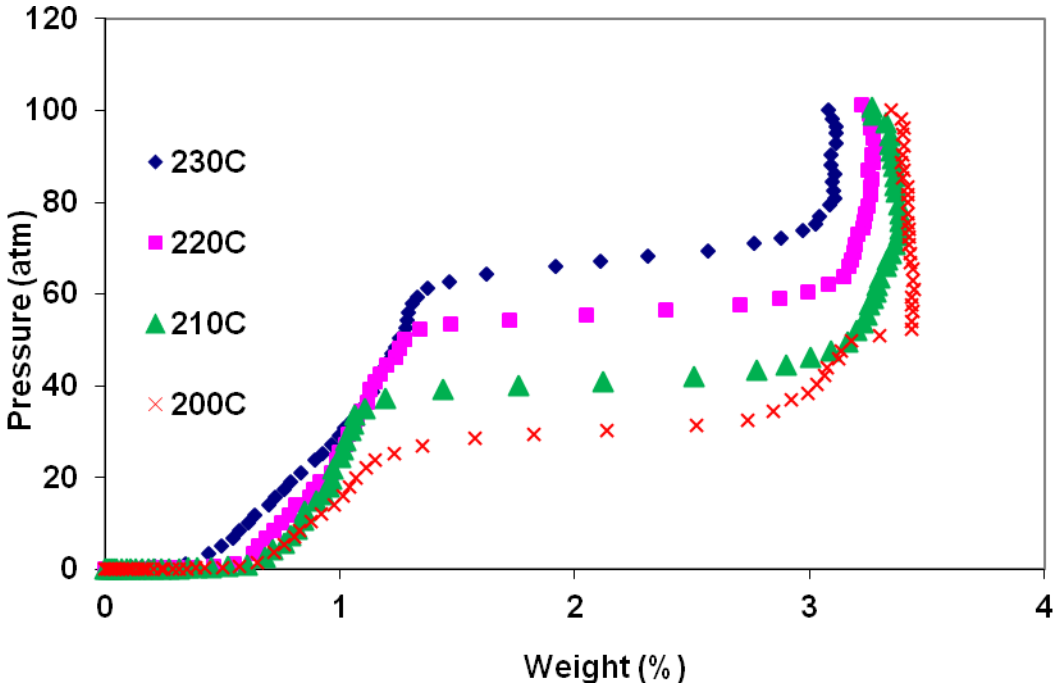

Figure 5.3a Desorption PCT isotherms for the CsH-doped $2LiNH_2/1.1MgH_2$ mixture

The desorption PCI for the RbH doped and the un-doped samples at various temperatures had been reported in chapter 4. Figure 5.3a shows the desorption PCI for the CsH doped sample while Fig. 5.3b shows the desorption temperatures for all samples at 210 ^{o}C.

Table 5.1 shows that the mixture with the lowest plateau pressure at 210 ^{o}C has the highest desorption temperature.

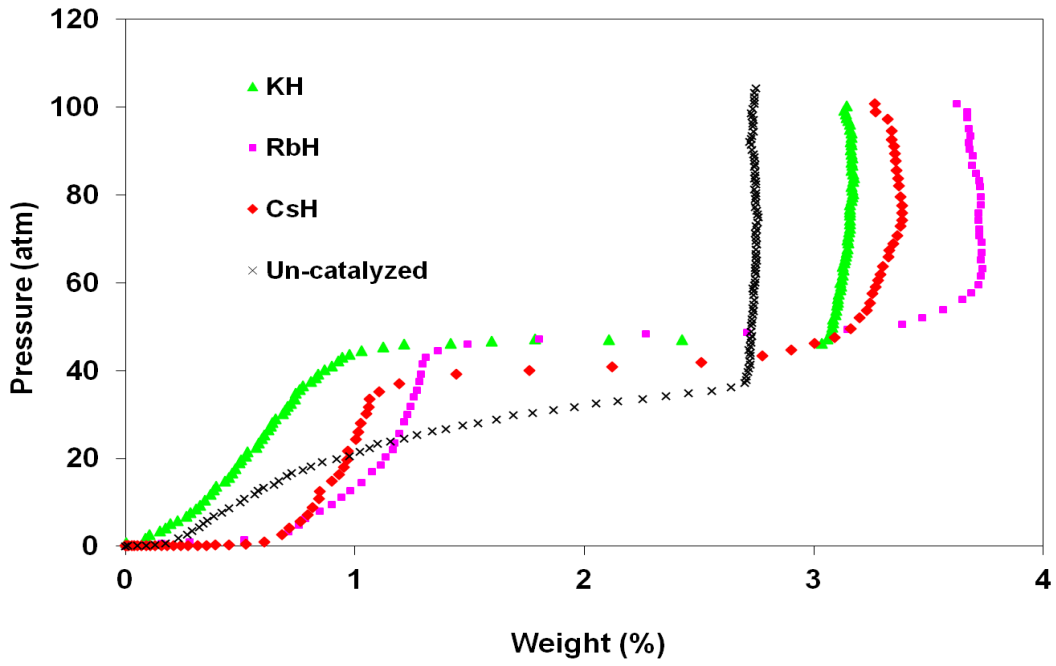

Figure 5.3b Desorption PCT isotherms for the doped and un-doped $2LiNH_2/1.1MgH_2$ mixture

5.4 Van't HOFF PLOTS

Thermodynamic stabilities were determined from pressure composition temperature (PCT) isotherm measurements that were done on the catalyzed and un-catalyzed mixtures. Measurements were made in the 200 - 230 ^{o}C range. The plateau pressures were used to construct van't Hoff plots and the slopes were used to determine the ΔH values for the desorption reactions. Van't Hoff plots for the RbH-doped, KH-doped and un-doped samples are shown in Figure 5.4. The enthalpy values obtained for the different

mixtures are shown in Table 5.1. The desorption enthalpy values obtained for the CsH doped mixture (45.7 kJ/mol), RbH doped mixture (42.7 kJ/mol) and the KH doped mixture (42.0 kJ/mol) are within the same range. These enthalpies are significantly lower than the (65 kJ/mol) found for the un-doped mixture.

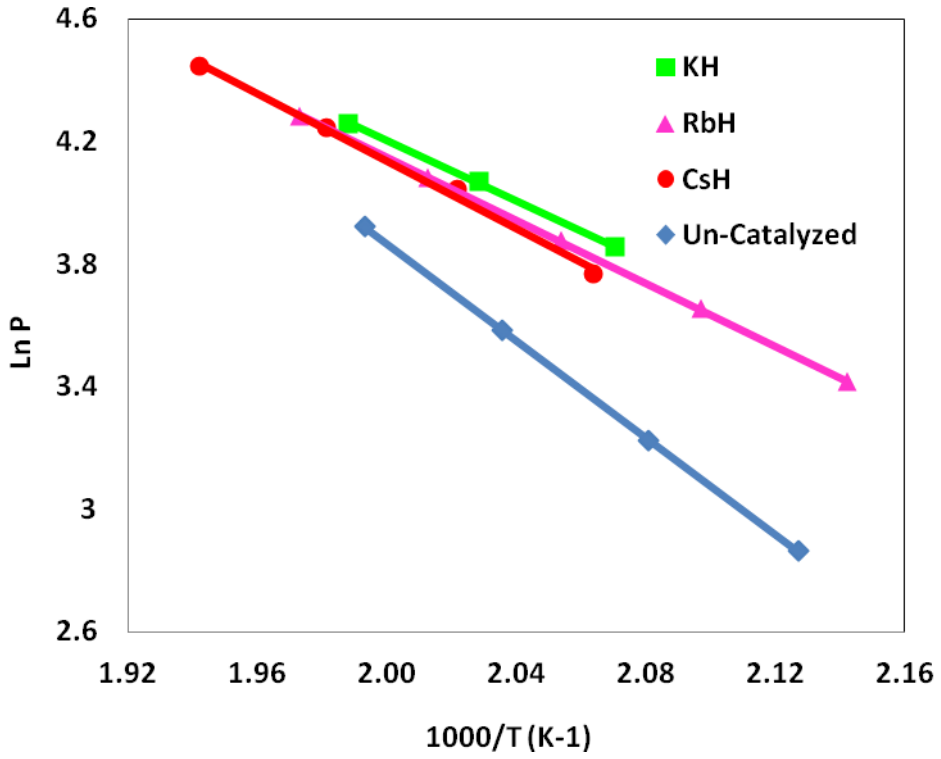

Figure 5.4 Van't Hoff plots for hydrogen desorption from the catalyzed and un-catalyzed $2LiNH_2/1.1MgH_2$ mixtures.

Table 5.1 Summary of desorption parameters for thermodynamics and kinetics results

Samples / Parameters	KH	RbH	CsH	Un-catalyzed
Onset Temp. (^{o}C)	75	76	63	109
Electronegativity of M	0.820	0.820	0.790	-
Desop. Temp., T_d, (^{o}C)	146	143	159	237
Desop. ΔH (KJ/mol)	42.0±0.12	42.7±0.03	45.7±0.03	65.8±0.04
Ratio NH_3/H_2 release	0.00283	0.00795	0.000649	0.0590
Ea (KJ/mol)	87.0±0.7	86.8±0.1	109.1±0.3	119.0±1.7
Pm at 210 ^{o}C (atm)	46.1	48.3	40.9	34.2
T_{90} (min)	62	27	76	1600
RbH ratio compared	2.3	1	2.8	59.3
"m" values	0.587	0.652	0.632	0.647

5.5 DTA MEASUREMENTS AND KISSINGER PLOTS

Differential Thermal Analysis curves (DTA) were carried out in order to better understand the effects of the additives on the dehydrogenation of the doped and un-doped $2LiNH_2/1.1MgH_2$ mixtures. The DTAs were carried out for the doped and un-doped mixtures at different heating rates between 4 and 20 ^{o}C per minute. Figure 5.5 shows the DTA curves for the CsH doped mixture at different heating rates. The plots show that the desorption temperatures increase with increasing scan rates. These scans are typical of those that were obtained for the other mixtures. There is a relationship between the scan

rate and the activation energy that is described by the Kissinger equation (19) in chapter 3.

Kissinger plots for various mixtures were constructed from the data obtained from the DTA curves. The slopes of these plots, shown in Figure 5.6, were used to determine the activation energies of each mixture. The activation energies for KH, RbH and CsH doped mixtures are 87 kJ/mol, 86.8 kJ/mol and 109.1 kJ/mol respectively. These are all smaller than the activation energy (119 kJ/mol) for the un-catalyzed mixture. Table 5.1 shows the activation energy values of all the mixtures.

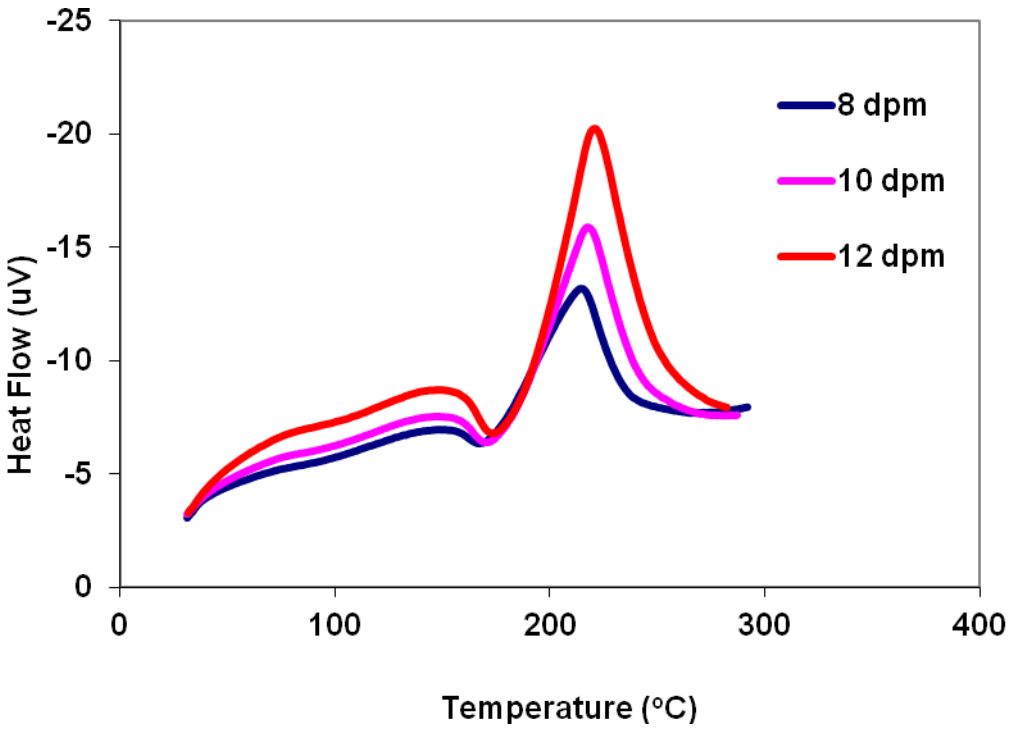

Figure 5.5 Differential thermal analysis plots for a $2LiNH_2/1.1MgH_2$ mixture catalyzed by CsH

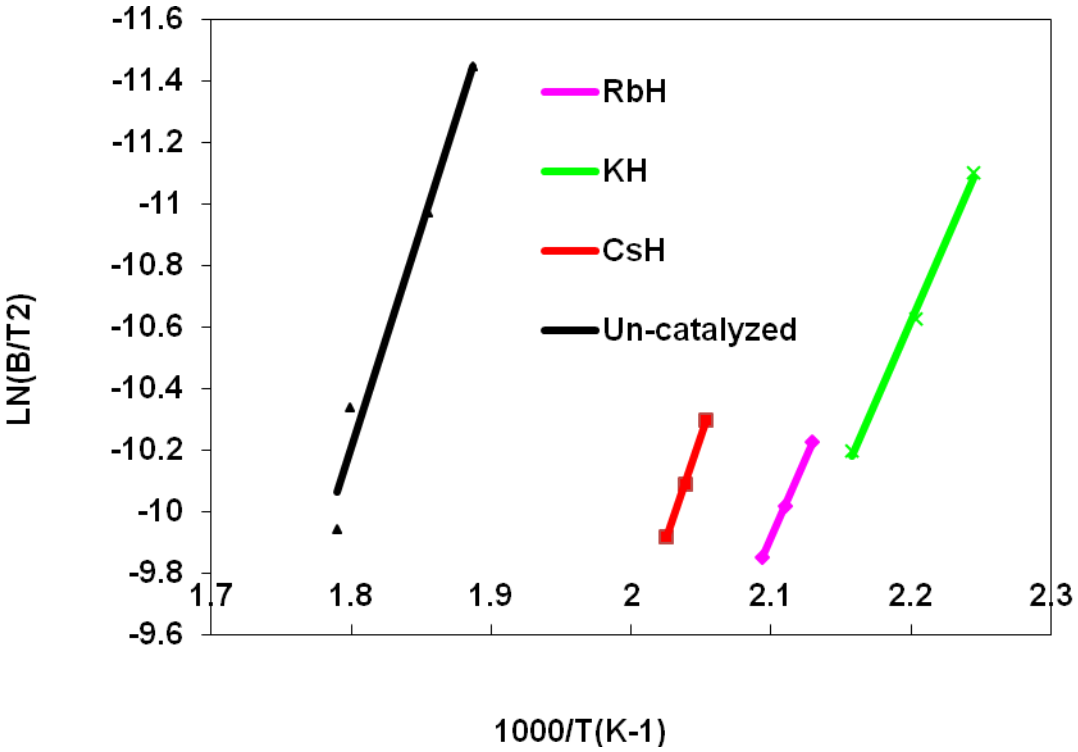

Figure 5.6 Kissinger plots for catalyzed and un-catalyzed $2LiNH_2/1.1MgH_2$ mixtures

5.6 KINETIC MEASUREMENTS

Comparisons were made of the desorption kinetics of the catalyzed and un-catalyzed systems. Kinetics measurements were carried out for each mixture in the two-phase plateau region at 210 ^oC using constant pressure thermodynamics forces described in chapter 3. Again, here an N-Value of 10 was applied to all samples. Figure 5.7a contains the desorption kinetics plots of $2LiNH_2/1.1MgH_2$ mixtures with and without RbH, KH and CsH catalysts. Figure 5.7b shows the full scale graph. It can be seen that the order of reaction kinetic rates is RbH > KH > CsH >>> Un-catalyzed. The RbH doped mixture desorbs hydrogen about twice as fast as the KH doped, thrice as fast as the CsH and about

60 times as fast as the un-catalyzed mixture. The times taken by the various reactions to reach 90 % completion (T_{90}) are shown in Table 5.1.

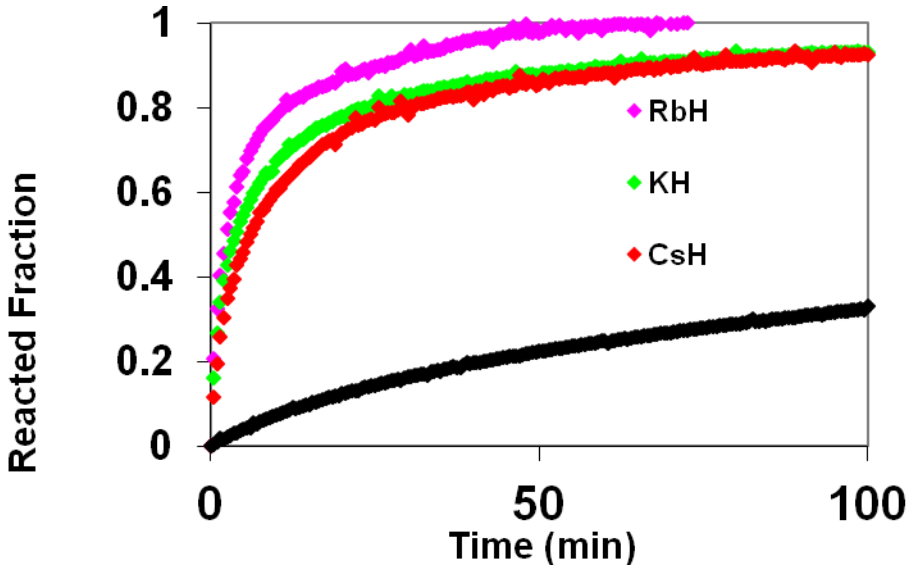

Figure 5.7a Desorption kinetics plots for catalyzed and un-catalyzed $2LiNH_2/1.1MgH_2$ mixtures at N=10 and 210 ^oC

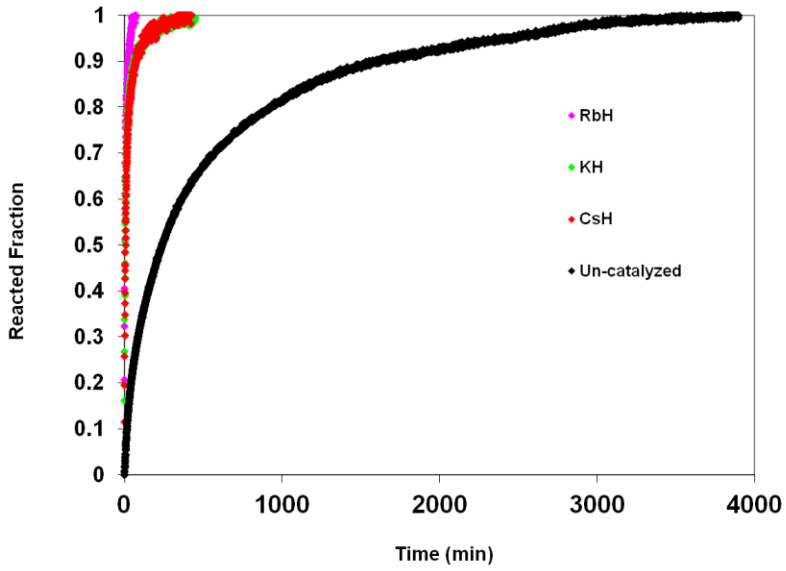

Figure 5.7b Desorption kinetics plots for catalyzed and un-catalyzed $2LiNH_2/1.1MgH_2$ mixtures at N=10 and 210 ^oC (Full scale plot)

5.7 KINETIC MODELING STUDIES

The kinetic modeling studies of the KH, RbH doped and un-doped mixtures had been reported in Chapter 4. The fact that the RbH and KH doped mixture desorbs hydrogen faster than CsH was unexpected based on the fact that Cs was supposed to be more reactive than both Rb and K, since reactivity increases from the top to the bottom in the metallic group on the periodic table. Therefore kinetics modeling studies were conducted to determine if there was an explanation for this by using the shrinking core model and Johnson-Mehl-Avrami (JMA) plot described in chapter 4. The overall rate of KH, RbH doped and un-doped mixtures are all diffusion controlled as reported in chapter 4. The desorption rate of the CsH doped mixture is also diffusion controlled. This is shown in figure 5.8.

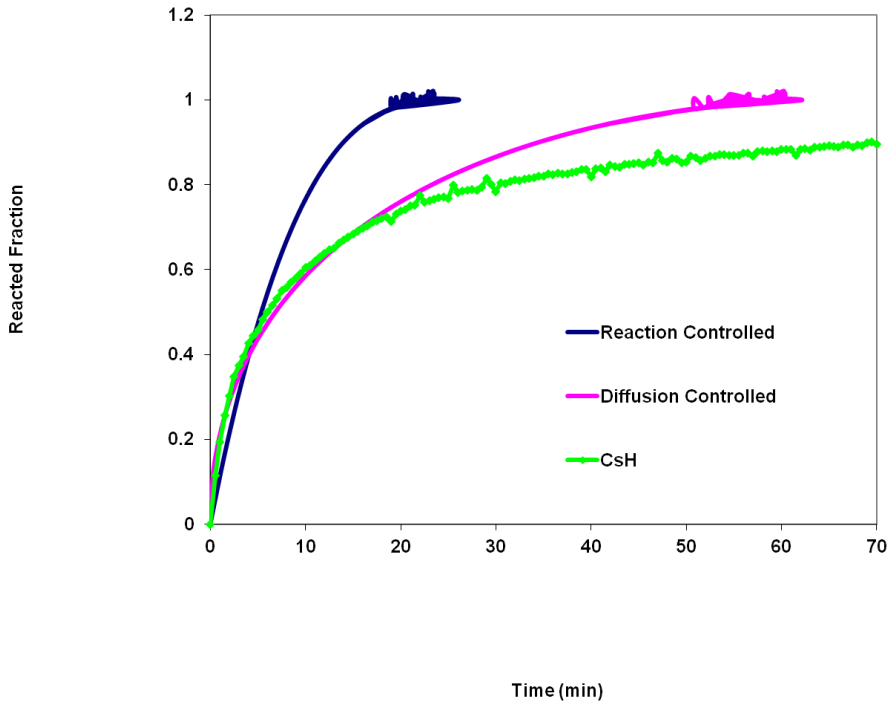

Figure 5.8 Modeling plots for the CsH doped mixture of $2LiNH_2/1.1MgH_2$ mixtures

The data generated from the model with diffusion controlling the overall rate fits the experimental data better than the data generated from the model with chemical reaction controlling the overall reaction rate. This is true only during the first 70 % of the reaction. During the last 30 % of the reaction, neither model was a good fit with the experimental data. The reason for this is that during the first 70 % of the reaction, desorption occurred along the plateau region where the pressure remained relatively constant. The N-Value was constant and thus the thermodynamic driving force was constant. When the reaction reached the left edge of the plateau region the pressure decreased sharply and the thermodynamic driving force decreased. At this point the kinetics slowed more rapidly than either model predicted. The modeling results for the KH, RbH doped and the un-doped mixtures showed the same pattern as well. This was reported in chapter 4.

A second modeling technique based on the classical equation for analysis of nucleation-and-growth developed by Hancock and Sharp [118] was used to confirm that the desorption rates are diffusion controlled. This method has been discussed in detail in chapter 3.

The values of ‘m’ obtained from the slope of the graph in Figure 5.9 for each mixture are tabulated in Table 5.1. The data shows that the values for all the systems correspond most closely to those expected for diffusion-controlled reactions.

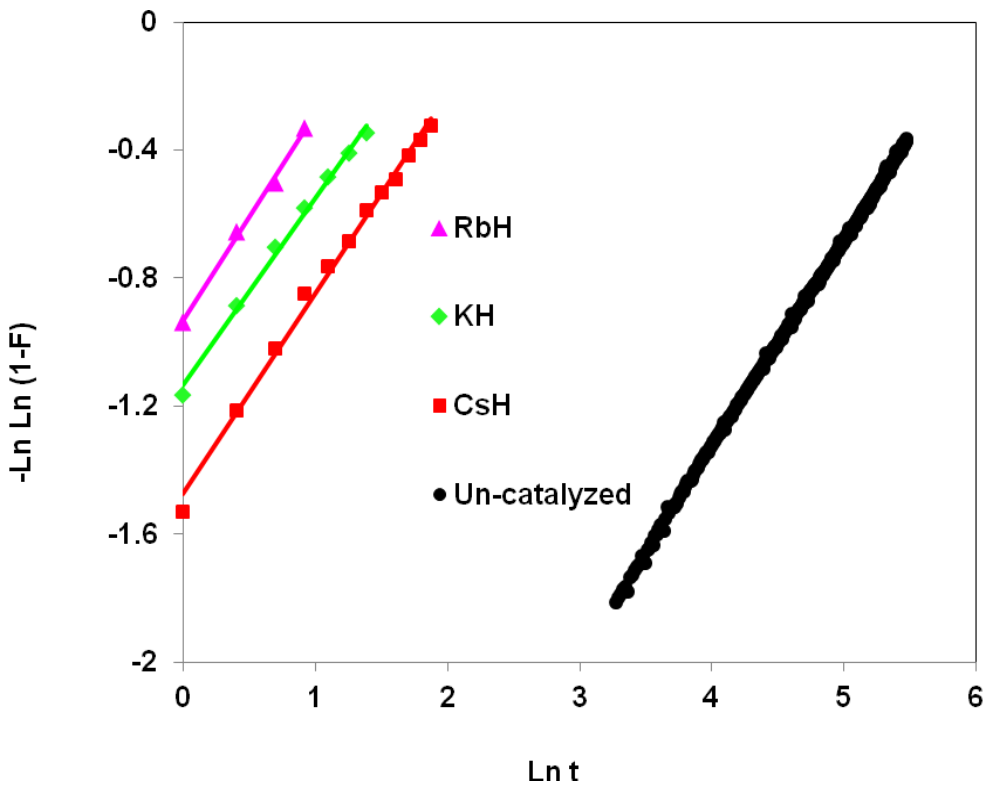

Figure 5.9 Modeling plots for catalyzed and un-catalyzed $2LiNH_2/1.1MgH_2$ mixtures based on the method of Hancock and Sharp

5.8 RGA MEASUREMENTS

Residual gas analyses were done on the various mixtures to determine the ratio of ammonia to hydrogen present in each mixture. The mixtures were analyzed 5 days after milling. Figure 5.10a-d shows the RGA analysis of the CsH, KH, RbH doped mixture and un-doped mixture respectively. Table 5.1 shows the ratio of ammonia to hydrogen present in the mixtures. The amount of ammonia present in the KH, RbH and CsH doped mixtures were small when compared to the un-catalyzed mixture. The CsH doped mixtures have the least ammonia release. Other random gases such as nitrogen, argon, air

and oxygen were also monitored along with hydrogen and ammonia, but these gases were not present. This shows there was no leak during the experimental measurements.

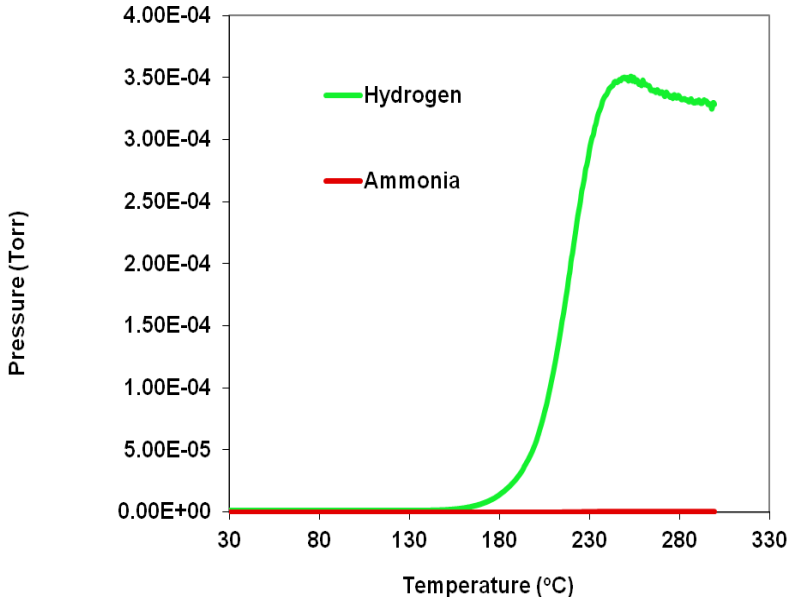

Figure 5.10a RGA Plot of CsH doped $2LiNH_2/1.1MgH_2$ mixtures

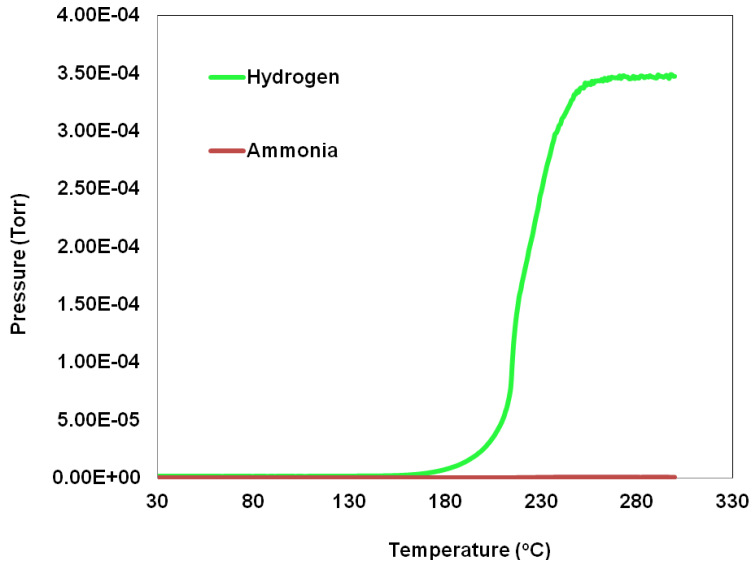

Figure 5.10b RGA Plot of KH doped $2LiNH_2/1.1MgH_2$ mixtures

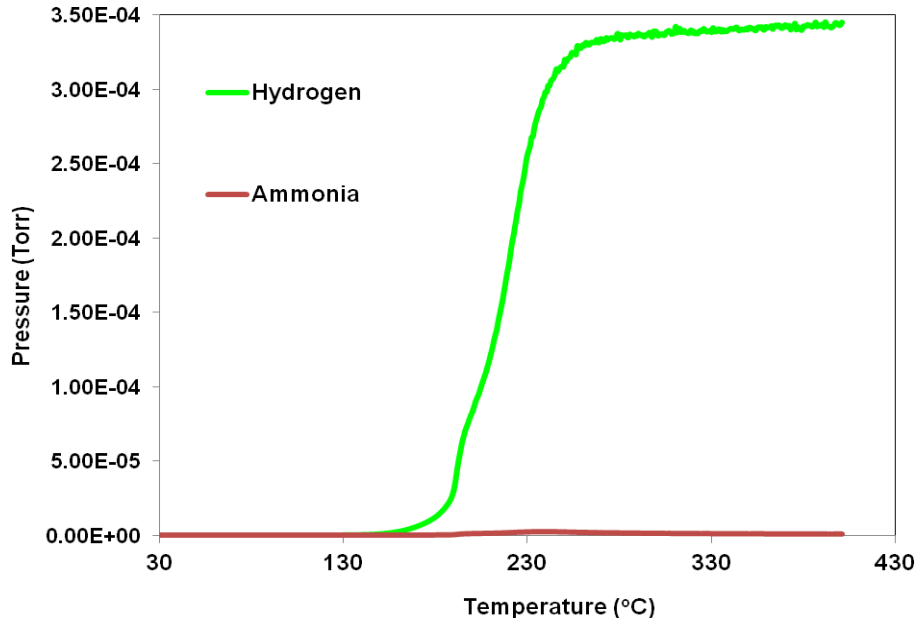

Figure 5.10c RGA Plot of RbH doped $2LiNH_2/1.1MgH_2$ mixtures

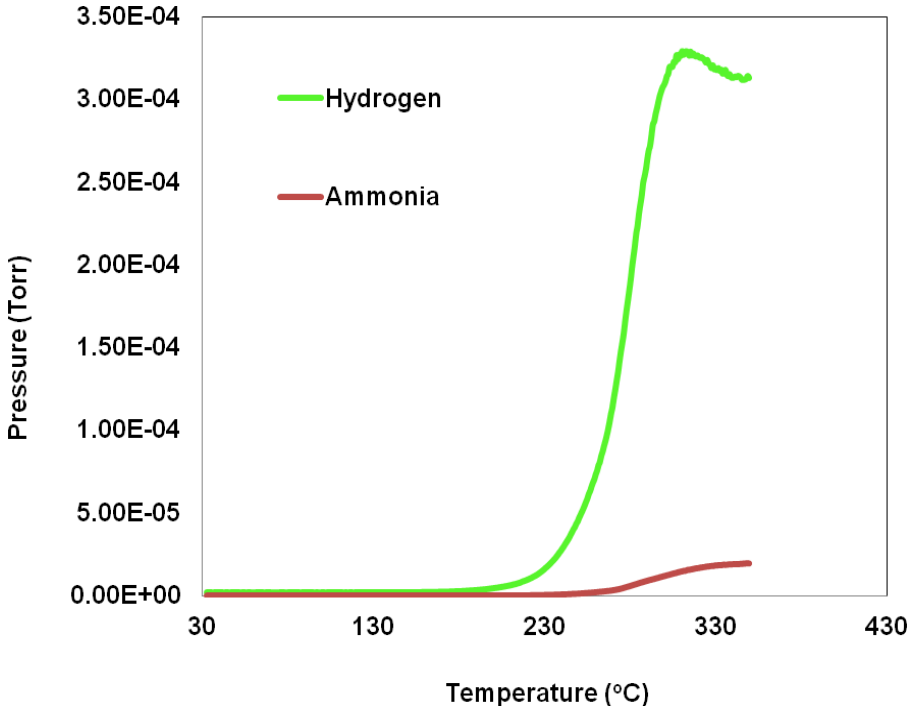

Figure 5.10d RGA Plot of un-doped $2LiNH_2/1.1MgH_2$ mixtures

5.9 FTIR MEASUREMENTS

Figure 5.11a shows the FTIR of the dopants. The FTIR of all the dopants have significant peaks at 704, 878, 1060, 1363 and 1447 cm^{-1}.

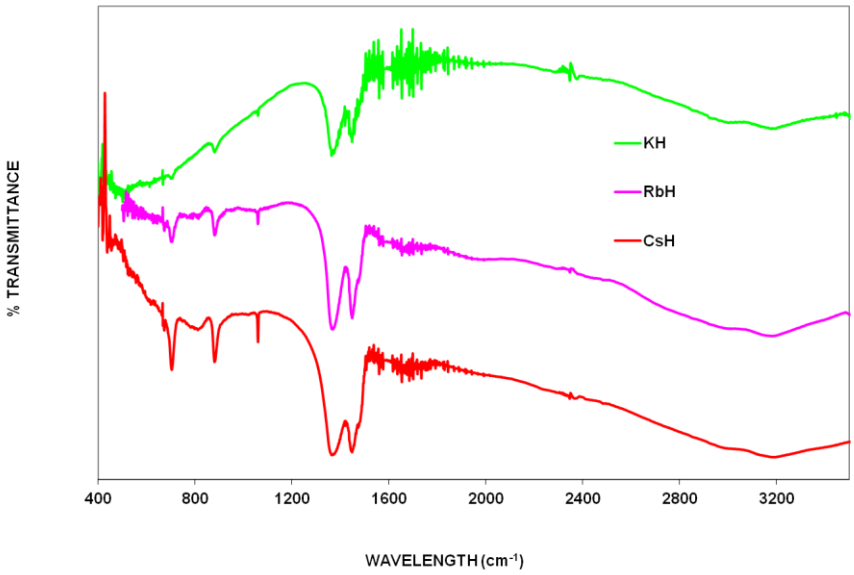

Figure 5.11a FTIR of dopants

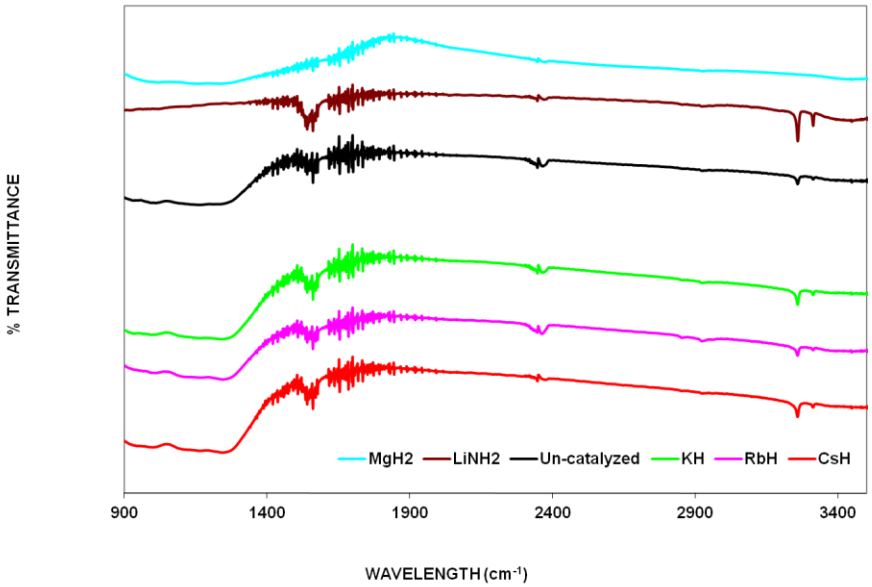

Figure 5.11b FTIR of doped and un-doped 'as milled' mixtures of $2LiNH_2/1.1MgH_2$

Figure 5.11b shows the FTIR of the "as milled " milled mixtures. The FTIR of the starting materials ($LiNH_2$ and MgH_2) are also included for comparism. The FTIR of the MgH_2 showed no peaks but that of the $LiNH_2$ showed peaks at 1554, 3259 and 3313 cm^{-1}.The peaks showed by the FTIR of both the doped and un-doped mixtures are the same as that shown by the $LiNH_2$. These results are in consistent with the XRD of the as milled mixtures that suggest no new phases are formed after 2 hrs of high energy milling and that the peaks shown in the XRD are that of MgH_2 and $LiNH_2$ peaks only. The FTIR peaks of the catalysts are also not visible in the as milled mixtures.

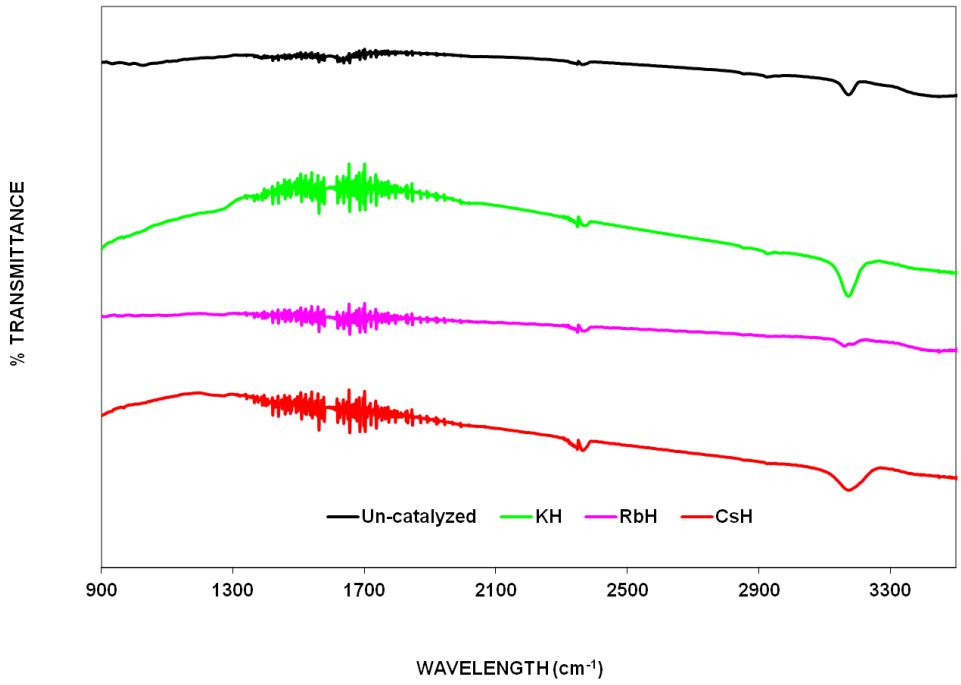

Figure 5.11c FTIR of doped and un-doped dehydrided mixtures of $2LiNH_2/1.1MgH_2$

Formation of a new phase can be seen in the FTIR of the dehydrided mixtures (Fig. 5.11c). The peak appearing at 3170 cm^{-1} is due to the formation of a new ternary compound $Li_2Mg(NH)_2$ that has been reported in several studies [70, 97, 100 and 107] for the un-doped mixture. This peak position is also consistent in the FTIR of the dehydrided doped mixtures. The peaks of the $LiNH_2$ seen in Fig. 5.11b are not visible. This also confirmed $LiNH_2$ is not present in the dehydrided mixtures.

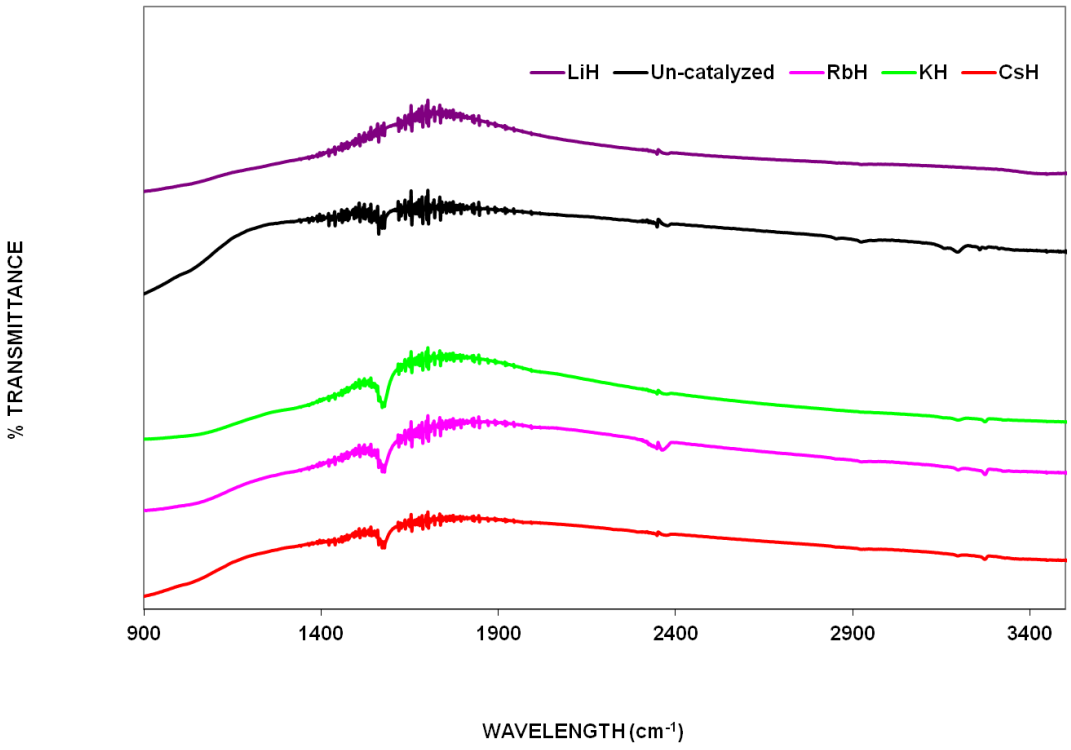

Figure 5.11d FTIR of doped and un-doped rehydrided mixtures of $2LiNH_2/1.1MgH_2$

Fig. 5.11d shows the FTIR of the rehydrided mixtures. The peaks at 1572 and 3258 cm^{-1} are characteristic peaks of $Mg(NH_2)_2$. The FTIR of LiH included showed no peaks.

However, this does not rule out the presence of LiH in the mixture. This can only confirm that the peaks are only due to $Mg(NH_2)_2$ according to eq. (7). The peaks of the catalysts are also not present in the dehydrided doped mixtures; this can be due to very small fraction of the catalysts present in the mixtures of the KBr for FTIR analysis.

5.10 CONCLUSION

The results show that all the dopants have the capabilities to lower desorption temperature and reduce the enthalpy of the $2LiNH_2/1.1MgH_2$ system. Hence we refer to the dopants as "catalytic additives". The results of this study show that the new catalytic additive, RbH, is significantly better than both KH and CsH for enhancing hydrogen desorption from the $2LiNH_2/1.1MgH_2$ system. The RbH and KH additives have nearly the same capability for lowering the hydrogen desorption temperature of the $2LiNH_2/1.1MgH_2$ mixture. This is believed to be largely due to the fact that both Rb and K have the same electronegativity and thus similar destabilizing effect on the N-H bond. The kinetics results show that the RbH-doped mixture releases hydrogen over twice as fast as the K doped mixture, thrice as fast as the Cs doped mixture and approximately 60 times faster than the un-catalyzed sample. The modeling studies using the shrinking core model and a method developed by Hancock and Sharp both indicated that the reaction rates for both the doped and un-doped mixtures are controlled by diffusion in the two-phase plateau region. The faster kinetics in the RbH doped mixture is attributed to the fact that Rb has a larger ionic radius (248 pm) than K (227 pm) and is thereby able to expand the lattice, thus facilitating the diffusion process. The Cs on the other hand has relatively larger radius (265 pm) than the Rb, however its relatively low hardness of 0.2

Mohs compared with the Rb (0.3 Mohs) and K (0.4 Mohs) prevents it from expanding the lattice just as the Rb did. FTIR of the doped and un-doped mixtures also confirmed the formation of a new ternary imide $Li_2Mg(NH)_2$ in the dehydrided mixtures. Presence of $Mg(NH_2)_2$ in the rehydrided mixture of the doped and un-doped samples was also confirmed by FTIR.

CHAPTER SIX

6.0 OVERALL CONCLUSION

This dissertation study has shown that KH has the ability to lower desorption temperature for both (1:1) and (2:1) ratios of $LiNH_2/MgH_2$ systems. It is much more effective for the (2:1) than the (1:1) mixture. KH hydride also has the ability to increase the desorption rates for the (2:1) mixtures of $LiNH_2/MgH_2$. KH has also shown to be ineffective for increasing the reaction rates of the (1:1) mixtures. The desorption rate improvement of the doped (2:1) was ~25 times faster than the un-doped mixture. Modeling studies indicated that the desorption rates of (1:1) and (2:1) mixtures are diffusion controlled except for the doped (1:1) mixture which appears to be controlled by reaction at the phase boundary. It was observed that samples with high activation energy tend to react slower than those with low activation energy.

This dissertation study also revealed the capabilities of KH, RbH and CsH to lower the desorption temperature and reduce the enthalpy of $2LiNH_2/1.1MgH_2$ mixture, hence they are referred to as "catalytic additives". RbH proved to be the most effective catalytic additive for lowering the desorption temperature and increasing the desorption rates. The order of reaction kinetic rates using constant pressure thermodynamic driving forces is RbH > KH > CsH >>> Un-catalyzed. Modeling studies for the doped and un-doped mixtures by using the shrinking core model and a method developed by Hancock and Sharp showed that the reaction rates are diffusion controlled in the two-phase plateau

region. The faster kinetics in the RbH doped mixture is attributed to the fact that Rb has a larger radius than K and is thereby able to expand the lattice, thus facilitating the diffusion process. The Cs on the other hand has relatively larger radius than the Rb but low hardness than Rb and K; this prevents Cs from expanding the lattice more than the Rb and K. FTIR confirmed the formation of $Li_2Mg(NH)_2$ in the dehydrided mixtures of both the doped and un-doped mixtures.

REFERENCES

1. Jain, I.P.; Jain, P.; Jain, A. Novel hydrogen storage materials: A review of lightweight complex hydrides. *J. Alloys Compd*. 503 **2010** 303–339.

2. Liang, C.; Liu, Y.; Fu, H.; Ding, Y.; Gao, M.; Pan, H. Li–Mg–N–H-based combination systems for hydrogen storage. *J. Alloys Compd.* 509 **2011** 7844–7853.

3. Grochala, W.; Edwards, P.P. Hydrides of the Chemical Elements for The Storage and Production of Hydrogen. *Chem. Rev*. 104 **2004** 1283–1315.

4. Fleischmann, M.; Pons, S. Electrochemically Induced Nuclear Fusion of Deuterium. *J. Electroanal. Chem*. 261**1989** 301–308.

5. Lipman, T. E.; DeLucchi, M. A. Hydrogen-fuelled vehicles. *Int. J. Vehicle Des*. 17 **1996** 562-589.

6. Irani, R. S. Hydrogen storage: high-pressure gas containment. *MRS Bull*. 27 **2002** 680-682.

7. Wolf, J. Liquid-hydrogen technology for vehicles. *MRS Bull*. 27 **2002** 684-687.

8. Grand challenge for basic and applied research in hydrogen storage available at

   http://www1.eere.energy.gov/hydrogenandfuelcells/pdfs/1_milliken_final.pdf (Last accessed on: March 19, 2013).

9. Jain, I. P.; Lal, C.; Jain, A. Hydrogen storage in Mg: A most promising material *Int. J. Hydrogen Energy* 35 **2010** 5133-5144.

10. Jain, A.; Agarwal, S.; Jain, I. P. Correlation between the milling time and hydrogen-storage properties of nanostructured ZrFeNi ternary alloy. *J. Alloys Comp*. 480 **2009** 325–328.

11. Tibbetts, G. G.; Gregory, P. M.; Charles, H. O. Hydrogen storage capacity of carbon nanotubes, filaments, and vapor-grown fibers. *Carbon* 39 **2001** 2291–2301.

12. Shiraishi, M.; Takenobu, T.; Ata, M. Gas-solid interactions in the hydrogen/single-walled carbon nanotube system. *Chem. Phys. Lett*., 367 **2003** 633–636.

13. Carpetis, C.; Peschka, W. A study on hydrogen storage by use of cryoadsorbents. *Int. J. Hydrogen Energy* 5 **1980** 539–554.

14. Agarwal, R.K.; Noh, J.S.; Schwarz, J.A.; Davini, P. Effect of surface acidity of activated carbon on hydrogen storage. *Carbon* 25 **1987** 219–226.

15. Targets for Onboard Hydrogen Storage Systems for Light-Duty Vehicles available at

    http://www1.eere.energy.gov/hydrogenandfuelcells/storage/pdfs/targets_onboard_hydro_storage_explanation.pdf (Last accessed on: March 19, 2013).

16. Conserve Energy Future available at

    http://www.conserve-energy-future.com/Advantages_Disadvantages_HydrogenEnergy.php (Last accessed on: March 19, 2013).

17. Fuel cell and hydrogen energy association available at

    http://www.fchea.org/index.php?id=47 (Last accessed on: March 19, 2013).

18. Fuel economy available at

    http://www.fueleconomy.gov/feg/fcv_benefits.shtml (Last accessed on: March 19, 2013).

19. U.S. Department of Energy- Hydrogen, Fuel Cells and Infrastructure Technologies Program available at http://www1.eere.energy.gov/hydrogenandfuelcells/mypp/pdfs/storage.pdf (Last accessed on: March 19, 2013).

20. Hydrogen storage technologies available at

    http://www1.eere.energy.gov/hydrogenandfuelcells/storage/current_technology.html?m=1& (Last accessed on: March 19, 2013).

21. Parliamentary Office of Science and Technology- Prospects For a Hydrogen Economy available at

    http://www.parliament.uk/post/pn186.pdf (Last accessed on: March 19, 2013).

22. Advanced Hydrogen Storage Materials available at

    http://ec.europa.eu/research/energy/pdf/efchp_hydrogen4.pdf (Last accessed on: March 19, 2013).

23. Hydrogen and Fuel Cell Technologies Program: Storage available at

http://h2bestpractices.org/storage/cryogenic_liquid/storage_vessels/ (Last accessed on: March 19, 2013).

24. Using metal hydrides to store hydrogen available at

http://sti.srs.gov/fulltext/ms2003172/ms2003172.pdf (Last accessed on: March 19, 2013).

25. Zuttel, A. Materials for Hydrogen Storage. *Materials Today* **2003**, 6(9), 24-33.

26. Pukazhselvan, D.; Kumar, V.; Singh, S. K. High capacity hydrogen storage: Basic aspects, new developments and milestones, *Nano Energy* **2012,** 1(4), 566-589.

27. Fuel From the Water- Hydrogen Storage available at http://www.fuelfromthewater.com/storage.htm (Last accessed on: March 19,

2013).

28. Arroyo, C. P.; Dompablo, Y.; Ceder, G. First principles investigations of complex hydrides AMH_4 and A_3MH_6 (A=Li, Na, K, M=B, Al, Ga) as hydrogen storage systems, *J. Alloys Compd.* **2004**, 364(1-2), 6-12.

29. Finholt, A. E.; Jacobson, E. C.; Ogard, A. E.; Thompson, P. Organic Reductions by Sodium Aluminum Hydride. *J.Am.Chem. Soc*. 77 **1955** 4163.

30. Finholt, A. E.; Bond Jr., A. C.; Schlesinger, H. I. Lithium Aluminum Hydride, Aluminum Hydride and Lithium Gallium Hydride, and Some of their Applications in Organic and Inorganic Chemistry. *J. Am. Chem. Soc*. 69 **1947** 1199–1203.

31. George, L.; Saxena, S.K. Structural stability of metal hydrides, alanates and borohydrides of alkali and alkali- earth elements: A review. *Int. J. Hydrogen Energy* 35 (11) **2010** 5454–5470.

32. Ashby, E.C.; Brendel, G.J.; Redman, H.E. Direct synthesis of complex metal hydrides. *Inorg. Chem*. 2 **1963** 499–504.

33. Resan, M.; Hampton, M.D.; Lomness, J.K.; Slattery, D.K.Effect of catalysts on hydrogen storage properties of $LiAlH_4$ and $NaAlH_4$. *Int. J. Hydrogen Energy* 30 (13–14) **2005** 1417-1421.

34. Claudy, P.; Bonnetot, B.; Bastide, J.; Jean-Marie, L. Lithium Aluminum Hydride, Aluminum Hydride and Lithium Gallium Hydride, and Some of their Applications in Organic and Inorganic Chemistry. *Mater. Res. Bull*. 17 **1982** 1499–1504.

35. Sartori, S.; Qi, X.; Eigen, N.; Muller, J.; Klassen, T.; Dornheim, M.; Hauback, B.C. A search for new Mg- and K-containing alanates for hydrogen storage. *Int. J. Hydrogen Energy* 34 (10) **2009** 4582-4586.

36. Ronnebro, E.; Majzoub, E. H. Crystal Structure, Raman Spectroscopy, and Ab Initio Calculations of a New Bialkali Alanate K_2LiAlH_6. *J. Phys. Chem. B*110 **2006** 25686–25691.

37. Mamatha, M.; Bogdanovi´ c, B.; Felderhoff, M.; Pommerin, A.; Schmidt, W.; Schüth, F.; Weidenthaler, C. Mechanochemical preparation and investigation of properties of magnesium, calcium and lithium–magnesium alanates. *J. Alloys Comp*. 407 **2006** 78–86.

38. James, B.D.; Wallbridge, M.G.H. Excellent review of metal tetrahydroborates. *Prog. Inorg. Chem*. 11 **1970** 99.

39. Schlesinger, H.I. ; Herbert, C. B.; Henry, R.H.; Louis, R.R. Reactions of Diborane with Alkali Metal Hydrides and Their Addition Compounds. New Syntheses of Borohydrides. Sodium and Potassium Borohydrides. *J. Am. Chem. Soc*. 75 **1953** 199–204.

40. C˘erny´, R.; Severa, G.; Ravnsbæk, D.B.; Filinchuk, Y.; D'Anna, V.; Hagemann, H.; Haase, D.; Jensen, C.M.; Jensen, T.R. NaSc(BH4)4: A Novel Scandium-Based Borohydride. *J. Phys. Chem. C* 114 **2010** 1357–1364.

41. Yuan, F.; Gu, Q.; Chen, X.; Tan, Y.; Guo, Y.; Yu, X. Complex Ammine Titanium(III) Borohydrides as Advanced Solid Hydrogen-Storage Materials with Favorable Dehydrogenation Properties. *Chem. Mater*. 24 (17) **2012** 3370–3379.

42. Fakioğlua, E.; Yürüma, Y.; Veziroğlub, T.N. A review of hydrogen storage systems based on boron and its compounds. *Int. J. Hydrogen Energy*. 29 (13) **2004** 1371–1376.

43. FJanot, R.; Eymery, J.B.; Tarascon, J.M. Decomposition of $LiAl(NH_2)_4$ and Reaction with LiH for a Possible Reversible Hydrogen Storage. *J. Phys. Chem. C* 111 (5) **2007** 2335–2340.

44. Nakamori, Y.; Kitahara, G.; Orimo, S. Synthesis and dehydriding studies of Mg–N–H systems. *J. Power Sources* 138 **2004** 309–312.

45. Kojima, Y.; Kawai, Y.; Ohba, N. Hydrogen storage of metal nitrides by a mechanochemical reaction. *J. Power Sources* 159 **2006** 81–87.

46. Leng, H.; Ichikawa, T.; Hino, S.; Hanada, N.; Isobe, S.; Fujii, H . Synthesis and decomposition reactions of metal amides in metal-N-H hydrogen storage system. *J. Power Sources* 156 **2006** 166–170.

47. Senker, J.; Jacobs, H.; Muller, M.; Press, W.; Mayer, H.M.; Ibberson, R.M. Structure determination of a low temperature phase of calcium and strontium amide by means of neutron powder diffraction on $Ca(ND_2)_2$ and $Sr(ND_2)_2$. *Z. Anorg Allg. Chem.* 625 **1999** 2025-2032.

48. Toyokoda, K.; Hino, S,; Ichikawa, T.; Okamoto, K.; Fujii, H. Hydrogen desorption/absorption properties of Li–Ca–N–H system. *J. Alloys Compd*. 439 **2007** 337–341.

49. Chen, P.; Xiong, Z.; Wu, G.; Liu, Y.;Hu, J.; Luo, W. Metal–N–H systems for the hydrogen storage-Viewpoint paper. *Scripta Materialia*. 56 **2007** 817–822

50. Erwin, M. Conversion of dihydridodiammineboron(III) borohydride to ammonia-borane without hydrogen evolution. *Inorg. Chem*. 12 **1973** 1954-1955.

51. Shore, S.G.; Parry, R.W. Chemical Evidence for the Structure of the "Diammoniate of Diborane." III. The Reactions of Borohydride Salts with Lithium Halides and Aluminum Chloride. *J. Am. Chem. Soc*. 80 **1958** 12-15.

52. Shore, S.G.; Parry, R.W. Chemical Evidence for the Structure of the "Diammoniate of Diborane." II. The Preparation of Ammonia-Borane. *J. Am. Chem. Soc*. 80 **1958** 8-12.

53. Hu, M.G.; Van Paasschen, J.M.; Geanangel, R.A. New synthetic approaches to ammonia-borane and its deuterated derivatives. *J. Inorg. Nucl. Chem*. 39 **1977** 2147-2150.

54. Appel, M.; Frankel, J.P. Production of Aluminum Hydride by Hydrogen-Ion Bombardment. *J. Chem. Phys*. 42 **1965** 3984-3988.

55. Brower, F.M.; Matzek, N.E.; Reigler, P.F.; Rinn, H.W.; Roberts, C.B. Schmidt, D.L.; Snover, J.A.; Terada, K. Preparation and properties of aluminum hydride, *J. Am. Chem. Soc*. 98 **1976** 2450–2453.

56. Sandrock, G. Gross, K. Thomas, G. Effect of Ti-catalyst content on the reversible hydrogen storage properties of the sodium alanates. *J. Alloys Comp*. 339 **2002** 299–308.

57. Lee, G.; Shim, J.; Cho, Y.; Lee, K. Reversible hydrogen storage in $NaAlH_4$ catalyzed with lanthanide oxides. *Int. J. Hydrogen Energy*, 32 **2007** 1911–1915.

58. Durojaiye T.; Goudy A. J. Desorption kinetics of lithium amide/magnesium hydride systems at constant pressure thermodynamic driving forces, *Int. J. Hydrogen Energy.* 37(4) **2012**, , 3298-3304.

59. Yang, H.; Ibikunle, A.; Goudy A.J. Effects of Ti-Based Additives on the Hydrogen Storage Properties of a $LiBH_4/CaH_2$ Destabilized System, *Adv. in Mat. Sci. and Eng*. 2010 **2010**, 138642-138649.

60. Ibikunle A.; Goudy A. J.; Yang H. Hydrogen storage in a $CaH_2/LiBH_4$ destabilized metal hydride system, *J. Alloys Compd*. **2009**, 475(1-2), 110-115.

61. Sabitu, S. T.; Goudy, A. J. Dehydrogenation kinetics and modeling studies of $2LiBH_4 + MgH_2$ enhanced by NbF_5 catalyst using constant pressure thermodynamic driving forces, *J. Phys. Chem. C* **2012** 116(25), 13545-13550.

62. Ibikunle, A.A.; Sabitu, S.T.; Goudy, A.J. Kinetics and modeling studies of the $CaH_2/LiBH_4$, $MgH_2/LiBH_4$, $Ca(BH_4)_2$ and $Mg(BH_4)_2$ systems. *J. Alloys Compd*, **2013** 556, 45-50.

63. Kim, J.; Shim, J.; Cho, Y.W. On the reversibility of hydrogen storage in Ti- and Nb-catalyzed $Ca(BH_4)_2$. *J. Power Sources*. 181 **2008** 140–143.

64. Kim, J.; Jin, S.; Shim, J.; Cho, Y.W. Reversible hydrogen storage in calcium borohydride $Ca(BH_4)_2$. *Scripta Mater*. 58 **2008** 481–483.

65. Yoon, C.W.; Sneddon, L.G. Ammonia Triborane: A Promising New Candidate for Amineborane-Based Chemical Hydrogen Storage. *J. Am. Chem. Soc*. 128 **2006** 13992-13993.

66. Hausdorf, S.; Baitalow, F.; Wolf, G.; Mertens, F. A procedure for the regeneration of ammonia borane from BNH-waste products. *Int. J. Hydrogen Energy* 33 **2008** 608–614.

67. Neiner, D.; Karkamkar, A.; Linehan, J.C.; Arey, B.; Autrey, T.; Kauzlarich, S.M. Promotion of Hydrogen Release from Ammonia Borane with Mechanically Activated Hexagonal Boron Nitride. *J. Phys. Chem. C* 113 **2009** 1098–1103.

68. Orimo, S.; Nakamori, Y.; Kato, T.; Brown, C. Jensen, C.M. Intrinsic and mechanically modified thermal stabilities of α-, β- and γ-aluminum trihydrides AlH_3. *Appl. Phys. A* 83 **2006** 5-8.

69. Luo, W.F. ($LiNH_2$–MgH_2): a viable hydrogen storage system. *J. Alloy. Compd*. 381 **2004** 284–287.

70. Luo, W.F; Sickafoose, S. Thermodynamic and structural characterization of the Mg–Li–N–H hydrogen storage system. *J. Alloys Compd*. 407 **2006** 274–281.

71. Xiong, Z.T.; Wu, G.T.; Hu, J.J.; Chen, P. Ternary Imides for Hydrogen Storage. *Adv. Mater*. 16 **2004** 1522–1525.

72. Xiong, Z.T.; Hu, J.J.; Wu, G.T.; Chen, P.; Luo, W.F.; Gross, K.; Wang, J. Thermodynamic and kinetic investigations of the hydrogen storage in the Li–Mg–N–H system. *J. Alloys Compd*. 398 **2005** 235–239.

73. Ichikawa, T.; Tokoyoda, K.; Leng, H.; Fujii, H. Hydrogen absorption properties of Li–Mg–N–H system. *J. Alloys Compd*. 400 **2005** 245–248.

74. Orimo, S.; Nakamori, Y.; Kitahara, G.; Miwa, K.; Ohba, N. Noritake, T.; Towata, S. Destabilization and enhanced dehydriding reaction of $LiNH_2$: an electronic structure viewpoint. *Appl. Phys. A* 79 **2004** 1765–1767.

75. Alapati, S. V.; Johnson, J. K.; Sholl, D. S. Identification of Destabilized Metal Hydrides for Hydrogen Storage Using First Principles Calculations. *J. Phys. Chem. B* 110(17) **2006** 8769-8776.

76. Lu, J.; Fang, Z. Z.; Choi, Y. J.; Sohn, H.J. Potential of Binary Lithium Magnesium Nitride for Hydrogen Storage Applications. *J. Phys. Chem. C*. 111 (32) **2007** 12129–12134.

77. Osborn, W.; Markmaitree, T.; Shaw, L. L. Evaluation of the hydrogen storage behavior of a $LiNH_2$+MgH_2 system with 1:1 ratio. *J. Power Sources*. 172 **2007** 376-378.

78. Liu, Y.; Zhong, K.; Gao, M.; Wang, J.; Pan, H.; Wang, Q. Hydrogen Storage in a $LiNH_2$−MgH_2 (1:1) System. *Chem. Mater*. 20 (10) **2008** 3521–3527.

79. Liang, C.; Liu, Y.; Luo, K.; Li, B.; Gao, M.; Pan, H.; Wang, Q. Reaction pathways determined by mechanical milling process for dehydrogenation/hydrogenation of the $LiNH_2$/MgH_2 system. *Chemistry*. 16(2) **2010** 693-702.

80. Anton, D. L.; Price, C. J.; Gray, J. Affects of Mechanical Milling and Metal Oxide Additives on Sorption Kinetics of 1:1 $LiNH_2$/MgH_2 Mixture. *Energies* 4(5) **2011** 826-844.

81. Price, C.; Gray, J.; Lascola Jr, R.; Anton, D. L. The effects of halide modifiers on the sorption kinetics of the Li-Mg-N-H System. *Int. J. Hydrogen Energy* 37 (3) **2012** 2742–2749.

82. Chen, P.; Xiong, Z.; Luo, J.; Lin, J.; Tan, K. Interaction of hydrogen with metal nitrides and imides. *Nature* 420 **2002** 302-304.

83. Chen, P.; Xiong, Z.; Luo, J.; Lin, J.; Tan, K. Interaction between Lithium Amide and Lithium Hydride. *J. Phys. Chem*. B 107 (39) **2003** 10967–10970.

84. Gregory D.H. Lithium nitrides, imides and amides as lightweight, reversible hydrogen stores. *J. Mater. Chem*. 18 **2008** 2321-2330.

85. Yang, J.; Sudik, A.; Wolverton, C. Activation of hydrogen storage materials in the Li–Mg–N–H system: Effect on storage properties. *J. Alloys and Compd*. 430 (1–2) **2007** 334-338.

86. Luo, W.; Rönnebro, E. Towards a viable hydrogen storage system for transportation application. *J. Alloys and Compd.* 404–406 **2005** 392-395.

87. Chen, Y.; Wu, C.; Wang, P.; Cheng, H. Structure and hydrogen storage property of ball-milled $LiNH_2/MgH_2$ mixture. *Int. J.Hydrogen Energy*. 31 (9) **2006** 1236-1240.

88. Xiong, Z.; Wu, G.; Hu, J.; Chen, P.; Luo, W.; Wang, J. Investigations on hydrogen storage over Li–Mg–N–H complex—the effect of compositional changes. *J. Alloys and Compd*. 417 (1–2) **2006** 190-194.

89. Chen, P.; Xiong, Z.; Yang, L.; Wu, G.; Luo, W. Mechanistic Investigations on the Heterogeneous Solid-State Reaction of Magnesium Amides and Lithium Hydrides. *J. Phys. Chem. B* **2006** 110 (29) 14221–14225.

90. Luo, S.; Flanagan, T.B.; Luo, W. The effect of exposure of the H-storage system ($LiNH_2$ + MgH_2) to water-saturated air. *J. Alloys and Compd*. 440 (1–2) **2007** L13-L17.

91. Sudik, A.; Yang, J.; Halliday, D.; Wolverton, C. Kinetic Improvement in the $Mg(NH_2)_2$−LiH Storage System by Product Seeding. *J. Phys. Chem. C* **2007** 111 (17) 6568–6573.

92. Luo, W.; Wang, J.; Stewart, K.; Clift, M.; Karl Gross. Li–Mg–N–H: Recent investigations and development. *J. Alloys and Compd.* 446–447 **2007** 336-341.

93. Aoki, M.; Noritake, T.; Nakamori, Y.; Towata, S.; Orimo, S. Dehydriding and rehydriding properties of $Mg(NH_2)_2$–LiH systems. *J. Alloys and Compd*. 446–447 **2007** 328-331.

94. Janot, R.; Eymery, J.; Tarascon, J. Investigation of the processes for reversible hydrogen storage in the Li–Mg–N–H system. *J. Power Sources* 164 (2) **2007** 496-502.

95. Rijssenbeek, J.; Gao, Y.; Hanson, J.; Huang, Q.; Jones, C.; Toby, B. Crystal structure determination and reaction pathway of amide–hydride mixtures. *J. Alloys and Compd*. 454 (1–2) **2008** 233-244.

96. Liu, Y.; Hu, J.; Wu, G.; Xiong, Z.; Chen, P. Formation and Equilibrium of Ammonia in the $Mg(NH_2)_2$−2LiH Hydrogen Storage System. *J. Phys. Chem. C* 112 (4) **2008** 1293–1298.

97. Markmaitree, T.; Osborn, W.; Shaw, L.L.. Comparisons between MgH2- and LiH-containing systems for hydrogen storage applications. *Int. J. Hydrogen Energy* 33 (14) **2008** 3915-3924.

98. Shahi, R.R.; Yadav, T.P.; Shaz, M.A.; Srivastava, O.N. Effects of mechanical milling on desorption kinetics and phase transformation of $LiNH_2/MgH_2$ mixture. *Int. J. Hydrogen Energy* 33 (21) **2008** 6188-6194.

99. Liu, Y.; Zhong, K.; Luo, K.; Gao, M.; Pan, H.; Wang, Q. Size-Dependent Kinetic Enhancement in Hydrogen Absorption and Desorption of the Li−Mg−N−H System. *J. Am. Chem*. Soc. 131 (5) **2009** 1862–1870.

100. Hu, J.; Fichtner, M. Formation and Stability of Ternary Imides in the Li−Mg−N−H Hydrogen Storage System. *Chem. Mater*. 21 **2009** 3485-3490.

101. Markmaitree, T.; Shaw, L.L. Synthesis and hydriding properties of $Li_2Mg(NH)_2$. *J. Power Sources* 195 (7) **2010** 1984-1991.

102. Chen, Y.; Wang, P,; Liu, C.; Cheng, H. Improved hydrogen storage performance of Li–Mg–N–H materials by optimizing composition and adding single-walled carbon nanotubes. *Int. J. Hydrogen Energy* 32 (9) **2007** 1262-1268.

103. Liu, Y.; Hu, J.; Xiong, Z.; Wu, G.; Chen, P. Improvement of the hydrogen-storage performances of Li–Mg–N–H system. *J. Mater. Res*. 22 (5) **2007** 1339 - 1345.

104. Lohstroh, W.; Fichtner, M. Reaction steps in the Li–Mg–N–H hydrogen storage system. *J. Alloys and Compd*. 446–447 **2007** 332-335.

105. Barison, S.; Agresti, F.; Lo Russo, S.; Maddalena, A.; Palade, P.; Principi, G.; Torzo, G. A study of the $LiNH_2$–MgH_2 system for solid state hydrogen storage. *J. Alloys and Compd*. 459 (1–2) **2008** 343-347.

106. Ma, L.; Dai, H.; Liang, Y.; Kang, X.; Fang, Z.; Wang, P.; Wang, P.; Cheng, H. Catalytically Enhanced Hydrogen Storage Properties of $Mg(NH_2)_2$ + 2LiH Material by Graphite-Supported Ru Nanoparticles. *J. Phys. Chem. C* 112 (46) **2008** 18280–18285.

107. Ma, L.; Dai, H.; Liang, Y.; Kang, X.; Fang, Z.; Wang, P.; Wang, P.; Cheng, H. Effect of Li3N additive on the hydrogen storage properties of Li-Mg-N-H system. *J. Mater. Res*. 24 (6) **2009** 1936 – 1942.

108. Wang, J.; Liu, T.; Wu, G.; Li, W.; Liu, Y.; Moysés Araújo, C.; Scheicher, R.; Blomqvist, A.; Ahuja, R.; Xiong, Z.; Yang, P.; Gao, M.; Pan, H.; Chen, P. Potassium-Modified $Mg(NH_2)_2$/2 LiH System for Hydrogen Storage. *Angew. Chem. Int. Ed*. 48 (32) **2009** 5828–5832.

109. Wang, Q.; Chen, Y.; Niu, G.; Wu, C.; Tao, M. Nature of Ti Species in the Li−Mg−N−H System for Hydrogen Storage: A Theoretical and Experimental Investigation. *Ind. Eng. Chem. Res.* 48 (11) **2009** 250–5254.

110. Shahi, R.R.; Yadav, T.P.; Shaz, M.A.; Srivastva, O.N. Studies on dehydrogenation characteristic of $Mg(NH_2)_2$/LiH mixture admixed with vanadium and vanadium based catalysts (V, V_2O_5 and VCl_3). *Int. J. Hydrogen Energy* 35 (1) **2010** 238-246.

111. Wang, J.; Hu, J.; Liu, Y.; Xiong, Z.; Wu, G..; Pan, H.; Chen, P. Effects of triphenyl phosphate on the hydrogen storage performance of the $Mg(NH_2)_2$–2LiH system. *J. Mater. Chem*. 19 **2009** 2141-2146.

112. Nayebossadri, S. Kinetic rate-limiting steps in dehydrogenation of Li–N–H and Li–Mg–N–H systems – Effects of elemental Si and Al. *Int. J. Hydrogen Energy* 36 (14) **2011** 8335-8343.

113. Liang, C.; Liu, Y.; Wei, Z.; Jiang, Y.; Wu, F.; Gao, M.; Pan, H. Enhanced dehydrogenation/hydrogenation kinetics of the $Mg(NH_2)_2$–2LiH system with NaOH additive. *Int. J. Hydrogen Energy* 36 (3) **2011** 2137-2144.

114. Luo, W.; Stavila, V.; Klebanoff, L.E. New insights into the mechanism of activation and hydrogen absorption of ($2LiNH_2$–MgH_2). *Int. J. Hydrogen Energy* 37 (8) **2012** 6646-6652.

115. Durojaiye, T.; Goudy, A. Desorption kinetics of lithium amide/magnesium hydride systems at constant pressure thermodynamic driving forces. *Int. J. Hydrogen Energy* 37 (4) **2012** 3298-3304.

116. Velikokhatnyi, O. I.; Kumta, P. N. Energetics of the lithium-magnesium imide–magnesium amide and lithium hydride reaction for hydrogen storage: An ab initio study. *Mat. Sci. and Eng. B* 140 (1–2) **2007** 114-122.

117. Elansari, L.; Antoine, L.; Janot, R.; Gachon, J.C.; Kuntz, J.J.; Guérard, D. Preparation of alkali metal hydrides by mechanical alloying. *J. Alloys and Compd*. 329 (1–2) **2001** L5-L8.

118. Hancock, J.D; Sharp, J.H. Method of comparing solid-state kinetic data and its application to the decomposition of kaolinite, brucite, and $BaCO_3$. *J Am Ceram Soc*. 55 **1972** 74-77.

119. Smith, G.; Goudy, A.J. Thermodynamics, kinetics and modeling studies of the $LaNi_{5-x}Co_x$ hydride system. *J. Alloys and Compd*. 316 (1–2) **2001** 93-98.

120. Jacobs, H.; Birkenbeul, J.; Kochelkorn, J. Darstellung und Eigenschaften der Amidomagnesate des Kaliums und Rubidiums $K_2[Mg(NH_2)_4]^-$ und $Rb_2[Mg(NH_2)_4]^-$Verbindungen mit Isolierten $[Mg(NH_2)_4]^{2-}$-Tetraedern. (Preparation and Properties of Amidomagnesate of potassium and rubidium $K_2[Mg(NH_2)_4]^-$ und $Rb_2[Mg(NH_2)_4]^-$ Connections with insulated $[Mg(NH_2)_4]^{2-}$-Tetrahedra). *J Less Common Met* **1984**, 97, 205-214.

121. Jacobs, H.; Birkenbeul, J.; Schmitz, D. Struktur verwandtschaft des dicaesiumamidomagnesats, $Cs_2[Mg(NH_2)_4]$, zum β-K_2SO_4-Typ (Structural relationship of dicaesiumamidomagnesats, $Cs_2[Mg(NH_2)_4]$, to β-K_2SO_4-Type*). J. Less Comm. Met*. 85 **1982** 79-86.

122. Lappert, M.; Protchenko, A.; Power, P.; Seeber A. Metal Amide Chemistry. *Wiley publications* **2009** Pg. 52. ISBN: 978-0-470-72184-1.

123. Smith, G.; Goudy, A.J. Thermodynamics, kinetics and modeling studies of the $LaNi_{5-x}Co_x$ hydride system. *J. Alloys and Compd*. 316 (1–2) **2001** 93-98.

TOLULOPE OLUMIDE DUROJAIYE

831 GibbS Drive, Middletown, Delaware, 19709, Phone # 302-765-7174,
tolusko@yahoo.com

Education

Delaware State University – Dover, Delaware
Ph.D., Applied Chemistry, May 2013

Delaware State University – Dover, Delaware
M.Sc., Chemistry, December 2008

University of Abeokuta – Ogun State, (Nigeria)

B.Sc., Biochemistry, April 2002

Professional/Research Experience

Graduate Assistant

(Hydrogen Storage Research Center) Delaware State University. Dover, DE.

January 2007-May 2013

- Synthesized non-commercially available catalyst (Rubidium and Cesium hydrides) using reactive ball milling approach
- Synthesized potential hydrogen storage materials (borohydrides and amides) suitable for hydrogen storage purposes
- Characterized synthesized samples using XRD and FTIR
- Conducted detailed research on the synthesis, characterization and thermodynamic studies of some double-cation borohydrides
- Conducted comparative kinetics and modeling studies on different ratios of lithium amide and magnesium hydride mixtures using potassium hydride as catalyst
- Designed and conducted detailed comparative studies of the effect of some alkali hydrides on lithium amide and magnesium hydride mixtures
- Analyzed and interpreted various data
- Prepared scientific reports for group meetings

- Supervision of first year graduate student on planning and execution of research/data analysis

Graduate Tutor

Delaware State University, Dover, DE. September 2009-December 2009

- Served as Chemistry Laboratory Instructor for Nursing students
- Assisted Undergraduate students with comprehension of Chemistry

Additional Experience

Laboratory Technician

Immunoassay Laboratory Limited. Lagos, (Nigeria) October 2002-December 2006

- Analyzed human serum for levels of various endocrine hormones using RIA/ELISA diagnostic kits
- Analyzed seminal fluids for sperm counts and morphology
- Analyzed human serum for Tumor markers
- Served as Head of Technical department

Internship

CPL Industries Limited. Lagos, (Nigeria) March 1997-February 1998

- Quality Control experience in Pharmaceutical and Cosmetic laboratories
- Physical/Chemical analysis of drugs and cosmetics

Technical skills

- UV-Spectroscopy, FTIR, NMR, Microscopy, Viscometers
- Characterization of solid state samples using X-ray diffractometer
- Planetary/Shaker miller for mixing samples
- Pressure Composition Isotherms Instruments (PCI) and Thermogravimetric/Differential Analyzer (TG/DTA) for thermodynamics analysis

- Mass Spectrometry using Residual Gas Analyzer (RGA) for desorbed gas analysis
- Sieverts apparatus for kinetics and reaction rate measurements
- Volumetric/Qualitative analysis
- Radioimmunoassay (RIA), Enzyme Linked Immunosorbent Assay (ELISA) techniques
- Ability to design and execute research with little or no supervision
- Excellent Communication/People skills
- Excellent problem-solving skills and good sense of responsibility
- Proficient use of MS Office suite

Thesis and Dissertation

MS

- Study of copper, manganese and zirconium metals as partial Substituents in double-cation borohydride complexes of $LiBH_4$ and $NaBH_4$ for hydrogen storage purposes

PhD

- Thermodynamics and kinetics enhancement of $LiNH_2$-MgH_2 systems using alkali metal hydride dopants for hydrogen storage

Publications

- Tolulope Durojaiye, Adeola Ibikunle, Andrew J. Goudy. Hydrogen storage in destabilized borohydride materials. International Journal of hydrogen energy 35 (2010) 10329-10333
- Tolulope Durojaiye and Andrew J. Goudy. Desorption kinetics of lithium amide/magnesium hydride systems at constant pressure thermodynamic driving forces. International Journal of hydrogen energy 37 (2012) 3298-3304
- Andrew Goudy, Adeola Ibikunle, Saidi Sabitu and Tolulope Durojaiye, "Thermodynamics and Kinetics of Complex Borohydride and Amide Hydrogen Storage Materials" Materials Challenges in Alternative and

Renewable Energy II in Ceramic Transactions, Vol 239, Edited by George Wicks, Wiley, 2013.

- Tolulope Durojaiye, Jalaal Hayes, Andrew J. Goudy. Rubidium hydride- An exceptional dehydrogenation catalyst for lithium amide-magnesium hydride system. Journal of Physical Chemistry C. (In Press)
- Tolulope Durojaiye, Jalaal Hayes, Andrew J. Goudy. Comparative studies of selected alkali metal hydrides of group I on $2LiNH_2/MgH_2$ system. (To be published soon in Journal of Chemistry of materials)

Conferences/Presentations

- Posters on the Hill

Capitol building, Washington DC, USA May 2009. *(Attendee)*

- Hydrogen Storage in lithium borohydride destabilized metal hydride materials

Gordon Research Conference, Lucca, Italy, July 2009*. (Poster Presentation)*

- Hydrogen Storage in modified lithium borohydride metal hydride materials

National Organization for the Professional advancement of Black Chemists and Chemical Engineers (NOBCChe). September 2009, Maryland, USA. *(Poster Presentation)*

- Desorption kinetics of lithium amide/magnesium hydride systems at constant pressure thermodynamic driving forces

Gordon Research Conference, Easton, MA, USA.July 2011.

(Poster Presentation)

- Improved kinetics of lithium amide/magnesium hydride systems for hydrogen storage

2nd Annual Graduate Research Symposium. Delaware State University. April 2012, Dover, USA *(Poster Presentation)*

Honors/Awards

- Most diligent staff, 2005
- Most dedicated staff, 2006
- 1st Runner up, Doctoral Poster Presentations, 2012
-

Affiliations

- Member; American Chemical Society (ACS)
- Member; Student Chemical Society of Nigeria (SCSN)